COO/2846-2
UC - 60

THE UNIVERSITY OF MICHIGAN

COLLEGE OF ENGINEERING

DEPARTMENT OF ELECTRICAL AND COMPUTER ENGINEERING

Radiation Laboratory

ELECTROMAGNETIC INTERFERENCE BY WIND TURBINE GENERATORS

Final Report No. 2

January 1977 - March 1978

D.L. Sengupta and T.B.A. Senior

March 1978

Prepared for:

Department of Energy
Division of Solar Technology
Wind Systems Branch
Washington, D. C. 20545

Work Performed Under Contract EY-76-S-02-2846.A001

Ann Arbor, Michigan

014438-2-F

ELECTROMAGNETIC INTERFERENCE BY WIND TURBINE GENERATORS

Final Report

By

D.L. Sengupta and T.B.A. Senior
Radiation Laboratory
Department of Electrical and Computer Engineering
The University of Michigan
Ann Arbor, Michigan 48109

Work Performed Under

Contract EY-76-S-02-2846.A001

Prepared for

Department of Energy
Division of Solar Technology
Wind Systems Branch
Washington, D.C. 20545

March 1978

NOTICE

ABSTRACT

The interference produced by horizontal axis wind turbine generators on a number of electromagnetic systems has been identified and quantified. The interference to TV reception has been exhaustively studied, and a method has been developed to approximate the interference zone of a WTG. This can be used to estimate the effects on a WTG on TV reception and thereby establish minimal criteria for siting of such a machine. No significant interference to FM broadcast reception has been found. Studies of the interference to two specific air navigation systems (VOR and DVOR) indicate that no significant degradation in the performance of these systems should occur if the WTG is sited according to the standard guidelines established by the FAA. The performance of a repeating station of a typical microwave communication link system located in the vicinity of a WTG has been analyzed and guidelines have been developed which can aid in siting a WTG so that it produces minimum impact on the link system performance.

TABLE OF CONTENTS

TABLE OF CONTENTS (Continued)

TABLE OF CONTENTS (Continued)

TABLE OF CONTENTS (Continued)

ELECTROMAGNETIC INTERFERENCE BY WTG

This is the final report of a second year's study of the effects of large horizontal axis wind turbine generators (WTG) or windmills on the electromagnetic environment. Since a large portion of the present research has been devoted to the interference to TV reception which was also the subject of our previous study [1], and since the results obtained supplement and extend those reported there, it is appropriate to begin by summarizing the key findings of the previous study and the methods used to obtain them.

1. Previous Study

The original one-year study consisted of a preliminary but wide ranging theoretical and experimental investigation of the effects of a horizontal axis windmill on the reception of TV signals in its vicinity. Theoretical considerations of the scattering from idealized models of a blade showed that the rotating blades of a WTG could serve to pulse amplitude modulate the total signals received in its vicinity; and a simple signal analysis of the basic detection process of a TV receiver indicated that such extraneous modulation could cause video but not audio distortion.

During field tests performed at Plum Brook (Ohio) with the NASA/ERDA 100 Kw WTG and a local UHF TV signal, video distortion was observed at a distance of 0.5 km from the WTG when it was slewed to direct the specularly scattered signals to the test receiver. Simulation tests were also carried out in the laboratory using sinusoidal and unidirectional rectangular pulse amplitude modulations of the received signal. These confirmed that the modulation which a WTG could create does indeed produce video distortion, and suggested a threshold level that the modulation must exceed for the distortion to be severe or unacceptable.

With a rectangular metal plate as a model for a WTG blade and a distant TV transmitter, expressions for the primary (direct) and secondary (blade-scattered) fields at the receiver were obtained using the rigorous theory for the propagation of electromagnetic waves over a smooth homogeneous spherical earth. The approximate shapes and amplitudes of the modulation pulses of the total field at a point in the vicinity of the WTG were then derived, and from a knowledge of the modulation level necessary for severe video distortion, a computer method was developed to determine the TV interference zone around a WTG.

The most significant finding of the first year's work was that the rotating blades of a WTG pulse amplitude modulate the total field received in the vicinity of the machine, and that the modulation pulses can be sufficiently strong to produce unacceptable distortion of the video portion of the TV reproduction, especially at the higher UHF frequencies. Nevertheless, the study was preliminary in many aspects. Only a limited number of field tests had been performed, the modulation used in the laboratory simulation did not faithfully reproduce that generated by a moving blade, the scattering model for the blade was undesirably crude, and the determination of the modulation threshold was tentative at best, with no consideration of its possible dependence on the ambient signal level, the pulse width, the test receiver, etc. In addition, the method developed for predicting the TV interference zones was too inefficient and time-consuming to be used in the assessment of a large number of potential WTG sites. Thus, in spite of the successes achieved, it was desirable to pursue the study further to obtain a better understanding of the interference that a WTG produces, as regards other forms of electromagnetic signal as well as TV.

2. Present Study

Having conclusively established that a WTG can interfere with TV reception, the investigation was broadened to include other electromagnetic

systems in addition to TV, and made deeper to determine how the TV interference depends upon the various parameters involved. The main objectives were now

(i) to obtain a better understanding of the problem of TV interference, and to develop simple and efficient techniques for predicting the zone about a WTG where the interference could be severe; and

(ii) to estimate the impact of WTG-produced interference on the performance of aircraft navigation and microwave link systems.

Although no significant interference to the reception of FM broadcast signals had been found when the signals were strong, it was required that we attempt to quantify these effects as well.

The resulting program was a rather comprehensive one involving laboratory measurements and simulations, field testing using the existing WTG at the NASA Plum Brook Facility, and theoretical analyses and computations. In a later section we summarize the work performed in several different areas and cite the main conclusions reached, but for a better appreciation of the studies that were carried out, it may be helpful to give an overview of the program as a whole.

A key objective was to devise a reliable and convenient method for predicting the zone about a WTG where the TV interference could be severe. Using the computer program developed during the first year, a graphical technique was arrived at by which the interference zone could be found given the equivalent scattering area A_e of a single windmill blade and the threshold value (m_o) of the modulation index, i.e., the maximum value of the modulation index for which the video distortion is still acceptable for short periods of viewing. The focus now shifted to the determination of A_e and m_o. To obtain the equivalent scattering area, measurements were made on small scale versions of three different windmill blades in the laboratory as well as on the (full scale) MOD-0 (metallic) and MOD-0A (composite) blades

onsite at Plum Brook. A_e can be related to the projected area A of a blade using the concept of the scattering efficiency η, and values were obtained for η for the MOD-0, MOD-0A and MOD-1 blades, valid for all frequencies of interest. In addition, a theory was developed with which the scattering areas of other (similar) blades could be found.

In parallel with this the nature of the modulation introduced by the rotating blades was being explored. Small scale model experiments revealed the type of amplitude modulation produced, and the various parameters characterizing the modulation pulses were related to the electrical size and rotation frequency of the blades. The results were in agreement with those obtained from a theoretical investigation, and were confirmed by measurements made using the MOD-0 WTG at Plum Brook, and provided the necessary information to permit simulation of the interference in the laboratory. A device was constructed to synthesize the modulation pulses produced by the rotating windmill blades and which could be attached to the input terminals of a TV receiver to amplitude modulate the net signal entering the receiver. It could be adjusted to provide a range of pulse widths and repetition frequencies, and with its aid an extensive series of controlled tests were performed to explore the degree of video distortion observed as a function of the TV channel number, the ambient signal level, the applied modulation index, the modulation pulse length, the delay between the direct and multipath (i.e., windmill scattered) signals, and the test receiver used. In particular, a threshold value for the modulation index was established for use in the graphical procedure for computing the interference zone. That portion of the zone which is produced by specular reflection off the blades is a cardioid centered at the WTG with its maximum pointing towards the TV transmitter. There is also a narrow lobe directed away from the transmitter resulting from forward scattering off the blades, and this generally provides the maximum distance from the WTG at which objectionable interference can occur. Though the shapes of the zones are independent of the TV channel number, their size increases with increasing number. The detailed procedure for determining the interference zone and other pertinent data are described in a separate report [2].

As a documentary record, video recordings were made of the video distortion to TV reception observed in the field and laboratory simulation tests. Selected ones have been reproduced on a single color video tape to which a narrative has been added, and this tape has been furnished to the sponsor. The original recordings are available for reference in The University of Michigan Radiation Laboratory.

Laboratory simulation techniques were also used to study the interference to FM radio reception. The same modulation pulse synthesizer was attached to the input terminals of a test receiver to amplitude modulate the input signal, and the interference assessed by listening to the quality of the audio reproduction as a function of the ambient level of the signal and the applied modulation index. The test receiver was a Ford-Autoneutronic Model 7710 typical of the FM stereo receivers in automobiles. When the ambient level of the input signal was high (signal to noise ratio S/N $\gtrsim$ 15 dB), no audio distortion was found until the modulation index reached 16 dB ($m \simeq 0.73$). Even with a weaker signal, i.e., S/N < 15 dB, there was no significant distortion for $m < 7$ dB ($\simeq 0.38$), but as m was increased beyond this level, there was an increasing amount of audio distortion in the form of a pulsed high frequency 'hiss' superimposed on the FM sound. The results are consistent with the known fact [3] that ordinary FM receivers are only susceptible to noise interference when operating in their 'threshold regions', i.e., for input S/N $\lesssim$ 12 dB. They also imply that the effects of WTG interference to FM radio reception will be negligible except possibly within a few tens of meters of the WTG, and even then the audio distortion will be perceptible only if the WTG is located in a region of low signal to noise ratio for that particular FM station.

Microwave communication links are widely used for the transmission and reception of a variety of information and there are few locations throughout the country that do not have a microwave link in their vicinity. To quantify the effect of WTG interference on the performance of typical communication links for telephone and television signals, a deterministic analysis was carried out on a free space basis, i.e., neglecting the presence of the earth.

Any degradation in performance depends on the sensitivity of a repeater receiver to the modulation that a windmill introduces, and this in turn is a function of the receiver characteristics. From a knowledge of the types of signals, modulation and modulation schemes used for the links, it was possible to specify a minimum level of interference which would adversely affect the link's performance. Using then the pattern of the receiving antenna and the equivalent scattering area of a windmill blade, the minimum level defines a 'forbidden' zone around a repeater station where the siting of a WTG could cause unacceptable interference. Not surprisingly, the largest dimension of the zone is along the microwave beam.

Navigational systems of varying types are also widely depolyed throughout the United States, and because of their vital role in ensuring safe and effective transportation, it is important to assess the potential impact of windmills on these systems. The VOR (Very High-Frequency Omnidirectional Range) and DVOR (Doppler VOR) systems are extensively used for (commercial) aircraft navigation over the continental United States, and in fact over the world. Due to this and their apparent vulnerability, we chose to analyze the impact of a rotating WTG on the performance of these two systems. The analysis was carried out by computing the direct and windmill-scattered VOR (DVOR) signals at an aircraft and then using the detection characteristics of the receivers to estimate the resulting error in the predicted aircraft location. The analytical procedures employed are logical extensions of those which the FAA has found acceptable in the case of static scatterers, and showed that the interference when the WTG blades are rotating is less troublesome than when the blades are stationary.

3. Task Summary

In the appendices to this report we detail the work performed in five different areas constituting the main lines of investigation. These are summarized in the following.

3.1 Interference Effects on VOR Indications (Appendix 1)

Scalloping errors in the bearing indications of a VOR (DVOR) system produced by the rotating blades of a WTG located in the vicinity of a VOR (DVOR) ground station are investigated. The analysis assumes the system to be in free space, the VOR receiver in the aircraft to be ideal, and neglects the vertical plane pattern characteristics of the VOR (DVOR) transmitting antenna system and the scattering effects of the WTG tower. A rectangular metal plate model for the WTG blade is used to obtain the windmill scattered VOR signals at the aircraft receiver.

The significant finding is that stationary WTG blades produce more scalloping errors than rotating ones. On the basis of the theory developed, some estimates of the errors produced by a common windmill are given. The results indicate that in choosing a site for a WTG in the vicinity of a VOR (DVOR) system it is sufficient to consider only the scattering effects of the stationary windmills. It therefore follows that the siting of a WTG can be carried out according to the standard guidelines established by the FAA.

3.2 Interference With Microwave Communication Link Systems (Appendix 2)

The possible effects of a WTG located in the vicinity of the repeater station of a typical microwave communication link (TD-) system used by the telephone companies are investigated theoretically. Using the threshold value for the interference to RF carrier signal ratio required by the telephone companies, and a knowledge of the signals scattered by the rectangular plate model of a (static) windmill blade, the concept of a forbidden zone around a microwave link receiver is developed, the zone being that where the placement of a windmill could produce unacceptable interference. The shape of the zone is primarily determined by the radiation pattern of the receiving antenna; its size is proportional to the equivalent scattering area of the WTG blade, and inversely proportional to the RF carrier wavelength and the specified threshold value of the interference signal relative to the desired signal at the receiver.

The effects of the blade rotation on the detected signal has been qualitatively assessed by examining the detection of the desired signals in the presence of the time varying modulation produced by the WTG. It is found that the blade rotation produces a frequency smearing of the received baseband signal energy, with the maximum frequency smear depending on the blade size and orientation, and its rotation frequency. For the MOD-0 blade, this maximum is much less than the total FDM (frequency division multiplex) bandwidth of the telephone channel. The degrading influence of the smear depends on the amplitude of the scattered signal at the receiver relative to that of the desired signal, and for a WTG outside the forbidden zone it would not appear that the blade rotation will produce significant interference effects.

3.3 Blade Scattering (Appendix 3)

The interference produced by the rotating blades of a WTG is directly proportional to the scattering from a single stationary blade, and is greatest for specular scattering off the broad face of a blade. For the MOD-0 and MOD-0A blades the backscattering cross sections have been measured on site at Plum Brook and compared with the values obtained in an anechoic chamber using small scale models at a scaled frequency. The equivalent scattering area of a blade, i.e., the area of a flat plate having the same specular cross section, is then deduced, and related to the projected area using the concept of scattering efficiency. The scattering areas of the MOD-0, MOD-0A and MOD-1 blades were found to be 12, 4.4 and 40 m^2 respectively, with corresponding scattering efficiencies 67, 24 and 63 percent respectively. The effect of adding different configurations of lightning arrestor strips to the (composite) MOD-0A blade has been explored, and a minimal configuration increases the scattering area to 5 m^2.

From a knowledge of the equivalent scattering area and the maximum dimension of the blade, the bistatic (specular) scattering can be determined using the physical optics approximation, and procedures are described for estimating the scattering from blades other than those which have been treated.

We have also examined the possibility of reducing the scattering of a blade of given physical area by using a non-metallic material or by applying some form of lossy coating to reduce the power reflection coefficient. Because of the wide range of frequencies that must be covered, it does not seem feasible to expect a substantial reduction from any coating that would be practicable, and for a composite blade the scattering is about 7 dB less than for the corresponding metal blade.

3.4 Amplitude Modulation by Rotating Objects (Appendix 4)

For a signal incident on a slowly rotating rectnagular metal plate the amplitude modulation produced has been studied theoretically and experimentally. In the analysis the physical optics approximation was used to obtain the scalloped fields. Experiments were carried out in an anechoic chamber to measure the modulation imposed on the signals scattered by a rectangular metal plate rotating about an axis through its center when illuminated by a plane electromagnetic wave of frequency 12.18 GHz. The modulation waveforms produced by a rotating scale model of the MOD-0 WTG blade were also measured using the same experimental setup.

The important findings of the study are:

(i) The nature of the modulation waveform depends on the orientation and electrical dimensions of the blade, its rotation speed, and most importantly, the directions of incidence and scattering.

(ii) For a plate rotating in its plane the modulation is independent of time in the directions where the scattering is maximum, i.e., in the specular and forward directions. In the direction near specular and forward , the modulation waveform is a sinusoid whose frequency is twice the rotation frequency; and away from these directions, the waveforms consist of sinc-like pulses repeating at twice the rotation frequency. The widths of the pulses are inversely proportional to the maximum linear dimension of the plate.

When the metal plate is skewed, i.e., not in its plate of rotation, the modulation waveforms in the specular and forward directions are sinusoids with frequency equal to the rotation frequency; in other directions the waveform is predominantly pulse-like, with the pulses repeating at the rotation frequency and the width of the main pulses are inversely proportional to the maximum plate dimension.

(iii) As regards the modulation waveform, a skewed rectangular plate is a satisfactory model of an actual WTG blade provided its dimensions are chosen appropriately and the skew angle approximates the average departure (including pitch as well as twist angle) of the blade surface from its plate of rotation.

3.5 Measurements of TV Interference (Appendix 5)

Results of two measurement programs to investigate and record the TV interference produced by a windmill are reported. The first program was a series of field tests using the NASA/ERDA 100 Kw WTG located at Plum Brook, Ohio, the sources of the RF energy being the TV transmitters available there. The second program consisted of a number of tests performed in a laboratory environment where the interference to reception of TV signals was studied under conditions simulating those experienced in the field, i.e., the direct signal was combined with an artificially-generated multipath signal so that the total signal input to the test receiver was amplitude modulated by a repetitive pulse of variable width and shape approximating that observed at Plum Brook. A method was developed to obtain reproducible video recordings of the observed distortions caused by the interference.

The main conclusions from the field tests are:

(i) The observed video distortion in the backward portion of the interference zone is a horizontal jittering of the received pictures in synchronism with the WTG blade rotating, whereas that in the forward portion appears as intensity fluctuations of the picture, also in synchronism with the blade rotation.

(ii) Singificant interference is observed in the backward region only when the WTG blade is positioned to direct the specularly reflected signals to the receiver. In fact, for given transmitter and receiver locations, interference is observed only if the wind is such as to position the WTG blades appropriately.

(iii) Each blade contributes individually and produces a sinc-like pulse amplitude modulation of the total received signal when the blade is close to horizontal.

(iv) All other conditions being equal, the interference and the resulting video distortion increase with increasing TV channel number (i.e., frequency) and decreasing distance from the WTG.

(v) The backward zone interference shows no significant dependence on the ambient level of the received signal and appears independent of the test receiver used.

The significant observations from the laboratory tests are:

(vi) In the backward zone the value of the critical modulation level m_c (required to produce minimum observable video distortion in a test receiver) is reasonably independent of the ambient level of the received signal, and in the forward zone m_c decreases with decreasing level of ambient signal.

(vii) The two test receivers showed similar vulnerability on the highest TV channels and in general, are more susceptible to backward zone interference.

(viii) A single modulation threshold level m_o of 2.6 dB ($\sim$ 15 percent) was defined as the largest value of the amplitude modulation index for the received signals for which the resulting video distortion is still judged acceptable for short periods of viewing.

4. Conclusions

The interference produced by horizontal axis wind turbine generators on a number of electromagnetic systems has been identified and quantified. The interference to TV reception has been exhaustively studied, and a method has been developed to approximate the interference zone of a WTG. This can be used to estimate the effects of a WTG on TV reception and thereby establish minimal criteria for siting of such a machine. No significant interference to FM broadcast reception has been found. Studies of the interference to two specific air navigation systems (VOR and DVOR) indicate that no significant degradation in the performance of these systems should occur if the WTG is sited according to the standard guidelines established by the FAA. The performance of a repeating station of a typical microwave communication link system located in the vicinity of a WTG has been analyzed and guidelines have been developed which can aid in siting a WTG so that it produces minimum impact on the link system performance.

Although the objectives of the present program have been accomplished, there are electromagnetic systems other than those considered here which may be susceptible to windmill interference. Many of these systems can be analyzed with the techniques developed in the present program. The TV signals being horizontally polarized, the scattering of these signals by a vertical axis WTG would be different and generally less, and this is one case where the interference should be examined. However, in the event that TV transmissions are made circularly polarized, even these machines could produce significant interference, and this change would affect the conclusions as regards other systems as well. The effects of circular polarization and vertical axis machines both warrant further study.

5. Acknowledgements

It is a pleasure to acknowledge the assistance of our colleagues in the performance of this study. We are particularly grateful to Mr. J.E. Ferris who was responsible for all of the field tests and for the measurements of

blade scattering; to Mr. I.J. LaHaie who carried out most of the study reported in Appendix 4, and in addition, assisted with the laboratory simulation of the interference, and to Mr. P.R. Jedrzejewski who developed many of the ideas reported in Appendix 2. Messrs I. Elrom and W.F. Parsons and Misses D.L. Michael and W.R. Ng all contributed to various portions of the sutyd. We are also grateful to the personnel of The University of Michigan Television Center for their advice and counsel with regard to our video tape recording, and those at the NASA Plum Brook facility for their cooperation in connection with the field tests.

6. References

[1] Senior, T.B.A., D.L. Sengupta and J.E. Ferris, "TV and FM Interference by Windmills", The University of Michigan Radiation Laboratory Final Report No. 014438-1-F, February 1977, Contract No. E(11-1)-2846, ERDA, Washington, D.C.

[2] Senior, T.B.A. and D.L. Sengupta, "Wind Turbine Generator Siting and TV Reception Handbook", The University of Michigan Radiation Laboratory Technical Report No. 014438-1-T, January 1978, Contract No. EY-76-S-02-2846.A001, DOE, Washington, D.C.

[3] Peebles, Jr., P.Z., Communication System Principles, Addison-Wesley Publishing Co., Inc., Reading, Mass, 1976, pp. 273-281.

APPENDIX 1: WINDMILL INTERFERENCE EFFECTS ON VOR INDICATIONS

The possible electromagnetic interference effects of a windmill on the bearing indications of conventional and Doppler VOR (Very High-Frequency Omni-directional Range) systems are theoretically investigated in the present Appendix.

The VOR is a short-range air navigation system which provides bearing information to a flying aircraft [1,2]. In an ideal situation the VOR ground station effectively radiates a VHF carrier signal (in the 108-118 MHz frequency range) which contains two synchronous 30 Hz modulation signals for reception by the airborne receiver. One modulation signal known as the reference signal is constant in phase and is independent of the aircraft azimuth; the other, known as the variable signal, varies directly in accordance with the bearing of the aircraft from the VOR ground station. A phase measuring device in the airborne receiver enables the pilot to determine his bearing by determining the phase difference between these two modulation signals.

In the absence of any multipath between the aircraft and the VOR transmitter, the accuracy of the bearing indications of the airborne VOR receiver is found to be satisfactory [2 - 5], but in the presence of multipath, the multipath signals combine with the desired signals to produce various types of siting errors in the VOR indications [2, 3, 6]. Those errors in the bearing indication which appear as a series of very slow rhythmic deviations from the desired course are known as course scalloping [2]. General discussions of observed course scalloping amplitudes produced by different types of static scattering objects are given in [2, 3, 6] and a rigorous theory of conventional VOR course scalloping amplitudes due to static multipath sources is presented in [7]. In the conventional VOR system, the variable phase signal is a 30 Hz amplitude modulation (AM) on the carrier while the constant phase or reference signal is the 30 Hz frequency modulation (FM) of 9.96 KHz subcarrier. In the Doppler VOR (DVOR) the roles of 30 Hz AM and FM signals are interchanged, i.e.,

the variable phase signal is applied as frequency modulation to the 9.96 KHz subcarrier while the 30 Hz AM signal acts as the reference signal. This makes the DVOR relatively immune to course scalloping errors due to site effects [2, 6]. Actual tests of DVOR show that scalloping errors on any given radial rarely exceed 1 percent whereas conventional VOR commonly has scalloping errors up to 2.5 percent [1].

The scattering from any windmill is time varying and because its frequency spectrum may well embrace 30 Hz and its harmonics, it is possible that the amount of course scalloping produced by a windmill may be different from that caused by a stationary object. In the following sections the course scalloping amplitude of conventional and Doppler VOR indications produced by a windmill are investigated theoretically. To simplify the electromagnetic analysis the following assumptions are made: (i) the VOR system and the windmill are in free space, i.e., ground effects are ignored, (ii) the effects of the elevation plane patterns of the VOR transmitting antennas are neglected and (iii) the receiving antenna is isotropic and the airborne receiver characteristics are ideal. In fact, many of the scalloping results given in [2] are based on the above assumptions and hence some of the findings of the present investigation may be considered as logical extensions of those in [2] to the case of a time varying multipath source.

1.1 The Conventional VOR

1.1.1 The Radiated Signal

The conventional VOR signal generation mechanism and the method of radiation by the antenna system are described in [2] and [4]. The reference phase signal is obtained by frequency modulating at 30 Hz a 9.96 KHz subcarrier which, in turn, amplitude modulates the RF carrier signal. The reference signal is radiated in the carrier mode of operation of the antenna system having an omnidirectional pattern in azimuth. The variable phase signal is produced by space amplitude modulating the RF carrier signal with 30 Hz side-band radiated energy [2, 4]. The variable phase signal is radiated by the antenna system in

the side-band mode of operation. The side-band mode pattern of the antenna system is a figure-of-eight in azimuth which effectively rotates in azimuth at 30 revolutions per second, thereby producing the variable phase signal.

The antenna system of a conventional VOR ground station consists of four co-planar Alford loops mounted above a 52 foot diameter conducting ground plane or counter-poise located about 15 feet above ground [2, 8]. The loops are mounted at the corners of a square and are 4 feet (slightly less than a half-wavelength) above the counter-poise. In the carrier mode of operation all the four loops are driven in phase. In the side-band mode of operation each diagonal pair of loops is driven from an output of a rotating capacitive goniometer and produces a horizontal figure-of-eight pattern in space. The antenna system radiates horizontally polarized waves. Theoretical expressions for the complete patterns of conventional VOR antenna systems are given in [9].

Assuming that the phase center of the antenna is located at the origin of a spherical coordinate system, the free space radiated VOR signal at an observation point (r, θ, ϕ) may be written as [7]:

$$E^i = K \frac{e^{i(\omega t - kr)}}{r} [S_c(\theta) \{1 + m \cos (\omega_s t + m_f \sin \omega_m t)\}$$

$$+ S_s(\theta) m \{\cos \omega_m t \sin (kd \cos \phi) + \sin \omega_m t \sin (kd \sin \phi)\}], \qquad (1.1)$$

where K is a constant,

ω is the carrier frequency in radians per second,

$k = \frac{2\pi}{\lambda}$ is the propagation constant in free space,

$S_c(\theta)$ is the free space carrier mode elevation plane far field complex pattern of the VOR transmitting antenna,

$S_s(\theta)$ is the free space side-band mode elevation plane far field pattern of the VOR transmitting antenna,

$2d$ is the diagonal separation between the two loops of each pair,

$\omega_s (f_s = 9.96$ KHz) is the subcarrier frequency in radians per second,

$\omega_m (f_m = 30$ Hz) is the modulation frequency in radians per second,
m_f is the frequency modulation index,
and m is the amplitude modulation index.

Except for the pattern terms $S_c(\theta)$ and $S_s(\theta)$, (1.1) is similar to that used in [6]. As mentioned earlier, for the present analysis it is assumed that $S_c(\theta) = S_s(\theta)$ and these two factors can be included in the constant K in (1.1). From the viewpoint of obtaining the azimuth information of the observation point, it is sufficient to consider the envelope of the unmodulated carrier and side-band signal terms in (1.1). Under these assumptions the signal of interest at the input to the receiver becomes

$$E^i = K \frac{e^{i(\omega t - kr)}}{r} [1 + m \cos \omega_m t \sin (kd \cos \phi) + m \sin \omega_m t \sin (kd \sin \phi)] , \quad (1.2)$$

which can be rewritten in the form:

$$E^i = K \frac{e^{i(\omega t - kr)}}{r} [1 + \rho \cos (\omega_m t - \beta)] , \quad (1.3)$$

where $\rho^2 = m^2 \sin^2 (kd \cos \phi) + m^2 \sin^2 (kd \sin \phi)$

$$\simeq m^2 (kd)^2, \text{ if } kd << 1, \quad (1.4)$$

and $$\tan \beta = \frac{\sin (kd \sin \phi)}{\sin (kd \cos \phi)} , \quad (1.5)$$

At the receiver, the FM channel constant phase signal yields on detection a signal of frequency ω_m. The detection of the variable phase signal given by (1.3) yields a signal of frequency ω_m and phase β. Thus, the VOR receiver indicates that the bearing of the observation point is β. Note that if $kd \simeq 0$, (1.5) gives $\beta = \phi$ which implies that the azimuth is determined without any error.

1.1.2 Basic Error in VOR Indications

As shown in the previous section, the physical arrangement of the four loops in the VOR transmitting antenna introduces some basic error in the

VOR bearing indications, and we now study this in more detail. The diagonal separation between the Alford loops of each pair is such that $kd \simeq 1$ [8]. If the bearing error is defined to be $\Delta\phi = \beta - \phi$ where β is given by (1.5), it follows that

$$\tan\Delta\phi = \frac{\sum_{0}^{\infty} J_{2n+1}(kd)\ \sin\{(2n+1)\phi\}\cos\phi - \sum_{0}^{\infty}(-1)^n J_{2n+1}(kd)\ \cos\{(2n+1)\phi\}\sin\phi}{\sum_{0}^{\infty}(-1)^n J_{2n+1}(kd)\cos\{(2n+1)\phi\}\cos\phi + \sum_{0}^{\infty} J_{2n+1}(kd)\ \sin\{(2n+1)\phi\}\sin\phi} \qquad (1.6)$$

where J_n is the Bessel function of the first kind and order n. Retaining the first significant terms in the numerator and denominator of (1.6) gives

$$\tan\Delta\phi \simeq \frac{J_3(kd)\ \sin 4\phi}{J_1(kd)} \quad . \qquad (1.7)$$

If it is now assumed that $\Delta\phi$ is small, the basic error in the conventional VOR indications becomes

$$\Delta\phi \simeq \tan\Delta\phi = \frac{J_3(kd)\ \sin 4\phi}{J_1(kd)} \quad . \qquad (1.8)$$

Typically, $kd \simeq 1$, $J_1(kd) \simeq 0.440$ and $J_3(kd) \simeq 0.0196$. Hence, the peak bearing error is approximately

$$\frac{J_3(1)}{J_1(1)} \simeq 2.55^\circ \ ,$$

in agreement with observed results [3,4].

For simplicity of analysis in the later sections, it will be assumed that $kd = 0$ and the direct VOR signal of interest at the input of the receiver is then

$$E^i = K\frac{e^{i(\omega t - kr)}}{r}[1 + m\cos(\omega_s t + m_f \sin\omega_m t) + m\cos(\omega_m t - \phi)]. \qquad (1.9)$$

This form of radiated VOR signal implies that in free space and in the absence of any multipath source, the basic bearing error associated with the four loop placement in the antenna is zero.

1.1.3 Stationary Multipath Source

The scalloping in the VOR indications produced by a stationary multipath source located in the vicinity of a VOR ground station are studied in this section. A detailed theoretical discussion of the problem is given in [7], and we shall here present a simplified free space analysis which is sufficient for our purpose. Let the phase center of the VOR transmitting antenna, the stationary multipath source (or scatterer) and a stationary aircraft be located as shown in Figure 1-1. It is assumed that the aircraft, the scatterer and the VOR antenna lie in the same plane and are all within the far zones of each other. Under this condition the direct signal at the input of the airborne receiver is given by (1.9). The scattered signal at P may be written as

$$E^S = K \frac{e^{i(\omega t - kr)}}{r} \Gamma_o e^{i\delta} [1 + m \cos (\omega_s t + m_f \sin \omega_m t) + m \cos (\omega_m t - \phi_1)] , \qquad (1.10)$$

where

$\delta = kd \cos (\phi_1 - \phi)$,

Γ_o = the magnitude of the scattered carrier signal at the input of the receiver relative to that of the direct carrier signal.

Note that Γ_o is a function of the distance d_s and of the scattering properties of the object S.

The envelope of the combined direct and scattered signals at the input of the airborne receiver can be written as

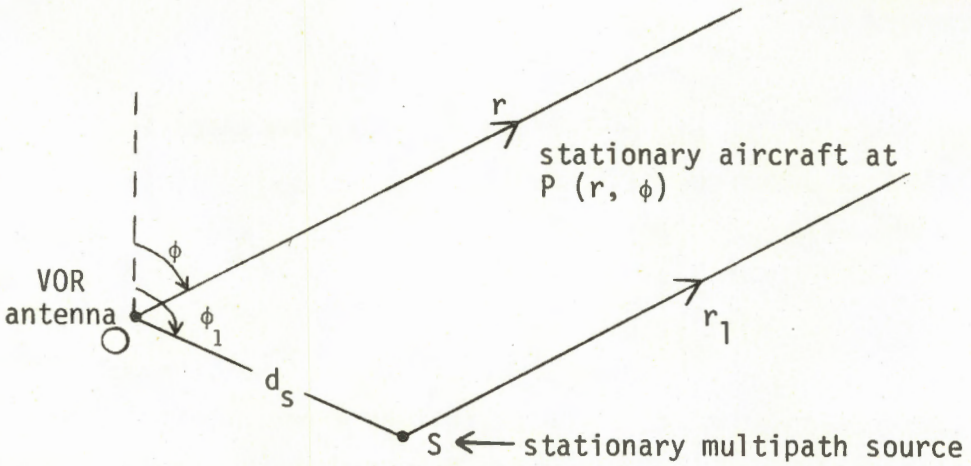

Figure 1-1: Geometry of the problem. Origin is at O.

$$f_v = 1 + m \cos(\omega_m t - \phi) + \Gamma_o \cos\delta\{1 + m \cos(\omega_m t - \phi_1)\} \quad , \tag{1.12}$$

i.e.,

$$f_v = (1 + \Gamma_o \cos\delta) + m\, m' \cos(\omega_m t - \phi + \beta), \tag{1.13}$$

where

$$|m'|^2 = 1 + \Gamma_o^2 \cos^2\delta + 2\,\Gamma_o \cos\delta \cos(\phi - \phi_1), \tag{1.14}$$

$$\tan\beta = \frac{\Gamma_o \cos\delta \sin(\phi - \phi_1)}{1 + \Gamma_o \cos\delta \cos(\phi - \phi_1)} \quad . \tag{1.15}$$

Observe that if $\Gamma_o << 1$, $m' \simeq 1$. From (1.13) it is found that the bearing indication $B = \phi - \beta$, and thus the bearing error $\Delta\phi = B - \phi$ is

$$\Delta\phi = B - \phi = -\beta = -\tan^{-1} \frac{\Gamma_o \cos\delta \sin(\phi - \phi_1)}{1 + \Gamma_o \cos\delta \cos(\phi - \phi_1)} \quad . \tag{1.16}$$

With the motion of the aircraft (in, say, an orbital flight) the parameter $\cos\delta$ will fluctuate at the RF carrier frequency between the values +1 and -1. The bearing error given by (1.16) will then fluctuate between some maximum and

minimum values. Thus the scalloping error, as obtained from (1.16), is given by

$$\Delta\phi_{\substack{1\\2}} = \mp \tan^{-1} \frac{\Gamma_o \sin(\phi - \phi_1)}{1 \pm \Gamma_o \cos(\phi - \phi_1)} , \tag{1.17}$$

where the upper and lower signs are associated with the subscripts 1 and 2 respectively. Assuming $\Gamma_o << 1$, the scalloping error due to a stationary multipath source is

$$\Delta\phi^{S}_{\substack{1\\2}} \simeq \mp \Gamma_o \sin(\phi - \phi_1) . \tag{1.18}$$

For example, if $\Gamma_o = 0.1$, the scalloping amplitude $|\Delta\phi^S|$ is approximately 5.7 degrees.

1.1.4 Time Varying Multipath Source

In this section the general effects produced by a time varying multipath source are studied. Such a scatterer will usually produce both amplitude and phase modulations of incident signals, but we shall consider the effects produced by the amplitude modulation only. With this restriction the magnitude of the scattered carrier signal relative to the direct carrier signal at the input of the receiver can be formally written as

$$\Gamma = \Gamma_o f_m(t) , \tag{1.19}$$

where Γ_o is the value of Γ for the stationary multipath source and $f_m(t)$ is the amplitude modulation function produced by the time varying scatterer. Note that in the stationary case $f_m(t) = 1$. It is assumed that the scatterer is undergoing a rotational motion, and that $f_m(t)$ can be expanded in the Fourier series

$$f_m(t) = \sum_{n=0}^{\infty} A_n \cos(\omega_n t - \alpha_n) , \tag{1.20}$$

where

ω_n's are harmonically related to the rotational frequency of the scatterer,

A_n is the amplitude of the component of angular frequency ω_n,

and α_n is the phase of each frequency component.

Without loss of generality it will be assumed that $\alpha_o \equiv 0$, which implies that the DC component ($\omega_o = 0$) of Γ is $\Gamma_o A_o$. With this notation, for the stationary multipath source $A_o = 1$ and $A_n = 0$ for $n \neq 0$, so that $\Gamma = \Gamma_o$.

In the present case the envelope of the combined signals at the input of the receiver can be written as

$$f_v = 1 + m \cos(\omega_m t - \phi) + \Gamma_o \cos\delta \sum_o^\infty A_n \cos(\omega_n t - \alpha_n)\{1 + m \cos(\omega_m t - \phi_1)\}, \tag{1.22}$$

where δ is as defined by (1.11). The VOR receiver obtains the azimuth information from the components of frequency ω_m. Thus, retaining only the ω_m components,

$$\begin{aligned} f_v = 1 &+ m \cos(\omega_m t - \phi) + \Gamma_o A_o m \cos\delta \cos(\omega_m t - \phi_1) \\ &+ \Gamma_o A_m m \cos\delta \cos(\omega_m t - \alpha_m) \\ &+ \Gamma_o \frac{A_{2m}}{2} m \cos\delta \cos(\omega_m t - \alpha_{2m} + \phi_1). \end{aligned} \tag{1.23}$$

As before, we rewrite this in the form

$$f_v = 1 + \rho \cos(\omega_m t - \phi + \beta), \tag{1.24}$$

where

$$\begin{aligned} \rho \cos\beta = m &+ \Gamma_o A_o m \cos\delta \cos(\phi - \phi_1) + \Gamma_o A_m \cos\delta \cos(\phi - \alpha_m) \\ &+ \Gamma_o \frac{A_{2m}}{2} m \cos\delta \cos(\phi - \alpha_{2m} + \phi_1), \end{aligned} \tag{1.25}$$

$$\rho \sin \beta = \Gamma_o A_o m \cos \delta \sin (\phi - \phi_1) + \Gamma_o A_m \cos \delta \sin (\phi - \alpha_m)$$

$$+ \Gamma_o \frac{A_{2m}}{2} m \cos \delta \sin (\phi - \alpha_{2m} + \phi_1) , \tag{1.26}$$

giving

$$\tan \beta = \frac{\Gamma_o A_o m \cos\delta\sin(\phi-\phi_1)+\Gamma_o A_m \cos\delta\sin(\phi-\alpha_m)+\Gamma_o \frac{A_{2m}}{2} m \cos\delta\sin(\phi-\alpha_{2m}+\phi_1)}{m+\Gamma_o A_o m \cos\delta\cos(\phi-\phi_1)+\Gamma_o A_m \cos\delta\cos(\phi-\alpha_m)+\Gamma_o \frac{A_{2m}}{2} m \cos\delta\cos(\phi-\alpha_{2m}+\phi_1)} . \tag{1.27}$$

The scalloping error can now be obtained from (1.27) as

$$\Delta\phi_{\frac{1}{2}} = \mp \tan^{-1} \frac{\Gamma_o A_o m \sin(\phi-\phi_1)+\Gamma_o A_m \sin(\phi-\alpha_m)+\Gamma_o \frac{A_{2m}}{2} m \sin(\phi-\alpha_{2m}+\phi_1)}{m \mp \Gamma_o A_o m \cos(\phi-\phi_1) \mp \Gamma_o A_m \cos(\phi-\alpha_m) \mp \Gamma_o \frac{A_{2m}}{2} m \cos(\phi-\alpha_{2m}+\phi_1)} . \tag{1.28}$$

Note that for a static scatterer $f_m(t) = 1$, implying $A_o = 1$ and $A_m = A_{2m} = 0$. Under these conditions (1.28) reduces to the expression (1.17) for the scalloping error in the stationary case.

If it is assumed that $\Gamma_o A_n << m$, (1.28) can be written in the more convenient form

$$\Delta\phi_{\frac{1}{2}} \simeq \mp \Gamma_o \left[A_o \sin (\phi - \phi_1) + \frac{A_m}{m} \sin (\phi - \alpha_m) + \frac{A_{2m}}{2} \sin (\phi - \alpha_{2m} + \phi_1)\right]. \tag{1.29}$$

This shows that the total scalloping is the sum of the scallopings due to the DC, ω_m and $2\omega_m$ components of the amplitude modulated signals introduced by the time varying scatterer. Normally the modulation index m is approximately 0.3. Thus, in an ideal situation, with equiamplitude frequencies in the modulation function, the ω_m component produces about 3.3 times more scalloping than the others. To obtain a quantitative estimate of the scalloping produced by a time varying scatterer, the amplitudes of the different modulation frequency components produced by the scatterer must be found, and this is done in the next section for a windmill.

1.1.5 Error Caused By A Windmill

The amplitude modulation of an incident electromagnetic wave produced by the rotating blades of a windmill was investigated in [10], and we shall now use some of the results to study the windmill interference effects on VOR indications

An analysis of the amplitude modulation of an incident signal by a windmill is a difficult electromagnetic boundary value problem, and to simplify the task the windmill blades will be replaced by a rectangular metal plate of equivalent area. The locations of the phase center of the VOR transmitting antenna, the aircraft and the simulated windmill blade (NN) at a particular instant of time are shown in Figure 1-2. It is assumed that the metal plate of length L and width W representing the windmill blades, is rotating around its center S at an angular frequency Ω_s in a plane normal to the plane of the paper and passing through NN in Figure 1-2. As depicted in Figure 1-2, a ray originating from the VOR antenna is specularly reflected to the aircraft. The VOR antenna, the scatterer L and the aircraft are assumed to be in the far zones of each other. Under these conditions, the magnitude of the scattered VOR carrier signal relative to the direct signal at the input to the airborne receiver is

$$\Gamma = \Gamma_o f_m(t), \tag{1.30}$$

where

$$f_m(t) = \frac{\sin[a \sin \Omega_s t]}{[a \sin \Omega_s t]} \tag{1.31}$$

with

$$a = \frac{kL}{2} \sin \phi. \tag{1.32}$$

Γ_o is the maximum value of Γ for the static case. In the present instance Γ_o may be approximated as

$$\Gamma_o = \frac{A_e}{\lambda d_s} f(\phi_1, \phi), \tag{1.33}$$

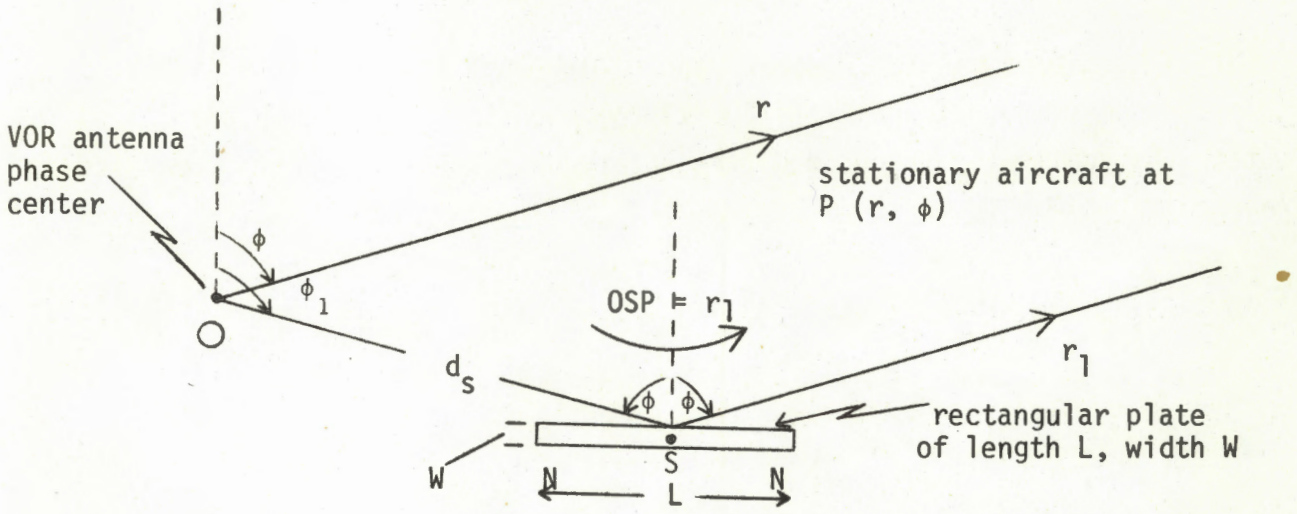

Figure 1-2: Orientation of VOR, aircraft and the windmill blades.

where A_e is the effective scattering area of the metal plate, $f(\phi_1,\phi) \leq 1$ is a normalized function describing the directional scattering characteristics of the linear element and d_s is the distance between the VOR antenna and the plate.

For large values of a and small values of Ω_s it can be shown [10] that the spectral components of $f_m(t)$ are given by

$$f_m(t) = \left[\frac{1}{a} + \frac{2}{a} \sum_{n=1}^{n\simeq a} \cos\ (n\ \omega_1 t)\right] \tag{1.34}$$

where $\omega_1 = 2\ \Omega_s$. (1.35)

Equation (1.34) should be compared with (1.20) which gives the general Fourier series expansion of the modulation function. Equation (1.34) indicates that the modulation contains even harmonics of Ω_s of constant amplitude, and that the spectrum extends up to $2n\ \Omega_s \simeq a$. Hence, depending on the value of a, the spectrum may extend up to a frequency many times larger than the rotation frequency Ω_s.

Let us assume that $a(= \frac{kL}{2} \sin\phi)$ and Ω_s are such that $f_m(t)$ in (1.34) contains both $\omega_m(= 30$ Hz) and $2\omega_m(= 60$ Hz) components. We can then use (1.29) to obtain the scalloping produced by the rotating scatterer. For this purpose we rewrite (1.29) as follows:

$$\Delta\phi_{\frac{1}{2}} \simeq \mp \Gamma_o \left[A_o \sin(\phi - \phi_1) + \frac{A_m}{m} \sin\phi + \frac{A_{2m}}{2} \sin(\phi + \phi_1) \right], \tag{1.36}$$

where

$$\left.\begin{aligned} A_o &= \frac{1}{a} \\ A_m &= A_{2m} = \frac{2}{a} \\ \alpha_o &= \alpha_m = \alpha_{2m} = 0 \end{aligned}\right\}. \tag{1.37}$$

Note that the existence of 30 Hz and 60 Hz components in $f_m(t)$ depends critically on the parameters a and Ω_s. For a given situation the existence of these components may be examined using the following relations:

$$\left.\begin{aligned} &\text{for } a \geq \frac{30}{f_s}, \quad A_m = A_{2m} = \frac{2}{a} \\ &\text{for } \frac{15}{f_s} \leq a \leq \frac{30}{f_s}, \quad A_m = \frac{2}{a}, \quad A_{2m} = 0 \\ &\text{for } a < \frac{15}{f_s}, \quad A_m = A_{2m} = 0 \end{aligned}\right\}, \tag{1.38}$$

where f_s is the rotation frequency of the scatterer.

The expansion of the modulation function in the Fourier series (1.34) is based on the assumption of large a $(= \frac{L}{\lambda})$ and small rotation frequency Ω_s. For intermediate values of a and Ω_s, a more rigorous expansion of the expression for $f_m(t)$ given in (1.31) should be used [10], but for the purposes of the present study it is sufficient to use the simpler (approximate) formulas given in this section.

1.1.6 Some Sample Calculations

It may be helpful to give some sample calculations to illustrate the possible scalloping errors produced by a windmill in the vicinity of a VOR ground station.

Example 1

This is an ideal case. We arbitrarily assume that a = 30 and f_s = 1 Hz, and under these conditions the windmill will introduce both 30 and 60 Hz modulation components to the scattered VOR signal (see 1.37). Let $|\Delta\phi^o|$, $|\Delta\phi^m|$ and $|\Delta\phi^{2m}|$ represent the scalloping amplitudes due to the DC, 30 Hz and 60 Hz components respectively of the modulation, and let Γ_o = 0.1, m = 0.3.

From (1.37) we obtain

$$A_o = 0.033, \quad A_m = A_{2m} = 0.067.$$

The resulting scalloping amplitudes are then

$$|\Delta\phi^o| = \Gamma_o A_o = 0.19 \text{ degrees},$$

$$|\Delta\phi^m| = \frac{\Gamma_o A_m}{m} = 1.26 \text{ degrees},$$

$$|\Delta\phi^{2m}| = \frac{\Gamma_o A_{2m}}{m} = 0.19 \text{ degrees},$$

and the maximum total scalloping is

$$|\Delta\phi^T| = 1.64 \text{ degrees}.$$

For the static case, i.e., when the scatterer is stationary, the maximum scalloping obtained from (1.18) is

$$|\Delta\phi^s| = \Gamma_o = 5.73 \text{ degrees}.$$

This example clearly indicates the dominance of the scalloping produced by the static scatterer.

Example 2

Consider the case of the NASA windmill at Plum Brook for which $L \simeq 18$ m. At the VOR carrier frequency $f = 115$ MHz ($\lambda = 2.61$ meters), $\frac{L}{\lambda} = 6.90$. For $\phi = 60°$, $a = \frac{kL}{2} \sin \phi = 18.96$. Although the typical rotation frequency of the windmill is 0.5 Hz we shall consider separately the two cases $f_s = 0.5$ Hz and $f_s = 1$ Hz. Assume $\Gamma_o = 0.1$.

Results for $f_s = \frac{1}{2}$ Hz:

$A_o = 0.053 \quad A_m = A_{2m} = 0$

$|\Delta\phi^o| = 0.30$ degrees.

Results for $f_s = 1$ Hz:

$A_o = 0.053 \quad A_m = 0.106 \quad A_{2m} = 0$

$|\Delta\phi^o| = 0.30$ degrees,

$|\Delta\phi^m| = 2.02$ degrees for $m = 0.3$.

Total scalloping = 2.32 degrees.

With $\Gamma = 0.1$, the maximum scalloping in the static case is $|\Delta\phi^s| = 5.7$ degrees. Here again we find the predominance of scalloping produced by the stationary windmill.

In the above we have assumed that $\Gamma_o = 0.1$. It is instructive to estimate the distance of the windmill from the VOR transmitting antenna for which $\Gamma_o = 0.1$. This can be obtained from (1.32). Assume that $f(\phi_1, \phi) = 1$, and

let the equivalent scattering area $A_e = 12\ m^2$. From (1.33) it is now found that for $\Gamma = 0.1$, the windmill to VOR antenna distance d is approximately 46 m. This is well within the FAA requirement that a region of about 500 m radius about a VOR station be cleared of any source of scattering.

In the vicinity of a VOR station the FAA also precludes the existence of any tall scattering object (like a water tower) which makes an angle of more than 2 degrees at the phase center of the VOR antenna. Assuming the windmill height to be 30 m, this would require the windmill to be located at least 1.4 km away. At this distance the static windmill blades would produce a maximum scalloping of about 0.17 degrees ($\Gamma_o \simeq 0.003$).

It is also of interest to estimate the interference produced by a windmill located at a distance of 6 miles (10 km) from a VOR station. Assuming the VOR carrier frequency to be 115 MHz, and the effective scattering area of the blade $A_e = 12\ m^2$, it is found that $\Gamma_o = 0.0005$. In the static case this would produce a maximum scalloping $|\Delta\phi^s| \simeq 0.03$. The rotating blades would produce scalloping much less than 0.03 and hence is not calculated here.

1.2 The Doppler VOR

1.2.1 The Radiating System

The DVOR signal generation mechanism and its radiation by the ground station are described in [5], and for present purposes it is sufficient to list only the key features of the ground station. The carrier frequency with 30 Hz AM reference signal is radiated by a central carrier antenna. Another RF signal spaced 9.96 KHz above the reference carrier is radiated by an antenna revolving at 30 Hz in a circle around the carrier antenna. Actually this circular motion of the antenna is simulated by a sequential feeding of radiators arranged uniformly along a circle. The resulting Doppler effect introduces a 30 Hz sinusoidal frequency modulation of the second RF signal; the phase of this FM signal contains the aximuth information [5]. This mode of operation of the DVOR system corresponds to single side band (SSB) modulation. The SSB method

has serious disadvantages due to the amplitude modulation introduced by the sequential switching of the antennas. This is avoided by using double side band (DSB) modulation where the two side band frequency signals, spaced 9.96 KHz above and below the RF carrier, are fed sequentially to two radiators located diametrically opposite on the circular arrangement of the antennas [11].

The individual antennas used are standard Alford loops [3] having circular patterns in the plane of the loops. The central carrier antenna system consists of the standard 4-loop array [3]. Fifty more Alford loops are arranged uniformly along a circle 22 feet in radius around the central antenna. The entire antenna system is mounted above a 150 foot diameter counterpoise located 10 feet above ground. More details of the antenna system, the signal generation and the switching mechanisms may be found in [5].

1.2.2 DVOR Radiated Signal

To obtain the radiated signal at a distant aircraft an idealized model of the DVOR ground antenna system is assumed. Figure 1-3 shows the horizontal plane geometry of the DVOR antenna system and a distant stationary aircraft. The antenna system consists of a point source C radiating the reference signal and a second point source S located at a distance d from C and rotating anti-clockwise around C at an angular frequency ω_m ($\omega_m/2\pi$ = 30 Hz). The rotating point source antenna S effectively radiates the variable phase signal. The origin of coordinates is at C and all angles are measured from the y-axis as shown in Figure 1-3. Note that the antenna model used is that appropriate for SSB operation which is sufficient for the present investigation.

For an assumed time dependence $e^{i\omega t}$, the signal received at P is

$$E'(P) = K\,(1 + m\cos\omega_m t)\,\frac{e^{i(\omega t - kr)}}{r} + n\,\frac{e^{i(\omega_1 t - k_1 r')}}{r'}, \qquad (1.39)$$

where K is a constant,

ω is the angular frequency of the reference signal carrier,

$k = \omega/c$ is the propagation constant corresponding to ω,

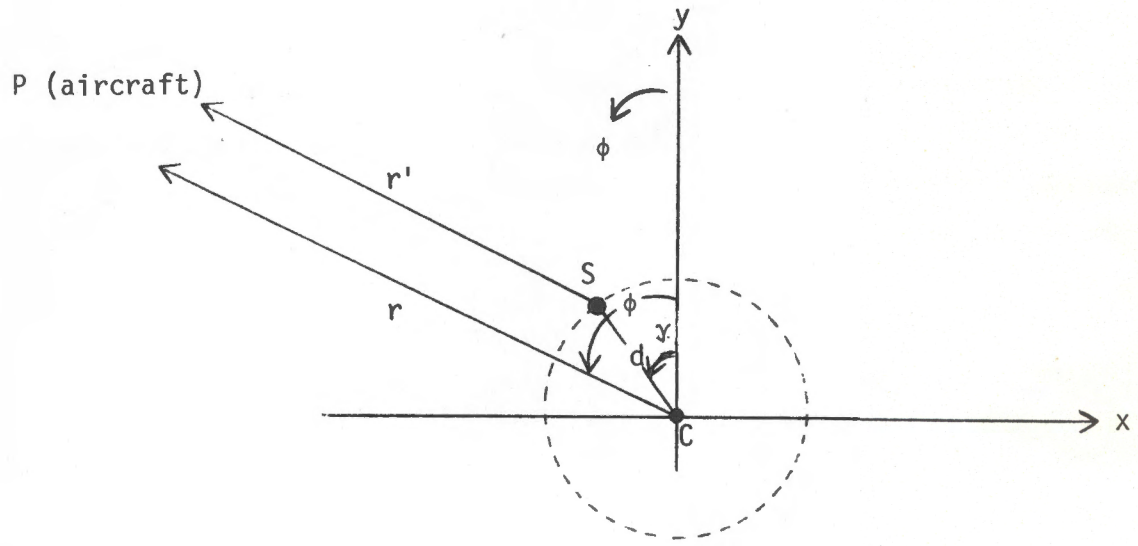

Figure 1-3: Idealized DVOR transmitting antenna and the coordinate system used.

m is the amplitude modulation index,

ω_m is the angular frequency of AM signal,

n is the level of the side-band signal relative to the reference carrier (normally $m = n = 0.3$),

ω_1 is the angular frequency of the side-band carrier; usually $\omega_1 = \omega + \Delta\omega$ and $\Delta\omega/2\pi = 9.96$ KHz,

and $k_1 = \omega_1/c$ is the propagation constant corresponding to ω_1.

Since P is in the far field we can make the approximation

$$r' \simeq r - d\cos(\phi - \gamma) = r - d\cos(\omega_m t - \phi) \tag{1.40}$$

in the exponent of the second term in (1.39) and take $r' = r_o$ in the denominator. Using (1.40), (1.39) yields the following real expression for the signal at P:

$$E(P) \simeq K\{(1 + m\cos\omega_m t)\frac{\cos(\omega t - kr)}{r} + \frac{n}{r}\cos[\omega_1 t - k_1 r + k_1 d\cos(\omega_m t - \phi)]\}, \tag{1.41}$$

in which the first term represents the reference signal and the second the variable phase signal. The first detector of the aircraft receiver envelope detects the signal represented by (1.41). Assuming $\omega_1 = \omega + \Delta\omega$ and $kr \simeq k_1 r$, this can be written as

$$E(P) = K \left[\{1 + m \cos \omega_m t + n \cos [\Delta\phi t + k_1 d \cos (\omega_m t - \phi)]\}^2 + n^2 \sin^2\{\Delta\omega t + k_1 d \cos (\omega_m t - \phi)\}\right]^{1/2} \frac{\cos (\omega t - kr - \psi)}{r} \qquad (1.42)$$

where

$$\tan \psi = \frac{- n \sin\{\Delta\phi t + k_1 d \cos (\omega_m t - \phi)\}}{1 + m \cos \omega_m t + n \cos\{\Delta\omega t + k_1 d \cos (\omega_m t - \phi)\}} . \qquad (1.43)$$

and by retaining only terms up to the first order in m and n in the amplitude of (1.42), we obtain the following simplified expression:

$$E(P) \simeq K \left[1 + m \cos \omega_m t + n \cos\{\Delta\phi t + k_1 d \cos (\omega_m t - \phi)\}\right] \cdot \frac{\cos (\omega t - kr - \psi)}{r} . \qquad (1.44)$$

It is easy to see now that envelope detection of the signal represented by (1.44) yields an undistorted reference modulation signal of frequency ω_m and an undistorted frequency modulated subcarrier signal containing the azimuth information ϕ. On second detection the latter will yield the variable phase signal of frequency ω_m and phase ϕ, so that in the absence of any multipath source the DVOR receiver will read the correct azimuth ϕ. It should be noted that the approximations involved in deriving the expressions (1.41) and (1.44) for the radiated signals and the assumption of ideal receiving characteristics imply that the DVOR has no zero-shift and run-out or spread errors [11].

1.2.3 Effects Of A Time Varying Multipath Source

The scalloping errors in the DVOR indications caused by a time varying multipath source located in the vicinity of a DVOR ground station are now

investigated. Let the phase center of the DVOR transmitting antenna system, the multipath source S and a stationary aircraft P be located as shown in Figure 1-1. The origin of the coordinate system is at O and the path lengths of the direct and multipath rays reaching P are as shown in Figure 1-1. The direct signal at the aircraft is then given by (1.41) and the scattered signal at P can be written as

$$E^S(P) \sim K\Gamma \left[(1 + m \cos \omega_m t) \frac{\cos (\omega t - kr_1 - \delta)}{r_1} \right.$$

$$\left. + n \frac{\cos \{\omega_1 t + k_1 d \cos (\omega_m t - \phi_1) - k_1 r_1 - \delta\}}{r_1} \right] , \qquad (1.45)$$

where Γ may be identified with the magnitude of the scattered signal at P relative to that of the direct signal, and δ is the RF phase change caused by the multipath source. Note that, in general, both Γ and δ depend on the scattering properties of the multipath source and its distance from the ground station. The total field at P is the sum of the direct and scattered fields given by (1.41) and (1.45), and by assuming $r_1 \simeq r$ in the denominators of the terms in (1.45) we obtain the following expression for the total field:

$$E^T(P) = E(P) + E^S(P)$$

$$\simeq \frac{K}{r} (1 + m \cos \omega_m t)\{\cos (\omega t - kr) + \Gamma \cos (\omega t - kr_1 - \delta)\}$$

$$+ n \cos\{\omega_1 t + k_1 d \cos (\omega_m t - \phi) - k_1 r\}$$

$$+ \Gamma n \cos\{\omega_1 t + k_1 d \cos (\omega_m t - \phi_1) - k_1 r_1 - \delta\} . \qquad (1.46)$$

To determine the azimuth information it is necessary to consider the instantaneous phase of the total variable phase signal. For this purpose it is sufficient to consider the phase of the following function:

$$f(t) = \cos\{\omega_1 t + k_1 d \cos(\omega_m t - \phi_1) - k_1 r\}$$

$$+ \Gamma\cos\{\omega_1 t + k_1 d \cos(\omega_m t - \phi_1) - k_1 r_1 - \delta)\} \quad . \tag{1.47}$$

Assuming $\Gamma << 1$, the instantaneous phase $\phi_p(t)$ of $f(t)$ may be written as

$$\phi_p(t) = k_1 d \cos(\omega_m t - \phi) - k_1 r$$

$$+ \Gamma\sin[k_1 d \cos(\omega_m t - \phi_1) - k_1 d \cos(\omega_m t - \phi) + k_1 (r - r_1) - \delta] \, , \tag{1.48}$$

which it is convenient to rewrite in the form

$$\Phi_p(t) = k_1 d \cos(\omega_m t - \phi) - k_1 r + \Gamma\sin\{\rho\sin\alpha(t)\}\cos\xi$$

$$+ \Gamma\cos\{\rho\sin\alpha(t)\}\sin\xi \, , \tag{1.49}$$

where

$$\left.\begin{aligned} \rho &= 2k_1 d \sin\left(\frac{\phi_1 - \phi}{2}\right) \\ \alpha(t) &= \omega_m t - \frac{\phi + \phi_1}{2} \\ \xi &= k_1 (r - r_1) - \delta \end{aligned}\right\} \quad . \tag{1.50}$$

After using the well-known expansions of $\sin(\rho\sin\theta)$ and $\cos(\rho\sin\theta)$ in the last two terms of (1.49) the final expression for the instantaneous phase of the variable phase signal is

$$\Phi_p(t) = k_1 d \cos(\omega_m t - \phi) - k_1 r + 2\Gamma\cos\xi$$

$$\times \sum_{n=0}^{\infty} J_{2n+1}(\rho) \sin\left\{(2n + 1)\left(\omega_m t - \frac{\phi + \phi_1}{2}\right)\right\}$$

$$+ \Gamma\sin\xi \left[J_0(\rho) + 2 \sum_{n=1}^{\infty} J_{2n}(\rho) \cos\left\{2n\left(\omega_m t - \frac{\phi + \phi_1}{2}\right)\right\}\right] \, , \tag{1.51}$$

where J_n is the Bessel function of the first kind of order n.

A time varying multipath source will produce both amplitude and phase modulations of incident signals, but we shall again consider only the effect produced by the amplitude modulation. With this restriction the magnitude of the scattered carrier signal relative to the direct carrier signal at the input of the airborne receiver is given by (1.19) and (1.20). Introducing these into (1.51) and retaining the terms in $\omega_m t$ we find

$$\begin{aligned}\Phi_p(t) = {} & k_1 d \cos(\omega_m t - \phi) - \beta_1 r_o + 2\Gamma_o \cos\xi \left[A_o J_1(\rho) \sin\left(\omega_m t - \frac{\phi + \phi_1}{2}\right) \right. \\ & - \frac{A_{2m}}{2} J_1(\rho) \sin\left(\omega_m t + \frac{\phi_1 + \phi}{2} - \alpha_{2m}\right) \\ & \left. + \frac{A_{2m}}{2} J_3(\rho) \sin\omega_m t - \frac{3}{2}(\phi + \phi_1) + \alpha_{2m} \right] \\ & + \Gamma_o \sin\xi\, A_m J_o(\rho) \cos(\omega_m t - \alpha_m) \\ & + \Gamma_o \sin\xi\, A_m J_2(\rho) \cos\{\omega_m t - (\phi + \phi_1) + \alpha_m\} \quad . \end{aligned} \tag{1.52}$$

The discriminator output current of the ideal receiver is proportional to the time derivative of $\Phi_p(t)$ given by (1.52), and is therefore

$$\begin{aligned} i_p(t) \simeq {} & \frac{d\Phi_p(t)}{dt} \\ = {} & k_1 d\, \omega_m \sin(\omega_m t - \phi) + 2\Gamma_o \omega_m \cos\xi \left[A_o J_1(\rho) \cos\left(\omega_m t - \frac{\phi + \phi_1}{2}\right) \right. \\ & - \frac{A_{2m}}{2} J_1(\rho) \cos\left(\omega_m t + \frac{\phi_1 + \phi}{2} - \alpha_{2m}\right) \\ & \left. + \frac{A_{2m}}{2} J_3(\rho) \cos\{\omega_m t - \frac{3}{2}(\phi + \phi_1) + \alpha_{2m}\} \right] \\ & - \Gamma_o \omega_m \sin\xi\, A_m J_o(\rho) \sin(\omega_m t - \alpha_m) \\ & - \Gamma_o \omega_m \sin\xi\, A_m J_2(\rho) \sin\{\omega_m t - (\phi + \phi_1) + \alpha_m\} \quad . \end{aligned} \tag{1.53}$$

The DVOR bearing indication is given by the phase of $i_p(t)$, and to obtain this we write (1.53) as

$$i_p = - B \sin (\omega_m t - \phi) + \sum_i C_i \cos (\omega_m t - \Phi_i)$$

$$- \sum_j D_j \sin (\omega_m t - \Phi'_j) , \qquad (1.54)$$

where the quantities B, C_i, Φ_i, D_j and Φ'_j may be obtained by identifying each term in (1.54) with the corresponding term in (1.53). Equation (1.54) can be written as

$$i_p = - \eta \sin (\omega_m t - \phi - \alpha) , \qquad (1.55)$$

where $$\eta \cos\alpha = B + \sum_i C_i \sin (\phi - \phi_i) + \sum_j D_j \cos (\phi - \phi'_j) , \qquad (1.56)$$

$$\eta \sin\alpha = \sum_i C_i \cos (\phi - \phi_i) - \sum_j D_j \sin (\phi - \phi'_j) . \qquad (1.57)$$

From (1.56) and (1.57) it follows that

$$\tan\alpha = \frac{\sum_i C_i \cos (\phi - \phi_i) - \sum_j D_j \sin (\phi - \phi'_j)}{B + \sum_i C_i \sin (\phi - \phi_i) + \sum_j D_j \cos (\phi - \phi'_j)} . \qquad (1.58)$$

The bearing or the azimuth of the aircraft as indicated by (1.55) is $\phi + \alpha$. The true bearing of the aircraft being ϕ, the bearing error in the DVOR indication caused by the multipath source is

$$\Delta\Phi = \alpha \qquad (1.59)$$

where α is given by (1.58). In terms of the original variables involved in (1.53) the final expression for the bearing error is therefore

$$\Delta\Phi = \tan^{-1} \frac{M}{N} , \qquad (1.60)$$

with

$$M = 2\Gamma_o \cos\xi\{A_o J_1(\rho) \cos\left(\frac{\phi - \phi_1}{2}\right) - \frac{A_{2m}}{2} J_1(\rho) \cos\left(\phi + \frac{\phi + \phi_1}{2} - \alpha_{2m}\right)$$

$$+ \frac{A_{2m}}{2} J_3(\rho) \cos\left(\phi_1 + \frac{\phi + \phi_1}{2} - \alpha_{2m}\right)\}$$

$$+ \Gamma_o A_m \sin\xi\{J_2(\rho) \sin(\phi_1 - \alpha_m) - J_o(\rho) \sin(\phi - \alpha_m) \qquad (1.61)$$

$$N = k_1 d + 2\Gamma_o \cos\xi\{A_o J_1(\rho) \sin\left(\frac{\phi - \phi_1}{2}\right) - \frac{A_{2m}}{2} J_1(\rho) \sin\left(\phi + \frac{\phi + \phi_1}{2} - \alpha_{2m}\right)$$

$$- \frac{A_{2m}}{2} J_3(\rho) \sin\left(\phi_1 + \frac{\phi + \phi_1}{2} - \alpha_{2m}\right)\}$$

$$- \Gamma_o A_m \sin\xi\{J_2(\rho) \cos(\phi_1 - \alpha_m) + J_o(\rho) \cos(\phi - \alpha_m)\} . \qquad (1.62)$$

Equations (1.60) - (1.62) give the most general expression for the bearing error in DVOR indications caused by a time varying multipath source. Under normal conditions $k_1 d$ is very large compared to the other terms in the expression for N given by (1.62). We can therefore make the approximation $N \simeq k_1 d$ in (1.62) to obtain the following simplified expression for $\Delta\Phi$:

$$\Delta\Phi \simeq \tan^{-1} \frac{M}{k_1 d} , \qquad (1.63)$$

where M is given by (1.61).

With the motion of the aircraft the terms $\cos\xi$ and $\sin\xi$ in the expression for M fluctuate at the RF carrier frequency between the values +1 and -1. The bearing error given by (1.63) will then fluctuate between some maximum and minimum values around the true value Φ, producing scalloping errors. In the present case the following two distinct scalloping errors are found.

(i) Type 1: this occurs when $\cos\xi = \pm 1$ and $\sin\xi = 0$. The scalloping errors are:

$$\Delta\Phi_{\substack{S_1 \\ 2}} = \pm \tan^{-1}\left[\frac{2\Gamma_o}{k_1 d}\left\{A_o J_1(\rho)\cos\left(\frac{\phi+\phi_1}{2}\right) - \frac{A_{2m}}{2}J_1(\rho)\cos\left(\phi+\frac{\phi+\phi_1}{2}-\alpha_{2m}\right)\right.\right.$$
$$\left.\left.+\frac{A_{2m}}{2}J_3(\rho)\cos\left(\phi_1+\frac{\phi+\phi_1}{2}-\alpha_{2m}\right)\right\}\right], \qquad (1.64)$$

where $\rho = 2k_1 d \sin\left(\frac{\phi_1-\phi}{2}\right)$ (1.65)

and the subscripts 1, 2 on the left hand side correspond to the + and - signs on the right hand side.

(ii) Type 2: this occurs when $\sin\xi = \pm 1$ and $\cos\xi = 0$. The scalloping error are:

$$\Delta\Phi_{\substack{S \\ 2}} = \pm \tan^{-1}\left[\frac{\Gamma_o A_m}{k_1 d}\left\{J_2(\rho)\sin(\phi_1-\alpha_m) - J_o(\rho)\sin(\phi-\alpha_m)\right\}\right]. \qquad (1.66)$$

Note that if the multipath source is static, $A_o = 1$ and $A_m = A_{2m} = 0$. Under these conditions the expressions for the scalloping errors reduce to

$$\Delta\Phi_{\substack{S_1 \\ 2}} = \pm \tan^{-1}\left[\frac{2\Gamma_o}{k_1 d}J_1(\rho)\cos\left(\frac{\phi-\phi_1}{2}\right)\right], \qquad (1.67)$$

which are the same as given in [3].

Usually $\Gamma_o << 1$, $k_1 d >> 1$ and $A_m << 1$ for all m. Under these conditions (1.64) and (1.66) may be further simplified by using the approximation $\tan^{-1} x \simeq x$ for $x << 1$. The final expressions for the scalloping errors caused by a time varying multipath source are then

$$\Delta\Phi_{\substack{S_1 \\ 2}} = \pm \frac{2\Gamma_o}{k_1 d}\left[A_o J_1(\rho)\cos\left(\frac{\phi-\phi_1}{2}\right) - \frac{A_{2m}}{2}J_1(\rho)\cos\left(\phi+\frac{\phi+\phi_1}{2}-\alpha_{2m}\right)\right.$$
$$\left.+\frac{A_{2m}}{2}J_3(\rho)\cos\left(\phi_1+\frac{\phi+\phi_1}{2}-\alpha_{2m}\right)\right]. \qquad (1.68)$$

$$\Delta\Phi_{\frac{1}{2}}^{S_1} = \pm \frac{\Gamma_o A_m}{k_1 d} \left[J_2(\rho) \sin(\phi_1 - \alpha_m) - J_o(\rho) \sin(\phi - \alpha_m) \right] . \qquad (1.69)$$

As indicated by (1.68), the total type 1 scalloping is given by the scallopings produced by the DC, ω_m and $2\omega_m$ components of the amplitude modulation of signals caused by the time varying scattering source. Equation (1.69) indicates that the total type 2 scalloping is contributed by the ω_m component of the modulation function, on the assumption that contributions due to larger harmonics of ω_m are negligible. To estimate quantitatively the scalloping produced by a time varying scatterer, the appropriate Fourier coefficients A_m, α_m for the modulation function of the scatterer must be known. These are obtained for a windmill in a manner discussed in Section 1.1.5.

1.2.4 Some Sample Calculations

Some sample calculations to illustrate the possible scalloping errors produced by a windmill in the vicinity of a DVOR ground station will now be given.

Example 1

This is an ideal case. We rather arbitrarily assume that a $(= \frac{kL}{2} \sin\phi) = 30$ and $f_s = 1$. Under this condition the windmill will introduce both 30 Hz and 60 Hz modulation components to the scattered DVOR signal. Let $\Gamma_o = 0.1$ and $k_1 d = 16$ (typical value at 155 MHz). From (1.37) we then obtain

$$A_o = 0.033$$
$$A_m = A_{2m} = 0.067$$
$$\alpha_o = \alpha_m = \alpha_{2m} \equiv 0$$

Type 1 Scalloping

Let $|\Delta\Phi^o|$, $|\Delta\Phi^{2m}|$ represent the scalloping amplitudes due to the DC and 60 Hz components. From (1.68) the resultant scalloping amplitudes are as follows.

$$|\Delta\Phi^{o}| = \frac{2\Gamma_o}{k_1 d} A_o J_1(\rho)_{max} , \qquad (1.70)$$

where $J_1(\rho)_{max}$ is the maximum value of $J_1(\rho)$

$$|\Delta\Phi^{2m}| = \frac{\Gamma_o A_{2m}}{k_1 d} \left[J_1(\rho)_{max} + J_3(\rho)|_{max} \right] . \qquad (1.71)$$

Thus

$$|\Delta\Phi^{o}| = \frac{2 \times 0.1 \times 0.033 \times 0.5819}{16} = 0.014 \text{ degrees},$$

$$|\Delta\Phi^{2m}| = \frac{0.1 \times 0.067}{16} [0.5819 + 0.4344] = 0.024 \text{ degrees},$$

and the maximum total scalloping is

$$|\Delta\Phi^{S_1}|_{max} = |\Delta\Phi^{o}| + |\Delta\Phi^{2m}| = 0.038 \text{ degrees}.$$

Type 2 Scalloping

From (1.69) it can be shown that the maximum value of the type 2 scalloping error is

$$|\Delta\Phi^{S_2}|_{max} \lesssim \frac{\Gamma_o A_m}{k_1 \phi} (J_2(\rho)|_{max} + J_o(\rho)|_{max})$$

$$= \frac{0.1 \times 0.067}{16} (0.4862 + 1.0000)$$

$$= 0.036 \text{ degrees}.$$

For the static case, maximum scalloping is:

$$\Delta\Phi^{S}_{max} = \frac{2\Gamma_o}{k_1 d} J_1(\rho)|_{max} = \frac{2 \times 0.1 \times 0.5819}{16} = 0.417 \text{ degrees}.$$

Thus, the scalloping produced by the rotating plate is about 1/10th of that due to the static plate. This clearly indicates the dominance of the scalloping produced by the static scatter as found also in the case of the conventional VOR.

Example 2

Consider the case of the NASA windmill at Plum Brook for which $L \simeq 18$ m. At the DVOR carrier frequency $f = 115$ MHz ($\lambda = 2.61$ m), $L/\lambda \simeq 6.90$. For $\phi = 60$ degrees, $a = kL/2 \sin\phi = 18.86$. Although the typical rotation frequency of the windmill is 0.5 Hz we shall consider separately the two cases $f_s = 0.5$ Hz and $f_s = 1$ Hz, and assume $\Gamma_o = 0.1$, $f(\phi, \phi_1) = 1$.

Results for $f_s = 0.5$ Hz

$A_o = 0.053 \quad A_m = A_{2m} = 0$

Maximum type 1 scalloping $|\Delta\Phi^{S_1}|_{max} = 0.022$ degrees

Type 2 scalloping error $\equiv 0$.

Results for $f_s = 1$ Hz

$A_o = 0.053 \quad A_m = 0.106 \quad A_{2m} = 0$

Maximum type 1 scalloping $|\Delta\Phi^{S_1}| = 0.022$ degrees

Maximum type 2 scalloping $|\Delta\Phi^{S_2}|_{max} \lesssim 0.029$ degrees.

It will be recalled that for $\Gamma = 0.1$ the maximum scalloping error produced by the static windmill blade is $|\Delta\Phi^{S}|_{max} = 0.417$ degrees.

1.3 Conclusions

Scalloping errors in conventional and Doppler VOR indications produced by time varying scattering objects (like a windmill) located in the vicinity of the VOR ground station have been theoretically investigated. The analysis

assumes the system to be in free space and neglects the vertical plane pattern characteristics of the VOR transmitting antenna system. A simple physical optics scattering model for the windmill blades has been adopted and any scattering effects from the windmill tower have been neglected.

It is found that the stationary windmill blades produce more scalloping errors than the rotating blades. This is because in the time varying case the scattered energy is distributed over a band of frequencies whereas the VOR receiver is sensitive to only 30 Hz modulated signals. On the basis of the approximate theory developed, some estimates of errors produced by a typical windmill have been obtained. The results indicate that in choosing a site for a windmill in the vicinity of a VOR it is sufficient to consider only the scattering effect of the stationary windmill. Thus the siting of a windmill may be carried out according to the FAA guidelines [2].

1.4 References

[1] Beck, G.E., Navigation Systems - A Survey of Modern Electronic Aids, VanNostrand-Reinhold, London, 1971, Chapter 9.

[2] "Handbook: VOR/VORTAC Siting Criteria", Federal Aviation Administration, Department of Transportation, Report 6700.11, August 7, 1968.

[3] Anderson, S.R., "VHF Omnirange Accuracy Improvements", IEEE Trans. Aerospace and Navigational Electronics, Vol. ANE-12, pp. 26-35, January, 1965.

[4] Hurley, C.H., S.R. Anderson and H.F. Keary, "The Civil Aeronautics Administration VHF Omnirange", Proc. IRE, Vol. 39, pp. 1506-1520, December, 1951.

[5] Anderson, S.R. and R.B. Flint, "The CAA Doppler Omnirange", Proc. IRE, Vol. 47, pp. 808-821, May, 1959.

[6] Anderson, S.R. and H.F. Keary, "VHF Omnirange Wave Reflections from Wires", Technical Report No. 126, Civil Aeronautics Administration Technical Development and Evaluation Center, Indianapolis, Indiana, May, 1952.

[7] Sengupta, D.L., "Theory of Scalloping Amplitude Errors in Standard VOR Bearing Indications", IEEE Trans. on Aerospace and Electronics Systems, Vol. AES-11, No. 1, pp. 86-93, January, 1975.

[8] Anderson, S.R., H.F. Keary and W.L. Wright, "The Four-loop VOR Antenna", Technical Report No. 210, Civic Aeronautics Administration Technical Development and Evaluation Center, Indianapolis, Indiana, June, 1953.

[9] Sengupta, D.L., "Theory of VOR Antenna Radiation Patterns", Electronics Letters, IEE (London), Vol. 7, No. 15, pp. 418-420, 1971.

[10] Sengupta, D.L., "Signal Analysis of TV Reception in the Presence of Various Multipath Sources", The University of Michigan Radiation Laboratory Memorandum No. 014438-514-M, Ann Arbor, Michigan, July, 1976.

[11] Flint, R.B. and E.R. Hollon, "VOR Evolutionary System Improvements in the United States", IEEE Trans., Vol. ANE-12, pp. 46-56, March, 1965.

APPENDIX 2: WINDMILL INTERFERENCE WITH MICROWAVE COMMUNICATION LINK SYSTEMS

In this appendix we examine theoretically the mechanism by which the interference produced by a windmill (WTG) may effect the performance of a microwave communication link. A rigorous investigation of the problem requires a detailed knowledge of the specific link: its function and how it operates, the radiation patterns of the transmitting and receiving antennas, the propagation characteristics in the region where the link is located, etc., as well as an understanding of how a windmill scatters any microwave energy incident upon it. Rather than attempting a precise assessment of how the performance of a particular microwave link could be affected, we shall instead confine ourselves to a consideration of the general effects of the extraneous modulation that a windmill can provide. The windmill, located in the vicinity of a microwave repeater station, will be treated as a time varying multipath source producing both amplitude and phase (or frequency) modulation of the signal picked up by the microwave receiving antenna. To simplify the analysis, the effects of the earth are ignored and the medium assumed to be free space.

Problems of inteference in microwave systems are usually treated statistically [1,2], but because of the source of the interference in the present case it is more convenient to follow a deterministic approach by assuming a simple model for the scattering of the microwave signal by the windmill blades. The effect of this scattering on the basic detection process of a typical microwave link receiving system is analyzed to provide an assessment of a windmill's interference with the link. It is believed that the results obtained are valid and meaningful in spite of the use of various idealized models in order to simplify the analysis.

2.1 Typical Microwave Link Systems

Microwave communication links may operate anywhere within the 300 MHz to 300 GHz portion of the electromagnetic spectrum. Various systems are in use

for a variety of purposes, but a study of the effects of windmill interference must of necessity concentrate on a specific type of system. Because of the availability of information about the link systems used by the telephone companies, it was decided to concentrate on these.

The telephone companies employ microwave links for long and short distance telephone communication as well as television and data transmissions [3]. The link systems utilize microwave repeaters at selected sites where the received signal is either detected and passed on to local customers, or amplified and transmitted to the next repeater. The three most common systems operate at 4, 6 and 11 GHz and are called the TD, TH and TJ systems respectively. Peak radiated power can range from 1 to 10 watts, with an average power of 1 to 5 watts. Highly directional pencil beam antennas, typically having $\pm$ 0.6° beamwidths and 35 dB gain (at 4 GHz), are used for transmission and reception. The TD system is normally used for 30 mile single-hop paths, and the TH and TJ systems for 25 and 10 mile hops respectively. Details and descriptions of all three systems can be found in [3], and we shall give here only the basic principles of operation of the TD system.

The system is structured to consist of 10 two-way broadband and two protection channels covering the frequency range 3.7 to 4.2 GHz. Protection channels are spares which are automatically switched in if a system failure occurs or defective equipment must be replaced. In one failure mode used, the noise level is monitored in the neighborhood of a pilot tone by measuring the level of energy present due to additive noise, interference and other factors. When this energy level exceeds a threshold value, the transmission is switched to the protection channel.

The total bandwidth of a transmit and receive channel is 40 MHz, and the transmit and receive midband frequencies are separated by 40 MHz [4]. Each channel has the capacity to handle two one-way television or 480 (or more) two-way telephone transmissions. To transmit many telephone conversations each having a 4 KHz spectrum a technique called frequency division multiplex (FDM) is used. Each telephone conversation is upconverted in frequency by an

amplitude modulation single sideband (AM-SSB) operation to occupy a contiguous frequency slot. The signal, either a television transmission or any other form of signal to be transmitted, is commonly referred to as the baseband signal. This is transformed into a low index frequency-modulated (FM) 70 MHz intermediate frequency (IF) carrier, and then upconverted to the radio frequency (RF) which is transmitted at approximately 4 GHz. The block diagram of a typical repeater station system for telephone conversations is shown in Figure 2-1. Since the modulation introduced on the IF carrier is a small deviation FM, this can be considered almost amplitude modulation (AM), a fact which is used in the subsequent analysis.

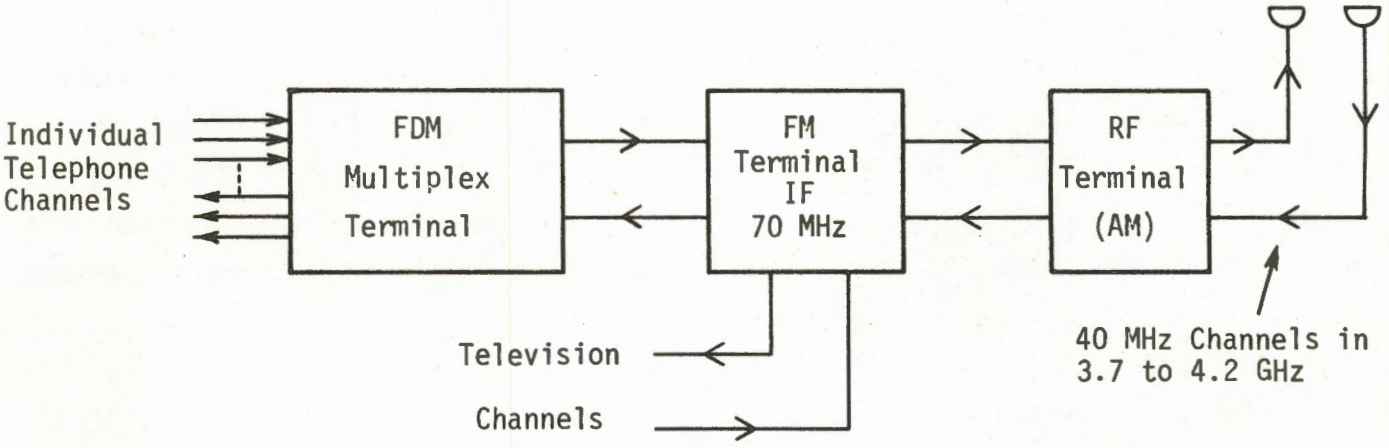

Figure 2-1. Block diagram of a TD system.

2.2 External Interference

For an efficient design of a microwave link system it is important to take into account the particular external sources of interference that may be present to which the system may be vulnerable. For example, an FM system is relatively immune to small amplitude disturbances but cannot tolerate a significant Doppler frequency shift of the received signal. Once the critical sources of interference have been pinpointed, it is necessary to establish a measure which can be used to relate the overall performance of the system to the level of inter-

ference. Quite often the measure chosen is the minimum acceptable signal to noise (or interference) ratio S/N at the receiver, and the design goal is then to protect the system against intolerable levels of S/N.

The most common types of interference in microwave communication systems are atmospheric fading and absorption, cross-talk between channels and multipath. The fading problem is usually handled statistically [1]. Given the minimum S/N required, the approach taken is to specify the percent time that this must be exceeded. Using this and a knowledge of the fading statistics in the region where the link is to be installed, the antenna gains, transmitter power, receiver to transmitter separation distance, etc., can be chosen. Atmospheric absorption effects are usually circumvented by judicious choice of frequency, and cross-talk minimized by locating the repeater stations in a zig-zag fashion or by frequency (or space) diversity schemes.

The most important source of interference is multipath and it is traditionally handled by path engineering, i.e., the proper choice of receiver and transmitter sites and antenna heights to minimize the possibility of interference between the direct and multipath signals at the receiver. The design is facilitated using the concept of the Fresnel zone. It is desirable to locate the two antennas at the foci of the first Fresnel zone (an ellipsoid of revolution) and to have this zone clear of any obstacles [7]. For satisfactory performance of a TD system in the absence of fading, it is sometimes required that any multipath interference be at least 40 dB down from the desired signal [4].

In our analysis a windmill is treated as a source of multipath interference to the microwave system. Were the blades not rotating, the siting of a windmill in the vicinity of a repeater station could be analyzed in the manner described above, but because of the blade rotation, a windmill will actually be a source of time-varying multipath, and the effect of this type of modulation of the total received signal must also be considered. To this end, a brief discussion of the basic detection process at a microwave repeater station is appropriate.

2.3 Basic Detection Process

We recall that at the transmitting terminal the baseband signals (multiplexed telephone conversations, television and/or other signals) are applied as a narrow band frequency modulation to a 70 MHz IF sub-carrier which is in turn upconverted by an AM process to the desired microwave frequency before being radiated by the antenna. At the receiving terminal the process is reversed: the received RF signal $e_s(t)$ is first envelope detected to obtain the IF signal $m(t)$ which is a narrow band FM signal containing the desired information $f(t)$, and $m(t)$ is then processed through a demodulator to yield $f(t)$. The recovery process is illustrated by the block diagram in Figure 2-2, where the following symbols are used:

$$e_s(t) = [1 + m(t)]\cos\omega_c t, \tag{2.1}$$

$\omega_c = 2\pi f_c$ = radian frequency of the RF carrier,

$$m(t) = \cos[\omega_o t + ka(t)] , \tag{2.2}$$

$\omega_o = 2\pi f_o$ = radian frequency of the IF sub-carrier,

k = modulation index (usually $<<$ 1)

and

$$a(t) = \int_o^t f(t)dt, \tag{2.3}$$

$f(t)$ being the desired information.

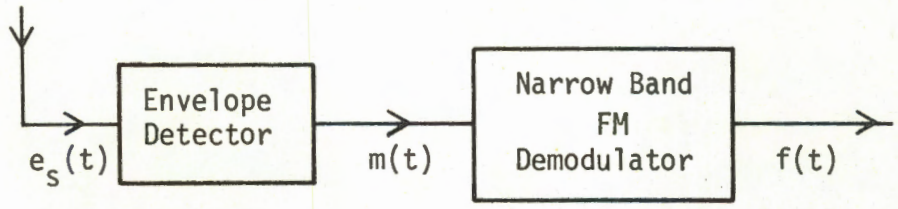

Figure 2-2. Basic detection process of a microwave link receiver.

The recovery of f(t) from the narrow band frequency modulation signal m(t) can be accomplished using a product device, and for the purposes of our analysis the narrow band FM demodulator in Figure 2-2 can be modelled as shown in Figure 2-3.

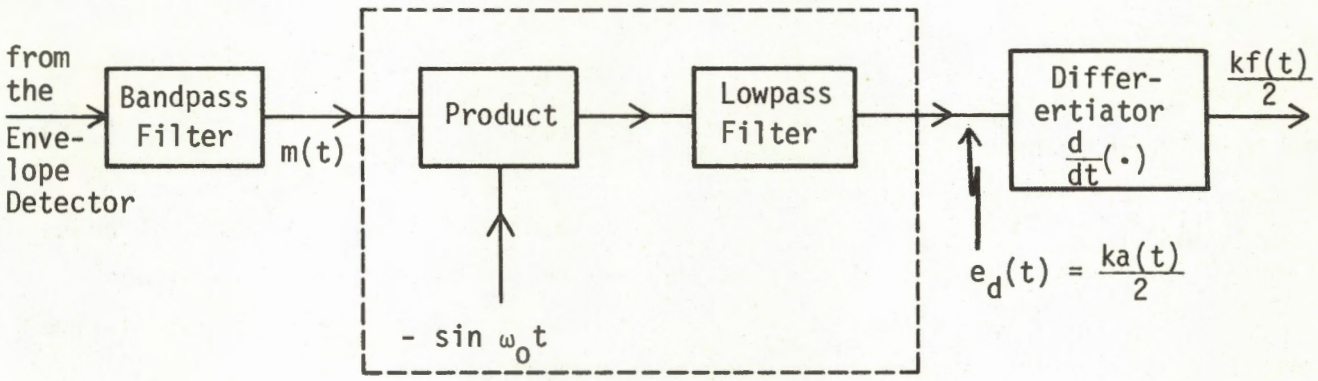

Figure 2-3. Block diagram of the demodulator for narrow band frequency modulated signal.

The purpose of the band pass filter is to pass the desired modulated signal. The portion of Figure 2-3 enclosed by dashed lines is a tuned device which passes only the spectral components within the message band, and the low pass filter removes the undesired spectral components generated by the product device. For a narrow band FM signal, the input m(t) to the product device can be written as

$$m(t) \simeq \cos \omega_o t - ka(t) \sin \omega_o t \ , \qquad (2.4)$$

and since the low pass filter is mathematically equivalent to an integrator, the input signal $e_d(t)$ to the differentiator in Figure 2-3 is obtained as

$$e_d(t) = -\frac{1}{T}\int_0^t m(t)\sin \omega_o t \, dt = \frac{1}{2} ka(t) \qquad (2.5)$$

provided a(t) varies slowly enough to be assumed constant over a period T of the IF carrier signal. From (2.5), the input follows by differentiation (see 2-3).

The above is based on the assumption of no interference, and in the presence of a time varying interference produced by a windmill, the net signal at the receiver can be written formally as

$$e_s(t) \simeq [1 + m(t)]\{1 + \Gamma(t)\cos \delta(t)\}\cos \omega_o t \qquad (2.6)$$

where $\Gamma(t)$ and $\delta(t)$ are the amplitude and phase of the interfering signal relative to the desired carrier signal at the receiver. Note that (2.6) assumes $|\Gamma(t)| << 1$. In a later section we examine in more detail the effect of a time varying interference source on the detected output of the receiver.

In the case of a static windmill, i.e., no blade rotation, $\Gamma(t) = \Gamma_o$ and $\delta(t) = \delta_o$, where Γ_o is directly proportional to the equivalent scattering area of a windmill blade and is inversely proportional to the distance between the windmill and the receiver. It can be shown that the output of the receiver is then

$$e_{out|static} = \frac{k}{2} f(t)\{1 + \Gamma_o \cos \delta_o\} , \qquad (2.7)$$

i.e., the output consists of the desired signal plus a replica with some added phase. The extent to which the performance of the system is affected by the second term depends mainly on the parameter Γ_o, and in the next section we use this equation to determine the region where a static windmill could impair a microwave link system.

2.4 Forbidden Zone for a Static Windmill

The region about a microwave link receiver where a windmill could produce unacceptable interference with reception will be called the forbidden zone, and

we now use (2.7) to find the forbidden zone associated with a static (i.e., blades stationary) windmill. The zone is that in which the amplitude Γ_o of the blade-scattered signal relative to the desired (direct) signal at the receiver exceeds a predetermined threshold value, and this threshold depends on the characteristics of the link system: its function, modulation used, etc. Telephone companies customarily demand [4,8] a threshold Γ_{ot} = - 75 dB for telephone channels, a margin of -40 dB for fading being included. The corresponding threshold for a television channel is Γ_{ot} = - 40 dB, i.e., $\Gamma_{ot} = 10^{-2}$, but if a - 40 dB margin for fading is also allowed here, the resulting threshold is Γ_{ot} = - 80 dB, i.e., $\Gamma_{ot} = 10^{-4}$. Our subsequent calculations will be carried out using either $\Gamma_{ot} = 10^{-2}$ (without fading) or 10^{-4} (with fading).

In seeking to relate Γ_o to the distance from the windmill, we ignore the presence of the earth and assume the medium to be free space. This simplification is believed adequate for the short distances of concern to us, but if desired the effects of the earth could be taken into account by performing the more rigorous propagation analysis described in [9].

Figure 2-4 shows the receiving antenna R and the windmill blade B exposed to the incident plane wave signal from the distant microwave transmitting antenna. The pattern $f(\phi)$ of the receiving antenna is assumed to be a pencil beam directed to receive the incoming signal, but it may also pick up some of the signal scattered off the windmill blade. It is obvious that to minimize this source of interference, the windmill must be out of the mainbeam and near sidelobes of R and, in addition, should be as far from R as possible. If E_o and E_s are the amplitudes of the direct and windmill-scattered (i.e., interfering) signals at R, their ratio is

$$\Gamma_o = \frac{E_s}{E_o} = \frac{A_e}{\lambda_c r} f(\phi) \qquad (2.8)$$

where λ_c = wavelength of the incident carrier,

r = distance of B from R,

and A_e = equivalent scattering area of a blade.

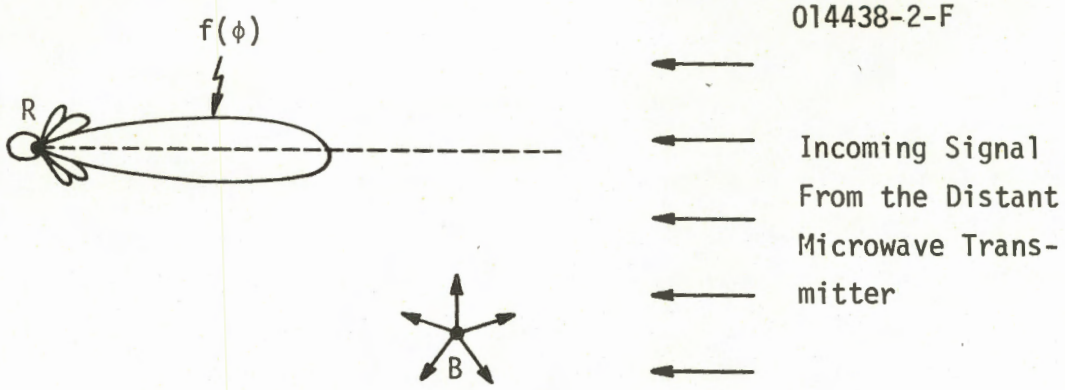

(a) Orientation of the phase centers of the receiving antenna (R) and the windmill blade (B) with respect to the incident signal.

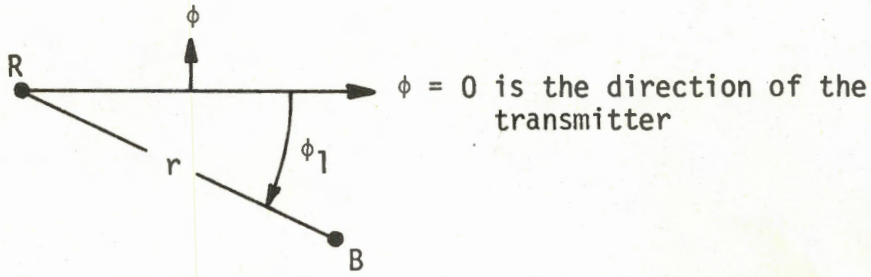

(b) Coordinate system used.

Figure 2-4. Geometry of the microwave receiving antenna, the windmill and the incident field direction.

As discussed later in Appendix 3, the blade scattering is predominantly in the specular and forward directions, with only one blade contributing at any given time. Detailed information about the blade scattering is given there, along with the equivalent scattering areas for a number of actual blades, and (2.8) is based on the assumption that the blade is so oriented as to direct the maximum (specularly) scattered signal to the receiver. With $\Gamma_o = \Gamma_{ot}$, the forbidden zone about the microwave receiver is now given by

$$r(\phi) = \frac{A_e}{\Gamma_{ot}\,\lambda_c} f(\phi) \ , \qquad 0 \leq \phi \leq \pi \ . \tag{2.9}$$

A key factor in (2.9) is the antenna radiation pattern $f(\phi)$. The antennas most frequently used for microwave repeaters are the horn-reflector and the 8-ft. diameter parabolic dish, and their patterns are shown in Figures 2-5(a),(b). Using these and a knowledge of A_e and Γ_{ot}, the forbidden zone can be computed from (2.9). Figure 2-6 shows the forbidden zone about the receiving station of a 4 GHz microwave link with a horn-reflector antenna when in the presence of a MOD-0 windmill for which $A_e = 12\ m^2$ (see Appendix 3). The threshold level used is $\Gamma_{ot} = 10^{-2}$. With an 8-ft. parabolic dish antenna instead, the corresponding zone for $\Gamma_{ot} = 10^{-2}$ and 10^{-4} (with fading) are given in Figures 7(a) and (b). The fact that the windmill must lie outside the mainbeam region is clearly shown, and the inclusion of the fading margin increases the zone size by a factor 100. For example, in the direction $\phi = 100°$ (the near sidelobe area) in Figures 7(a) and (b) the zones with and without the fading margin extend outwards to 0.08 and 8 Km respectively. Which zone is appropriate depends entirely on the threshold established by the link owner, and we remark in passing that the value $\Gamma_{ot} = 10^{-2}$ was the one used in our earlier assessments [10,11] of the interference problem at selected sites.

0.018, 1.8

2.5 Effects of Blade Rotation

The forbidden zone defined above is that in which the interference from a static windmill can exceed the specified threshold level. It is therefore also a region where an operating windmill should not be sited, but to see whether a still larger region is appropriate when the blades rotate, it is necessary to examine the effect of blade rotation on the type of interference produced. For this purpose we make use of the basic elements of the detection process in the receiver outlined in Section 2.3. To obtain an expression for the signal modulation, two simplified models for the scattering by a rotating blade are examined. The first is a rotating point scatterer illuminated by the plane wave signal, and though this is a highly idealized model, the results are relevant to the physical problem if the point is assumed coincident with the scattering center of an actual windmill blade. The second is somewhat more realistic and treats the blade as a rotating planar metal plate. Both models were employed in our earlier study [9].

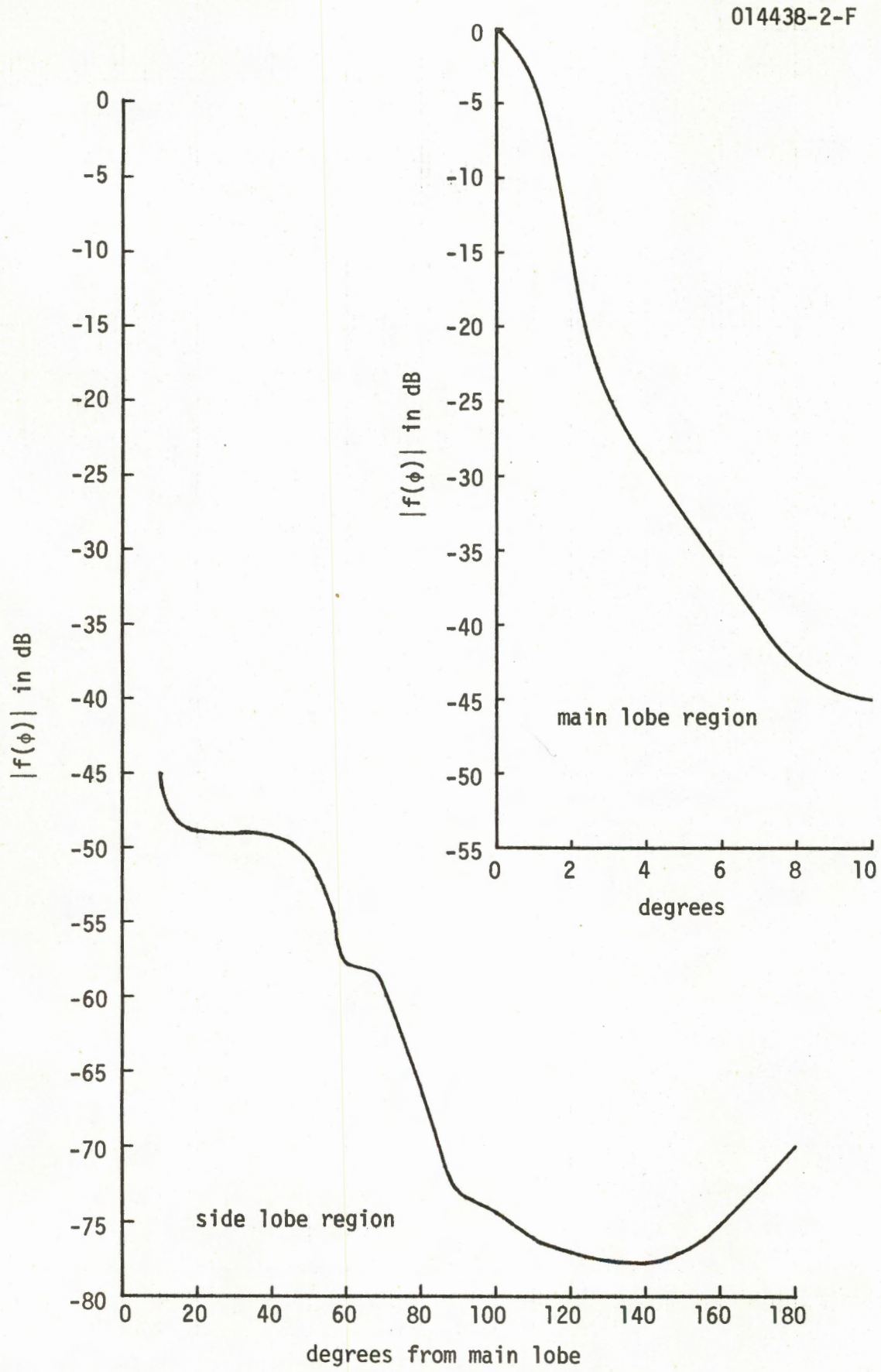

Figure 2-5(a): Smoothed radiation pattern in the horizontal plane for a horn-reflector antenna at 4 GHz (Reproduced from [4]).

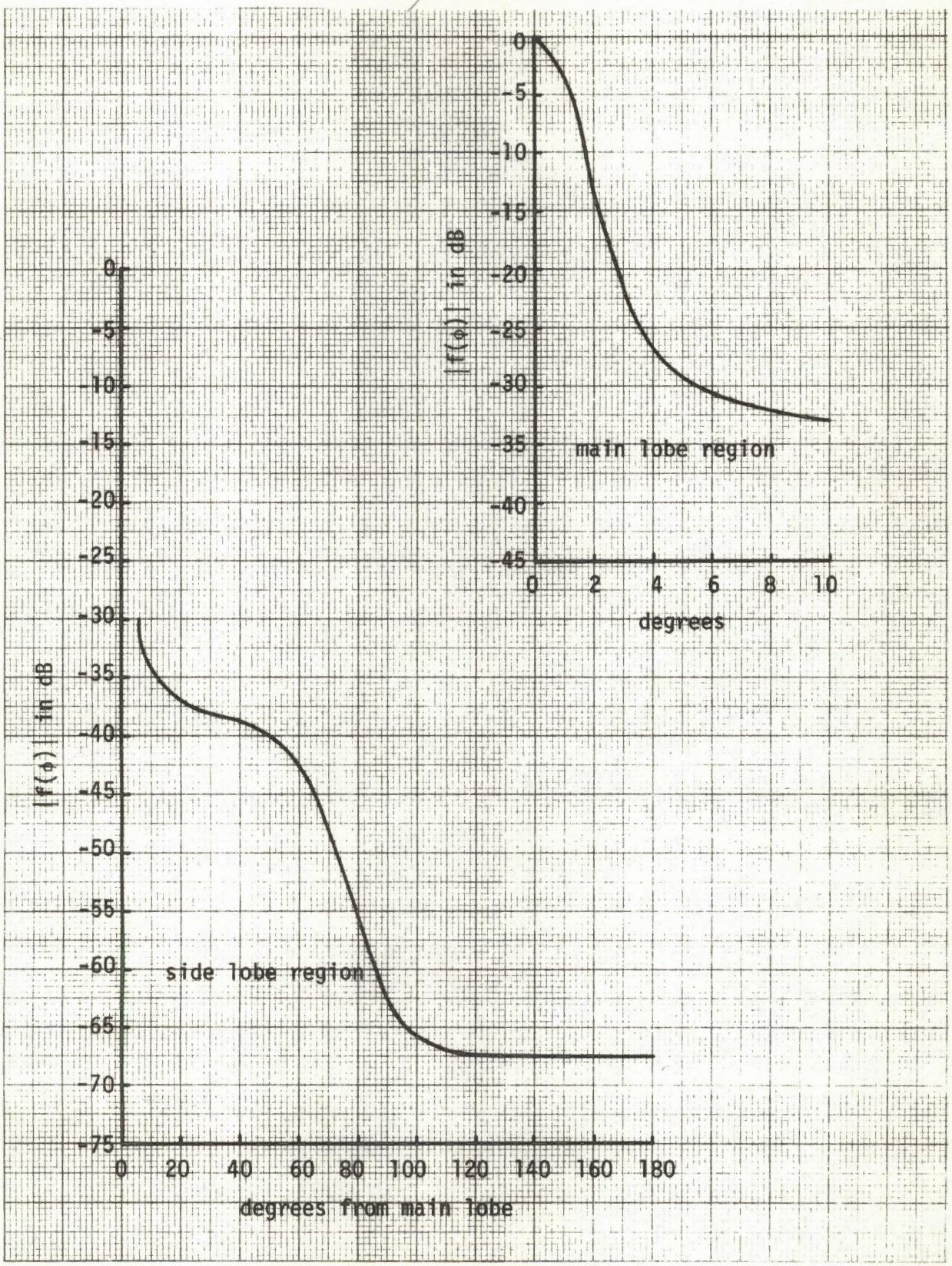

Figure 2-5(b): Smoothed radiation pattern in the horizontal plane for an 8-ft. parabolic dish antenna at 4 GHz (Reproduced from [4]).

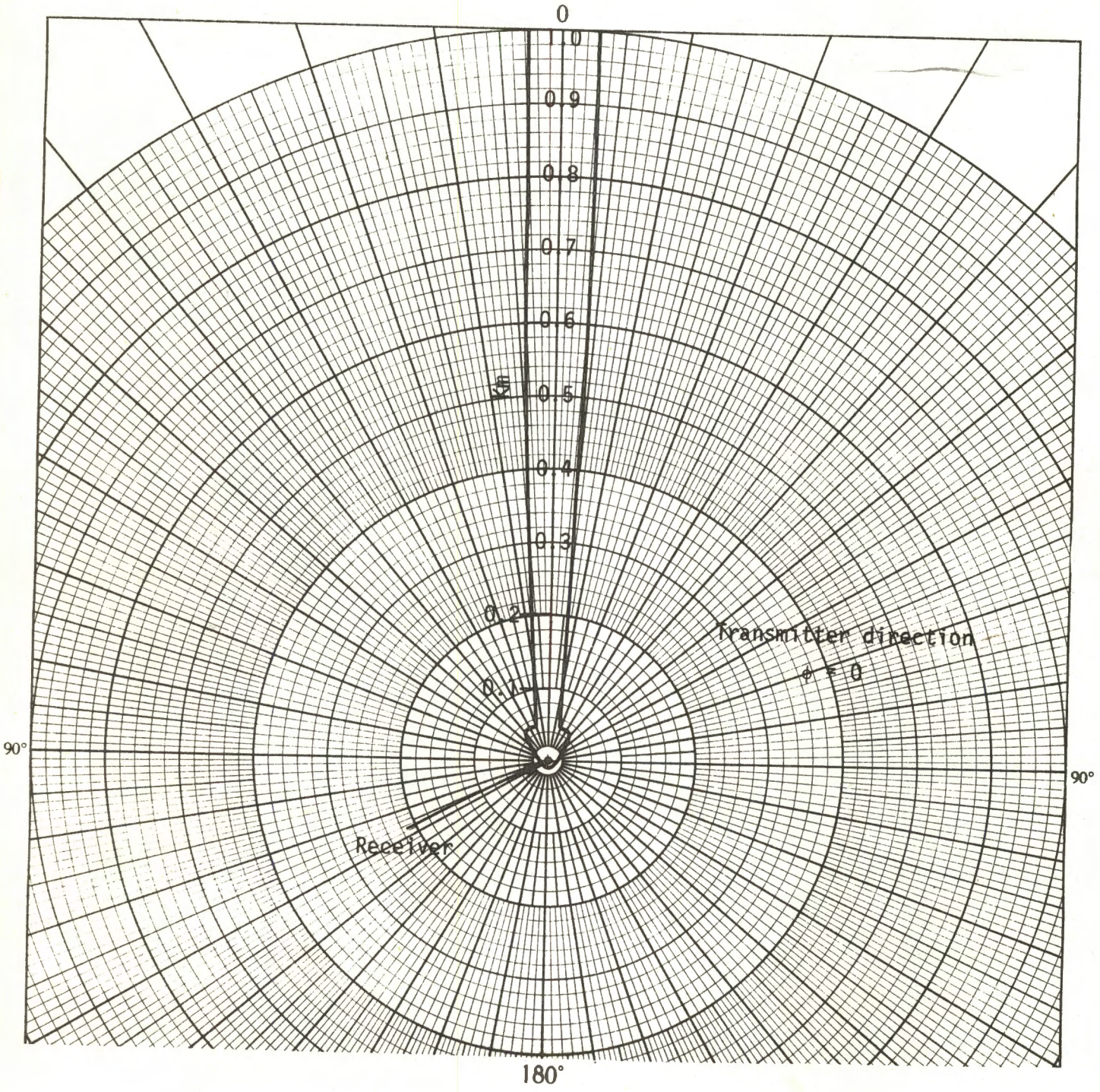

Figure 2-6: Forbidden zone of a 4 GHz microwave link receiver using a horn-reflector antenna. Threshold of interference to carrier signal level = -40 dB.

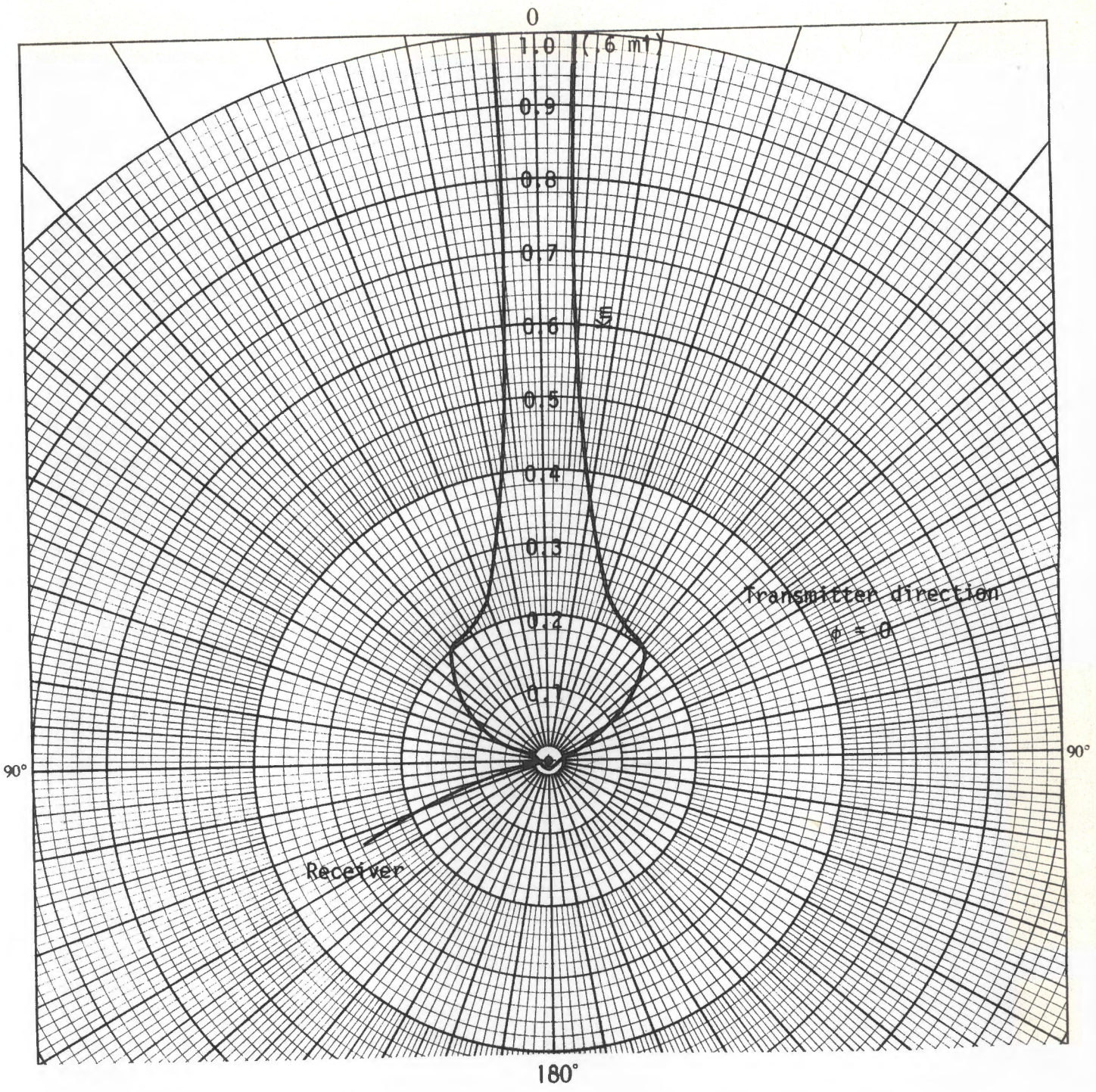

Figure 2-7(a): Forbidden zone of a 4 GHz microwave link receiver using a 8-foot parabolic dish antenna. Threshold of interference to carrier signal = -40 dB.

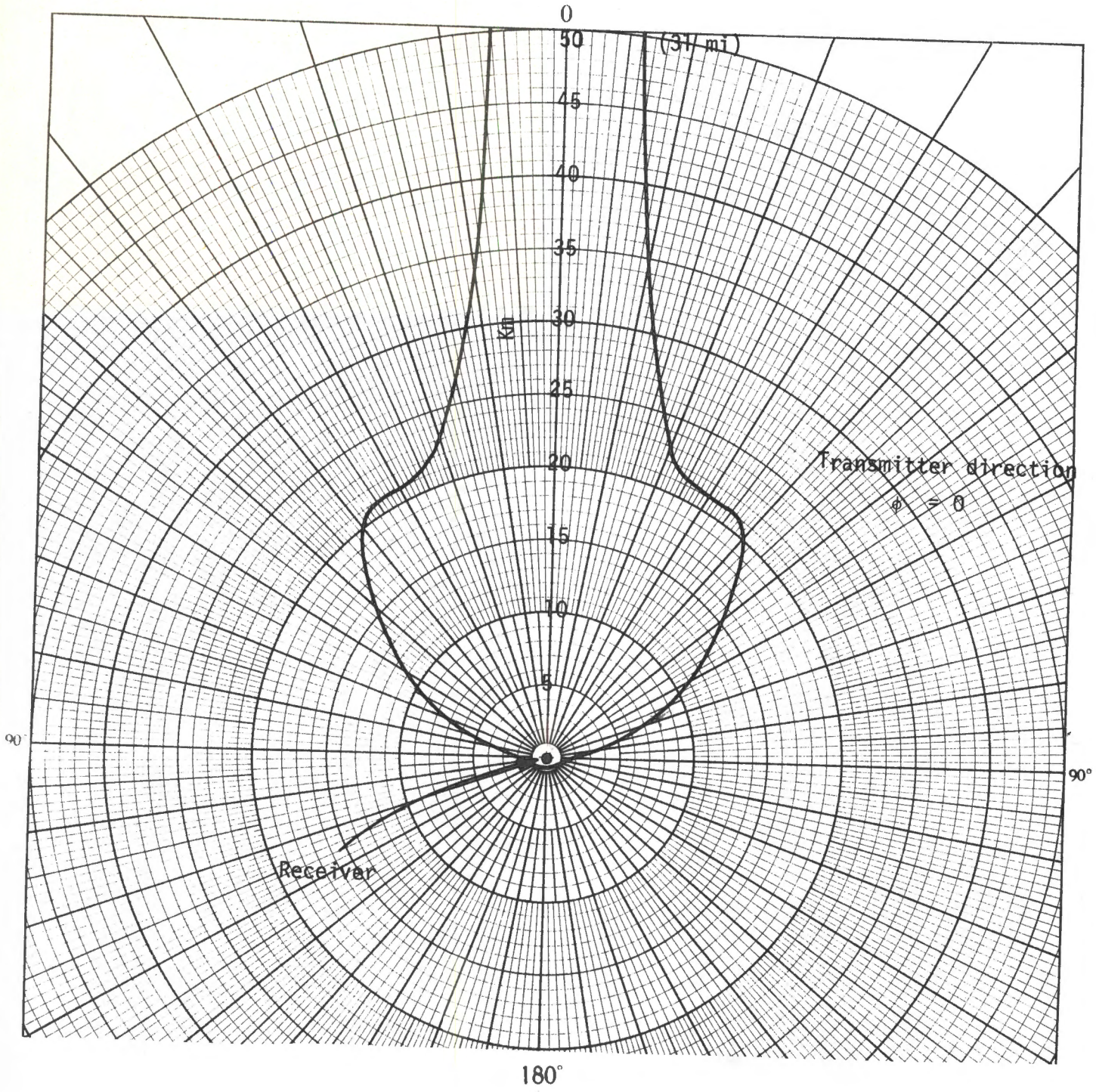

Figure 2-7(b): Forbidden zone of a 4 GHz microwave link receiver using a 8-foot parabolic dish antenna. Threshold of interference to carrier signal level = -80 dB.

2.5.1 Rotating Point Scatterer

An isotropic point scatterer S located at (ℓ, θ_s, ϕ_s) rotates in the plane $\phi = \phi_s$ of a spherical polar coordinate system at the angular frequency Ω_s such that

$$\theta_s = \Omega_s t = 2\pi f_s t \tag{2.10}$$

where f_s is the rotation frequency of the windmill blades. For simplicity the transmitter and the receiver are assumed to lie in the xy plane, i.e., the plane $\theta = \pi/2$, as shown in Figure 8. A plane wave is incident from the direction $\phi = \phi_o$ and the total field picked up by an omnidirectional receiving antenna R located at (r, ϕ) is then (see [9])

$$e_s(t) \simeq [1 + m(t)][1 + \Gamma_o \cos(\delta - k_c \ell p \sin \Omega_s t)]\cos \omega_c t \tag{2.11}$$

where

$\Gamma_o e^{i\delta}$ (with $\Gamma_o << 1$) is the ratio of the scattered field to the direct field at the receiver,

$k_c = 2\pi/\lambda_c$ is the propagation constant at the RF frequency,

$$p = \cos(\phi_o - \phi_s) + \cos(\phi - \phi_s) , \tag{2.12}$$

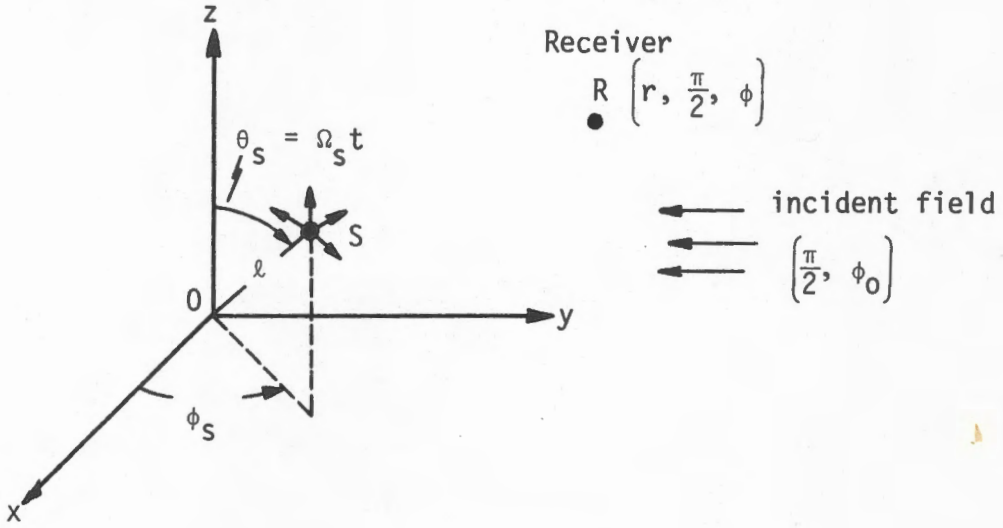

Figure 2-8. Geometry of rotating point scatterer.

and the other parameters are as defined before. Using the method given in Section 2.3, the output signal can be shown to be

$$e_{out}(t) \simeq \frac{1}{2} k\, f(t) + \frac{1}{2} k\, f(t)\, \Gamma_o \cos(\delta - k_c \ell p \sin \Omega_s t)$$

$$+ \frac{1}{2} k\, a(t)\, \Gamma_o k_c \ell p\, \Omega_s \cos \Omega_s t \sin(\delta - k_c \ell p \sin \Omega_s t) \,, \tag{2.13}$$

whereas if the scatterer is not rotating

$$e_{out|static} \simeq \frac{1}{2} k\, f(t) + \frac{1}{2} k\, f(t)\, \Gamma_o \cos(\delta - k_c \ell p \sin \theta_s) \tag{2.14}$$

in agreement with (2.7) if δ_o is identified with $(\delta - k_c \ell p \sin \theta_s)$.

Comparison of (2.13) with (2.7) or (2.14) reveals that the rotation of the multipath source introduces two rotation-dependent terms to the detected output in addition to the desired output $\frac{1}{2} k\, f(t)$. As remarked earlier, when the scatterer is stationary the added (multipath) signal is simply a replica of the desired baseband signal shifted by a constant phase, and though it is difficult to quantify the effect of the added terms in the dynamic case, we note the following:

(i) the term $\frac{1}{2} k\, f(t)\, \Gamma_o \cos(\delta - k_c \ell p \sin \Omega_s t)$ represents a time function of instantaneous frequency

$$f_{inst} \simeq \frac{2}{c} \pi \ell |p| f_o f_s \cos \Omega_s t \tag{2.15}$$

where f_o is the frequency of the IF sub-carrier and c is the velocity of light. For the typical values $\ell \simeq 9$m, $f_o = 70$ MHz and $f_s = 0.5$ Hz, the maximum value of f_{inst} is less than (about) 10 Hz, and the term therefore produces a frequency smearing of the desired baseband frequency response f(t). The net result is that the available baseband energy is smeared out over a narrow range ($\sim k_c \ell |p|$) of frequencies, but this is unlikely to be significant unless the amplitude Γ_o of the multipath signal is at least as large as the threshold established in the static case.

(ii) the second interference term in (2.13) also represents a time function having instantaneous frequency

$$f_{inst} \simeq \frac{2}{c} \pi \ell |p| \; f_o f_s \cos \Omega_s t \pm f_s .$$

Its maximum value is quite small (a few Hz only), though larger than the maximum value of (2.15). The quantity a(t) in the interference term is the integral of f(t) and its spectrum is therefore "de-emphasized", i.e., resembles that of f(t) except for a roll-off at higher frequencies whose rate depends on the parameter $\frac{1}{2} \Gamma_o \, k_c \ell |p| \, \Omega_s$. This interference term also serves to smear out the desired baseband signal output over a small range of frequencies and though it contains less high frequency energy than the first term, its amplitude is somewhat larger. Here again the practical significance depends on Γ_o and it seems probable that the effect of each term is comparable.

2.5.2 Rotating Rectangular Metal Plate

Consider a rectangular metal plate of dimensions L_1 and L_2 with $L_1 >> L_2$ lying in the xz plane with its center at the origin O of a spherical polar coordinate system. The directions of incidence and scattering are as shown in Figure 2-8, and the plate is assumed to rotate in the xz plane at the angular frequency Ω_s. It is known [2] that for any given direction of the incident signal, the only significant scattering is in the directions close to specular and forward, and for a receiver R in a direction close to one of these, the total received field can be shown to be [9]

$$e_s(t) \simeq [1 + m(t)]\left\{1 + \Gamma_o \, \text{sinc}\left(\frac{L_1}{\lambda_c} \sin \alpha \cos \Omega_s t \right)\right\} \qquad (2.17)$$

where Γ_o is proportional to the scattering area of the plate,
α is the angle measured from the direction of specular or forward scattering,
and $\text{sinc } x = \frac{\sin \pi x}{\pi x}$.

With the received signal given by (2.17), the detected output is

$$e_{out}(t) \simeq \frac{1}{2} k\, f(t) + \frac{1}{2} k\, f(t)\, \Gamma_o\, \mathrm{sinc}\left(\frac{L_1}{\lambda_c} \sin\alpha \cos\Omega_s t\right)$$
$$- \frac{1}{2} k\, a(t)\, \Gamma_o\, \Omega_s \tan\Omega_s t \left\{\cos\left(\frac{L_1}{\lambda_c} \sin\alpha \cos\Omega_s t\right)\right.$$
$$\left. - \mathrm{sinc}\left(\frac{L_1}{\lambda_c} \sin\alpha \cos\Omega_s t\right)\right\}. \qquad (2.18)$$

Observe that if $\alpha = 0$, i.e., the receiver is precisely in the direction of specular or forward scattering from the plate, the detected output reduces to that in the static case. This is in agreement with our previous finding [9] that the time varying modulation produced by a rotating plate is zero in these directions (see also Appendix 4). In contrast to the case of a rotating point scatterer, the present output contains interference terms which vary periodically with time like sinc pulses whose frequency spectrum extends out to only about $\Omega_s L_1/\lambda \sin\alpha$. In all other respects the frequency smearing of the detected baseband signal produced by the interference terms is similar to that for a rotating point scatterer, and once again the practical effect depends on the value of the parameter Γ_o. For $\Gamma_o < 10^{-4}$ (or even 10^{-2}), i.e., outside the forbidden zone for a static windmill, it seems probable that the effect is negligible.

2.6 Conclusions

There is a wide variety of communication link systems in use in the microwave region and because the effect of the interference caused by a nearby windmill depends on the characteristics of the system, e.g., modulation, format and form (digital or analog), it is impossible to provide a quantitative assessment that will hold in general. We have therefore confined our attention to the type of link systems used by telephone companies.

From a consideration of the scattering of signals by a static (i.e., blades stationary) windmill, the concept of a forbidden zone around a microwave link

receiver has been developed, the zone being that where the placement of a windmill could provide unacceptable interference effects. The shape of the zone is primarily determined by the radiation pattern of the receiving antenna. Its size is proportional to the equivalent scattering area of a windmill blade and inversely proportional to the carrier wavelength and to the specified threshold value of the interfering signal relative to the desired signal at the receiver. For typical TD microwave links, the forbidden zones have been calculated for the threshold $r_{ot} = 10^{-2}$ and 10^{-4} (with fading margin) and are, of course, 100 times larger in the latter case.

The effect of the blade rotation on the detection signal has been qualitatively assessed by examining the basic detection process in the receiver of a TD system. The rotation produces a frequency smearing of the received baseband signal energy, with the maximum frequency smear depending on the blade size and orientation and its rotation frequency. For the MOD-0 blade, this maximum is much less than the total FDM bandwidth of the telephone channel. The degrading influence of the smear depends on the amplitude of the scattered signal at the receiver relative to the desired signal, and for a windmill outside the forbidden zone determined from static considerations, it would not appear that the blade rotation will produce significant interference per se.

2.7 References

[1] Jakes, Jr., W.C., "Microwave Mobile Communications", John Wiley & Sons, New York, NY, 1974.

[2] Bennett, R, H.E. Curtis and S.O. Rice, "Interchannel Interference in FM and PM Systems Under Noise Loading Conditions", B.S.T.J., Vol. 34, May 1955, pp. 601-636.

[3] Members of the Technical Staff, "Transmission Systems for Communications", Third Edition, Bell Telephone Laboratories, Inc., 1964.

[4] Curtis, H.E., "Radio Frequency Interference Considerations in the TD-2 Radio Relay System", B.S.T.J., Vol. 39, March 1960, pp. 369-387.

[5] Peebles, Jr., P.Z., "Communication Systems Principles", Addison-Wesley Publishing Co., Reading, Mass., 1976, pp. 211-215.

[6] loc cit, pp. 222-225.

[7] ITT, "Reference Data for Radio Engineers", Sixth Edition, Howard W. Sams & Co., Inc., Indianapolis, Indiana, 1975, pp. 28-14—28-17.

[8] Campbell, R.D., "Radar Interference to Microwave Communication Services", Proc. of AIEE, Vol. 77, November 1958, pp. 717-722.

[9] Senior, T.B.A., D.L. Sengupta and J.E. Ferris, "TV and FM Interference by Windmills", Radiation Laboratory Final Report No. 014438-1-F, February 1977, Contract No. E(11-1)-2846, ERDA, Washington, D.C.

[10] Sengupta, D.L., "Windmill Interference With a Microwave Link", The University of Michigan Radiation Laboratory Memoranda No. 014438-521-M, November 8, 1976 and No. 014438-531-M, February 28, 1977.

[11] Senior, T.B.A., "Microwave Interference on Culebra", The University of Michigan Radiation Laboratory Memorandum No. 014438-529-M, February 15, 1977.

APPENDIX 3: BLADE SCATTERING

The interference produced by the rotating blades of a windmill is directly proportional to the scattering from a single blade, and the interference is greatest for specular scattering off the broad face of a blade. It is therefore important to determine the maximum scattered fields for the blades of interest, and to see how this is influenced by the geometry and material of the blade, as well as any lightning arrestor strips that may be present. To this end, a number of experiments have been carried out. These have included measurements of the scattering from the MOD-0 and MOD-0A blades on site at Plum Brook, and of the backscattering cross sections of several small scale model blades at a scaled frequency in an anechoic chamber. The results are summarized in Section 3-3 and used to predict the equivalent (flat plate scattering) area of the MOD-1 blade.

3.1 Full Scale Measurements

3.1.1 Blade Description

During the latter part of July examples of the MOD-0 and MOD-0A blades were available at the Plum Brook facility. The MOD-0 blade was identical to those permanently installed on the wind turbine and consists of an aluminum skin over a framework of girders. It is entirely metallic and similar in gross form to an airplane wing. As seen from Figure 3-1 its overall length is 58.5 feet (62.5 feet when measured from the axis of rotation). The variations of the chord, blade thickness and blade setting angle along its length are shown in Figure 3-2, and the maximum projected (planar) area of the blade has been computed to be 18.0 m^2.

The MOD-0A (composite) blade is made from a fiberglas-epoxy laminate and consists of two parts: a truncated conic section forming the leading edge of the blade and a fairing making up the trailing edge (see Figure 3-3). The

Dr. Spera disputes this description is wrong!

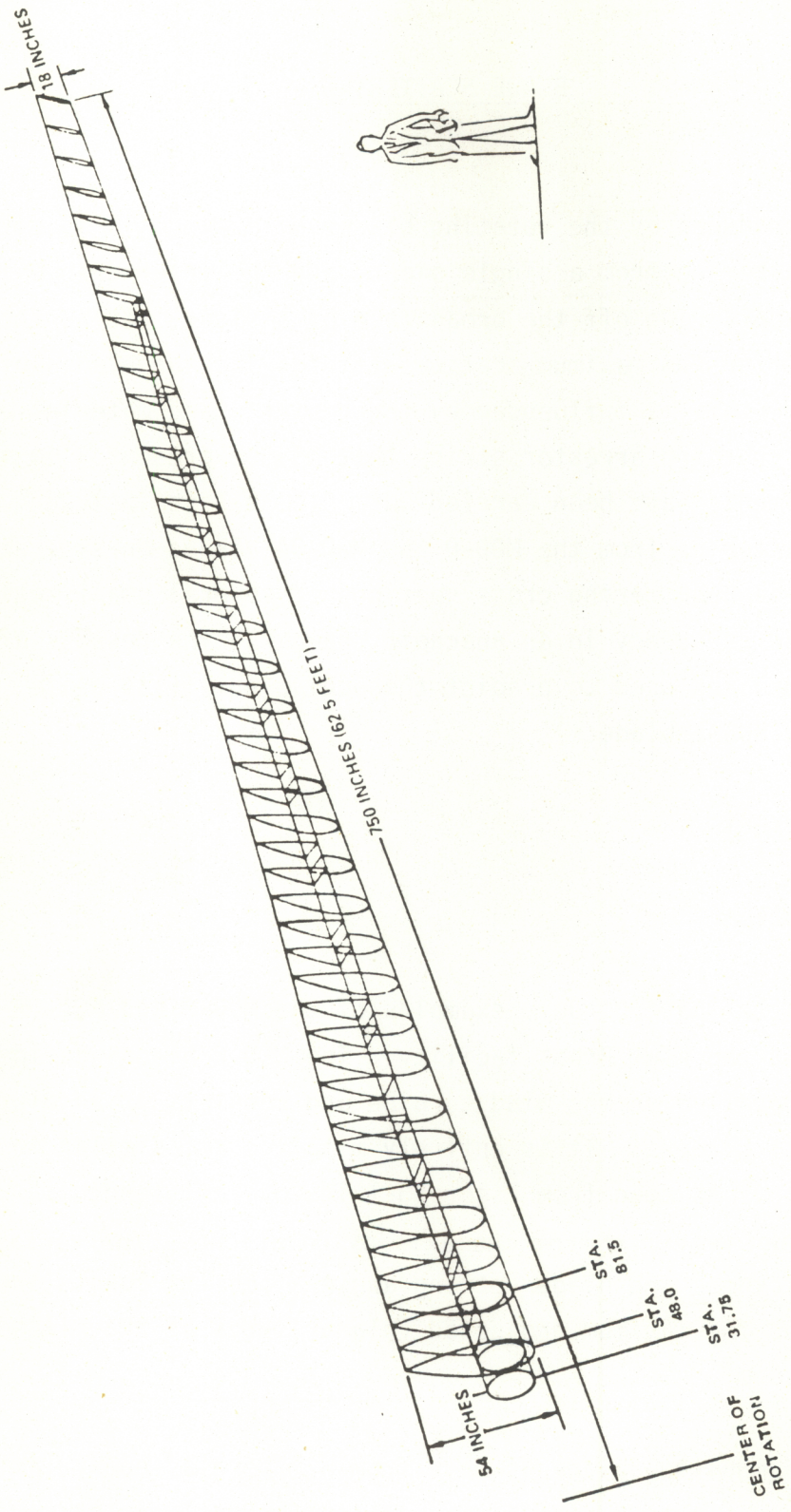

Figure 3-1: The MOD-0 blade.

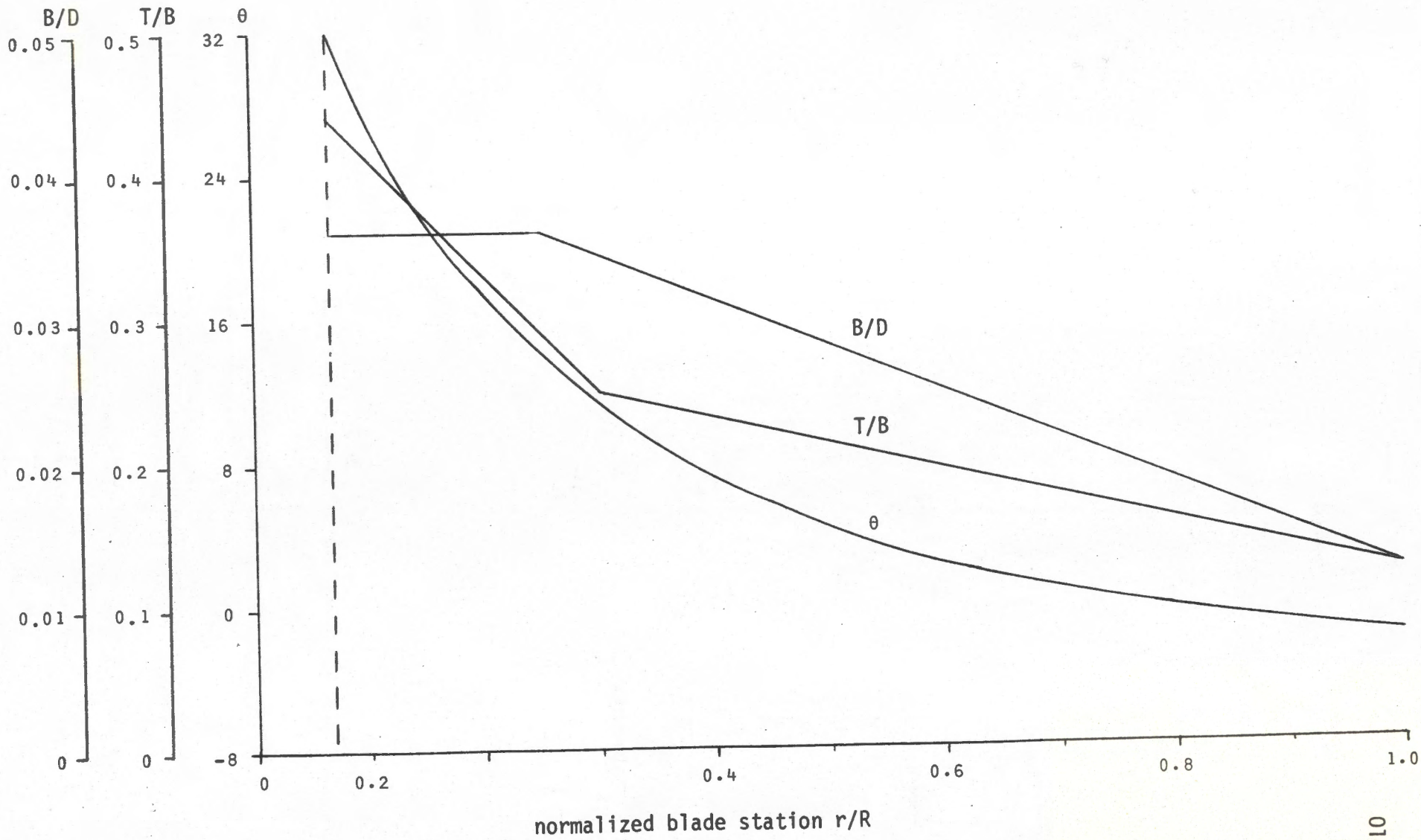

Figure 3-2: MOD-0 blade parameters B/D, T/B and θ vs. the non-dimensional blade station r/R where B is the blade width, D = 2R = 125 feet is the rotor diameter, T is the blade thickness and θ (in degrees) is the blade twist.

014438-2-F

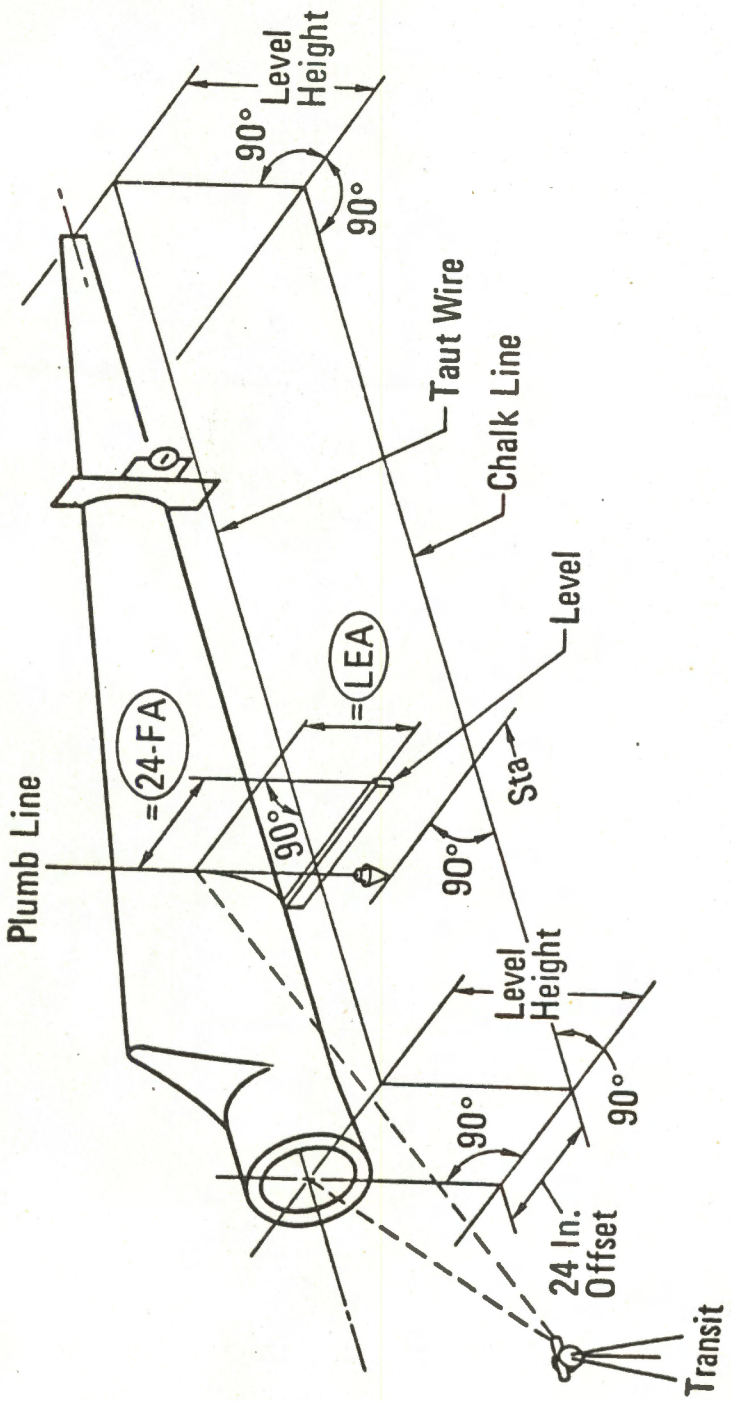

Figure 3-3: The MOD-0A blade.

thickness of the laminate is 0.5 inches and each section of the blade is hollow. The cone is about 60 feet long, and its base and truncated tip diameters are 3 and 0.5 feet respectively. The fairing is shaped somewhat similarly to the MOD-0 blade, but as seen from Figure 3-4, the actual distributions of chord, blade thickness and blade setting angle are different. The maximum projected area is estimated to be 18.0 m^2.

The blade is attached to the turbine hub by a metallic cylinder 3 feet in diameter and 1 foot long protruding from the end of the conic section. It should be noted that the cylinder was present on the blade used in our scattering measurements and, in addition, there were a number of strain gauge wires attached to the blade and covering an area approximately 30 feet by 1 foot.

3.1.2 Experimental Procedures

Using a local UHF TV transmitter as a source, the received field in the vicinity of a horizontally oriented blade was recorded as a function of time as the blade was slowly rotated in a horizontal plane. The blade was positioned with its leading edge parallel to the ground and the tip vertical, and was held in place at a height of 50 feet above the ground using a crane. Figure 3-5 is a photograph of the MOD-0 blade suspended from the crane. Ropes were attached at the root and tip, and these were pulled in a circle by two men to produce a manual rotation of the blade with the leading edge of the blade kept horizontal. The RF signal sources were the TV Channel 43 transmitter in Cleveland, 79.7 km away, and the Channel 24 transmitter in Toledo, 65.3 km away, whose (audio) frequencies are 649.75 and 535.75 MHz respectively. The receiving antenna was of the standard commercial type and was placed 17 feet above the ground (see Figure 3-6). The measured antenna pattern at a frequency of 600 MHz is shown in Figure VI.8 of [1] and during the experiments the main beam of the antenna was directed towards the test blade. A block diagram of the equipment used is given in Figure 3-7.

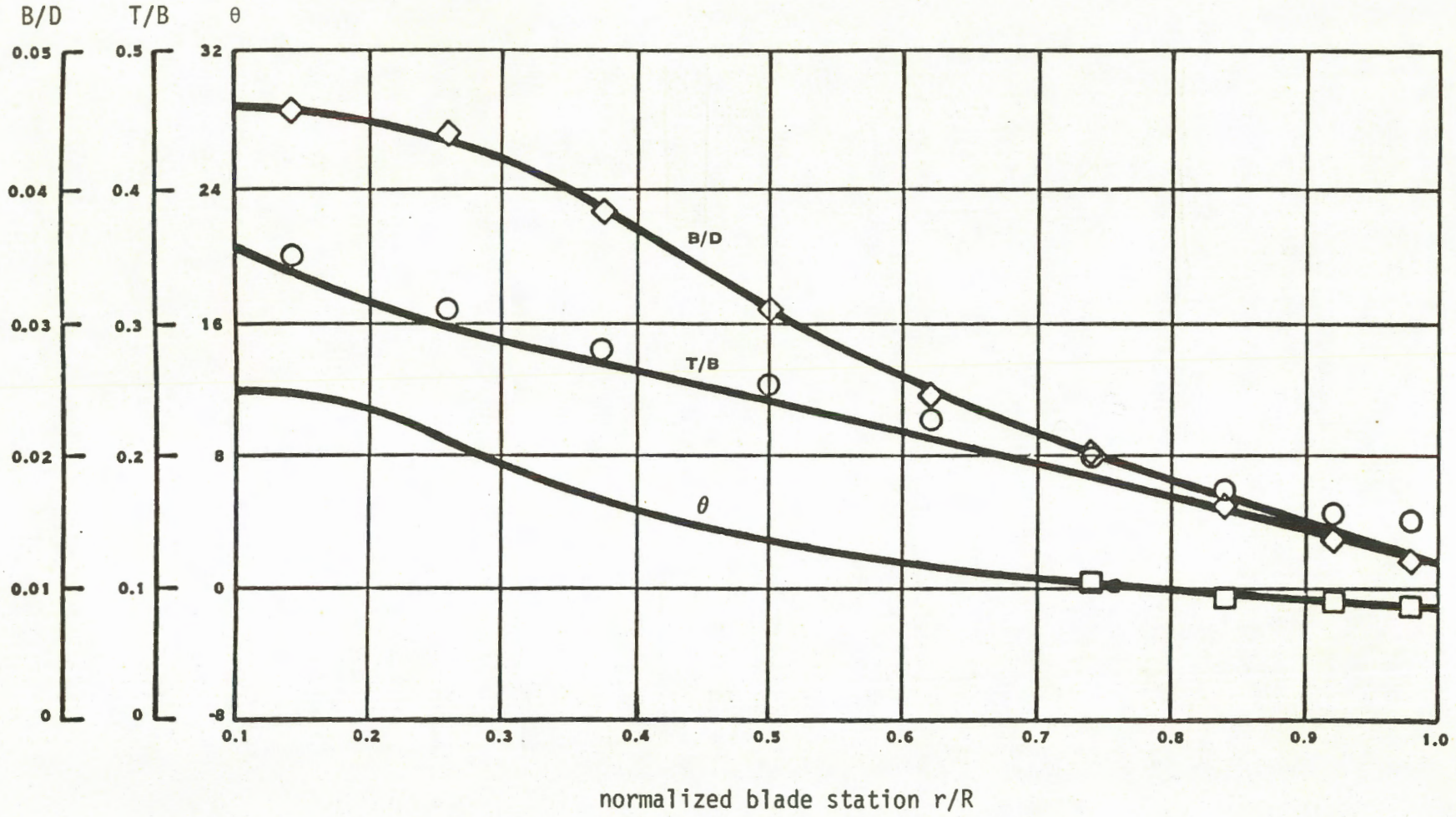

Figure 3-4: Theoretical (———) and measured (◊, ○, □) MOD-0A blade parameters, where the symbols are the same as in Figure 3-2.

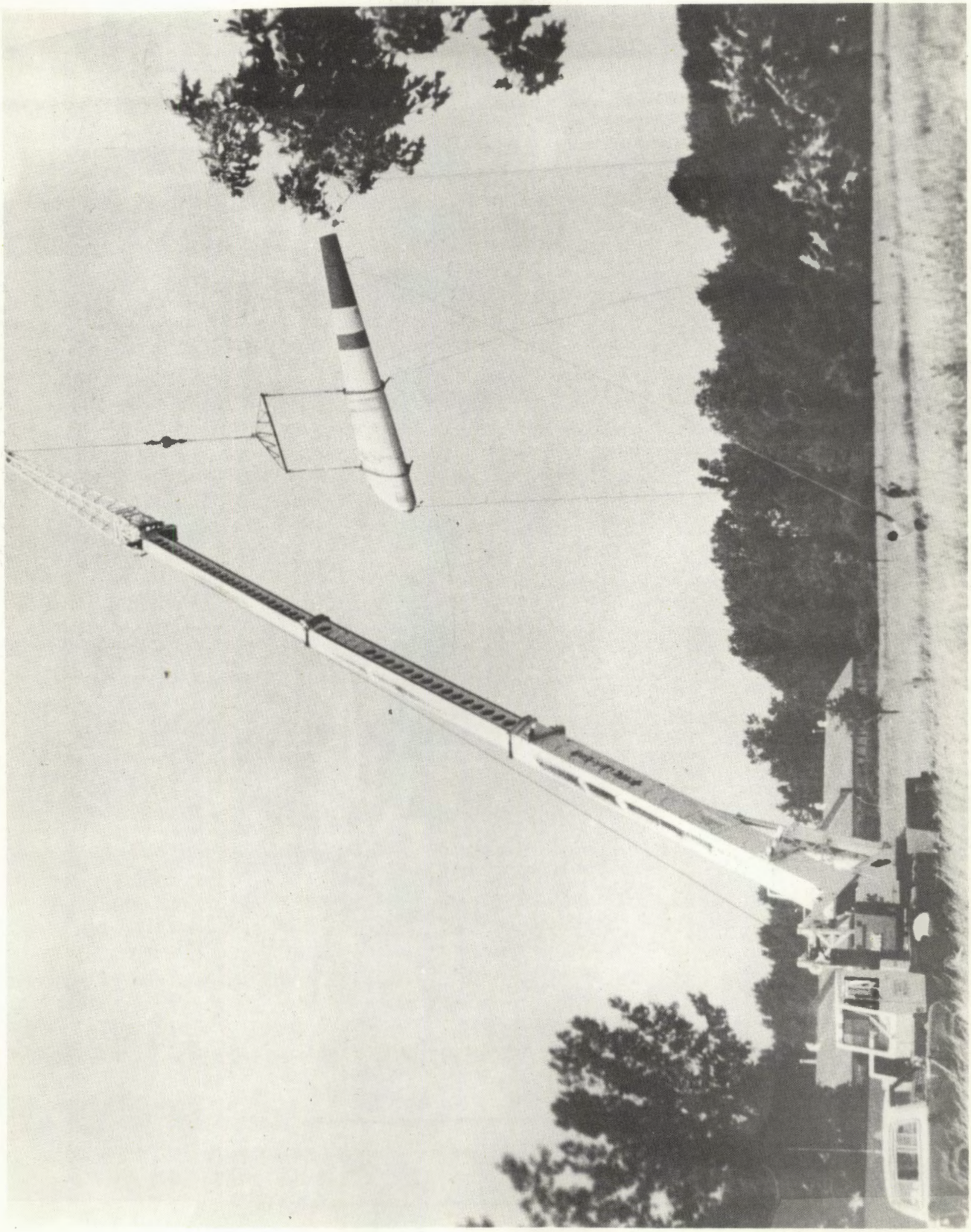

Figure 3-5: Photograph of the MOD-0 blade suspended from a crane.

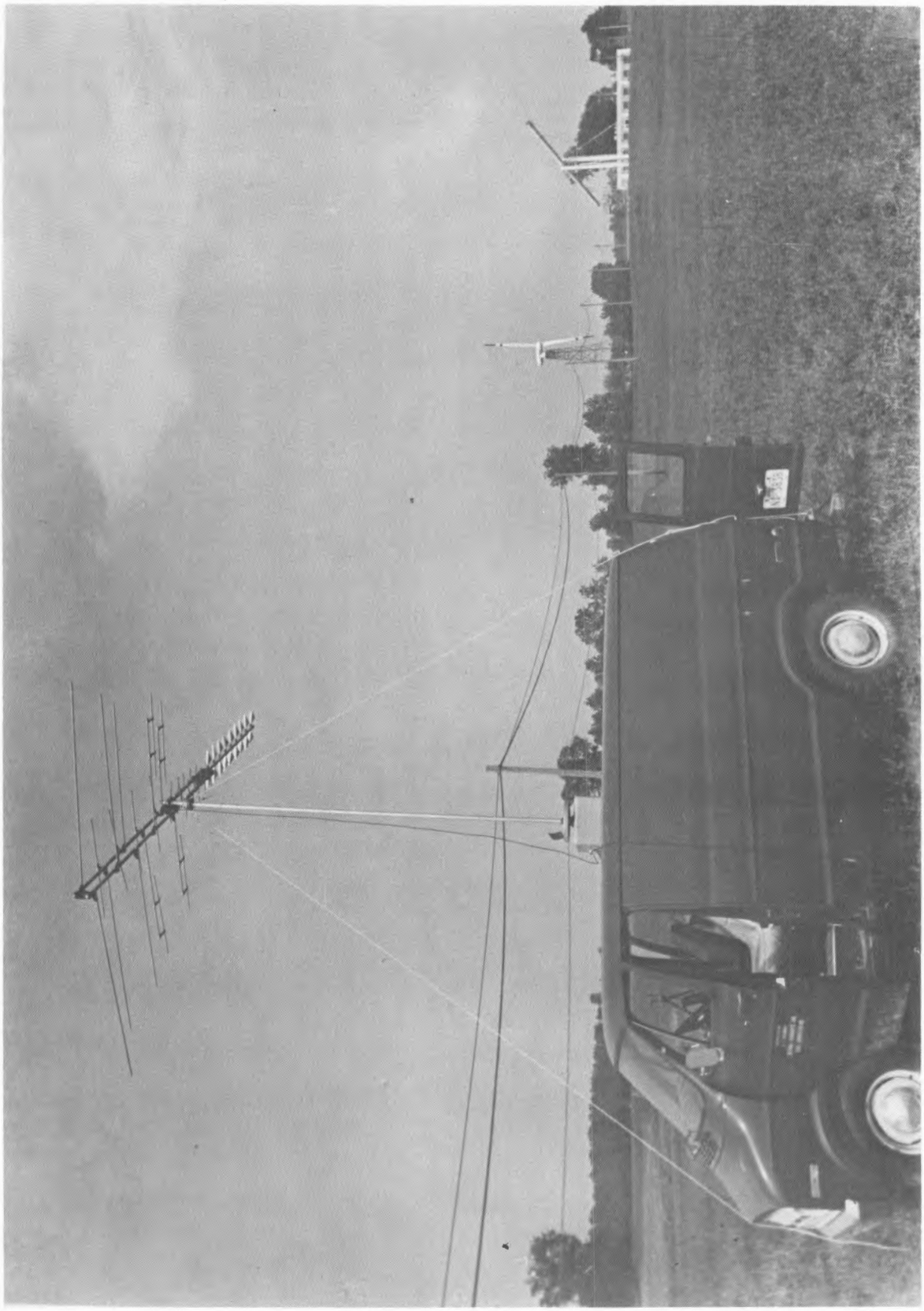

Figure 3-6: Receiving antenna arrangement used during the field tests at Plum Brook.

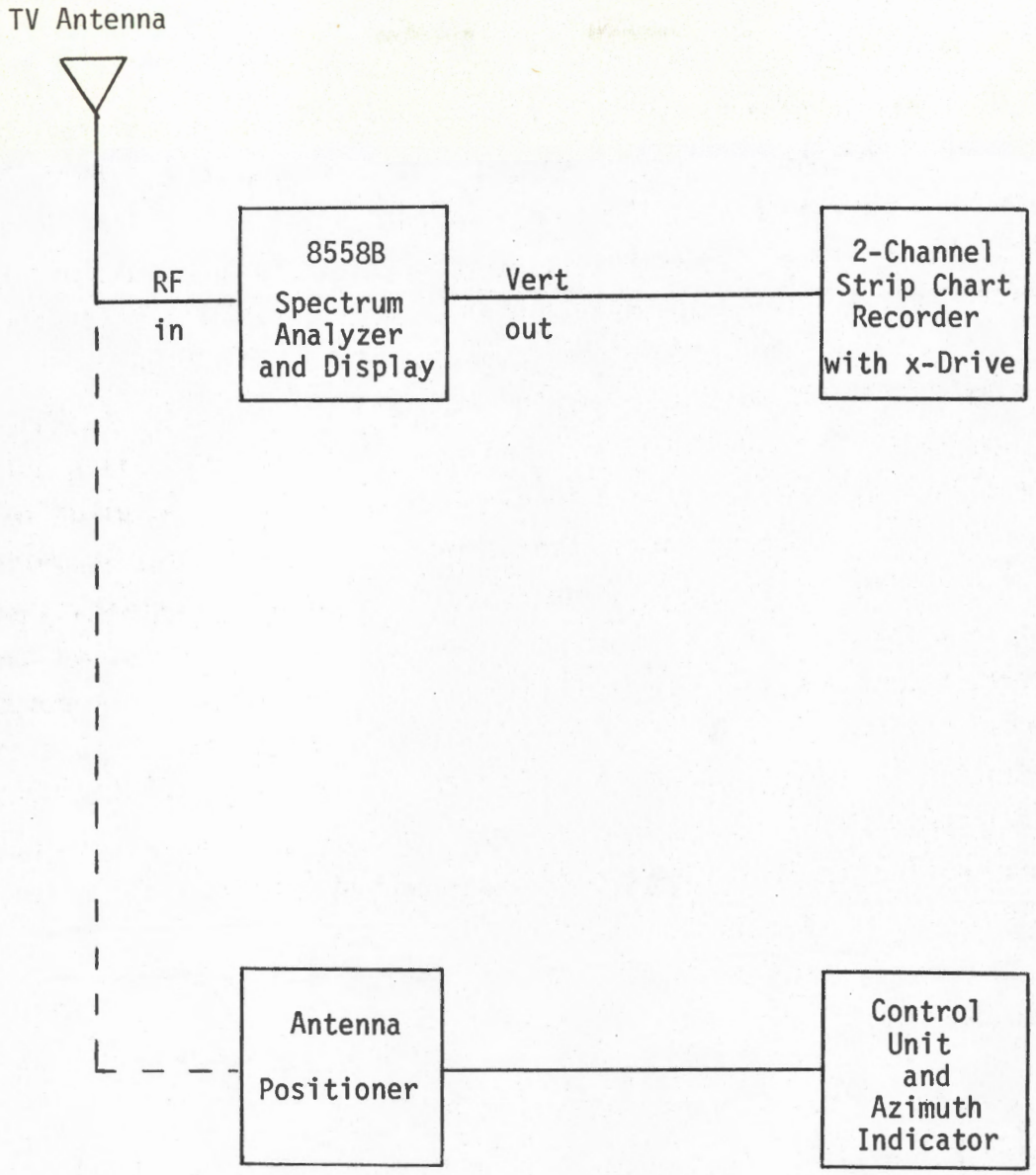

Figure 3-7: Block diagram of the field test equipment, mounted in and on a NASA van, with AC power supplied by a 25 Kw NASA generator.

Field tests in general are difficult to perform, and the present ones were no exception. For the scattered power to be interpreted as a scattering cross section it is necessary that the receiving antenna be in the far field of the scatterer, but in selecting the receiving site it was found impossible to satisfy the far field criterion and still obtain a scattered field of sufficient strength, particularly in the case of the composite blade. Ultimately, the two sites originally designated 9A and 9B were chosen, and the geometry of these sites is indicated in Figure 3-8. Erratic wind conditions also made it difficult to rotate the blade uniformly, and occasional gusts even caused the blade to swing like a pendulum, producing large changes in the scattered field received. In addition, the ambient RF signals on both channels were low and noisy, leading to variations in the levels of the received signal which sometimes masked the fields scattered from the blade. The problem was most serious with the composite blade whose scattering is small, and the only test where we were able to positively identify the scattering from this blade was that using Channel 24 at site 9A. Fortunately, the data obtained then are sufficient to determine the scattering from the blades at 535.70 MHz, and we shall confine attention to this one case.

3.1.3 Measured Data

Figures 3-9(a) and (b) show the received signals on Channel 24 at site 9A as functions of time for the MOD-0 and MOD-0A blades respectively, and are typical of the data obtained. The variations in the signal levels during the time intervals marked A-A are due to scattering from the blade as it rotated through the position for specular scattering to the receiving antenna, and as seen from the traces, the metallic and composite blades produce deviations in the signal of 12.5 and 5.0 dB respectively. The scattering cross sections and, hence, the scattering efficiencies of the blades can now be determined.

We present the details of the calculations only for the MOD-0 blade. From Figure 3-9(a) the field strength deviations above (Δ_1) and below ($-\Delta_2$) the ambient level are 5.5 and -7.0 dB respectively, and the modulation index m is then given by [1]

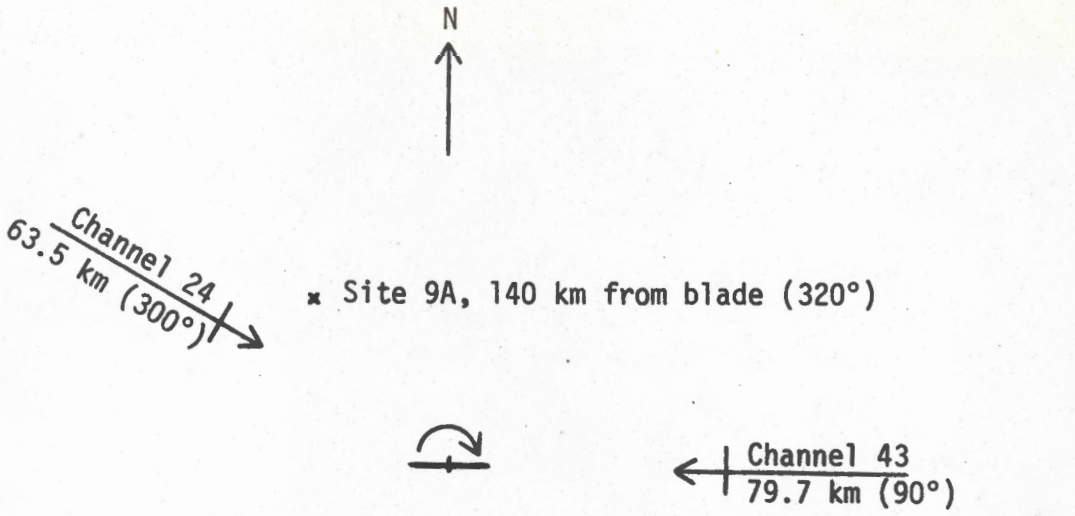

Figure 3-8: Geometry of the test sites. Angles are measured clockwise from North.

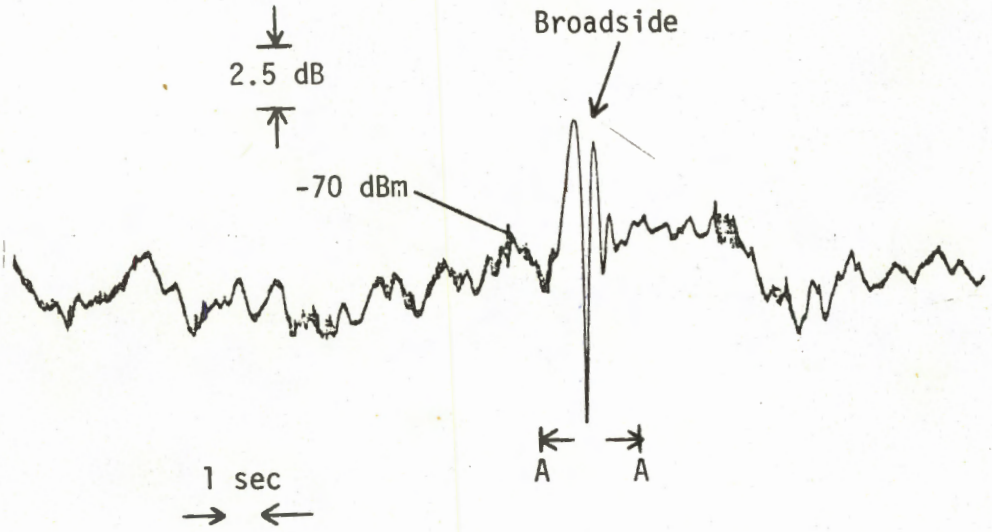

Figure 3-9(a): Observed MOD-0 blade scattering on Channel 24 at site 9A.

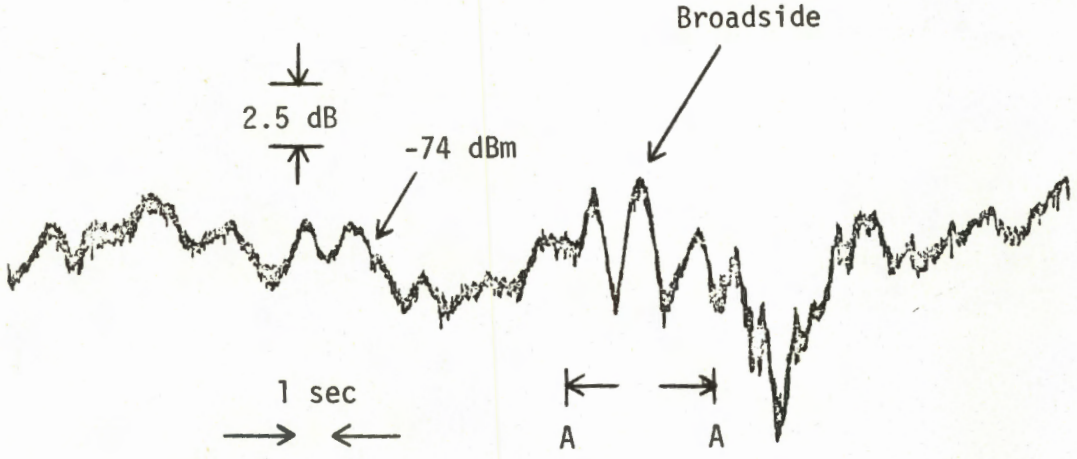

Figure 3-9(b): Observed MOD-0A blade scattering on Channel 24 at site 9A.

$$20 \log_{10} \frac{1 + m}{1 - m} = \Delta_1 - \Delta_2 , \tag{3.1}$$

yielding m = 0.62.

Were the scattering taking place in free space with the scattered field strength E^s measured at a large distance R from the blade, the scattering cross section would simply be

$$\sigma = 4\pi R^2 \left(\frac{E^s}{E^i}\right)^2 , \tag{3.2}$$

where E^i is the incident field strength at the blade, and insofar as this is the same as the ambient field strength at the receiving antenna,

$$\sigma = 4\pi R^2 m^2 . \tag{3.3}$$

For a perfectly conducting flat plate of area A_e, the backscattering cross section in the specular direction (i.e., broadside) is

$$\sigma = 4\pi A_e^2/\lambda^2 , \tag{3.4}$$

and the equivalent scattering area of the blade is

$$A_e = m\lambda R . \tag{3.5}$$

The scattering efficiency η defined as

$$\eta = \frac{\text{equivalent area } (A_e)}{\text{projected area } (A_p)} \tag{3.6}$$

is therefore

$$\eta = m\lambda R/A_p . \tag{3.7}$$

To make use of these formulas it is necessary to apply three corrections to the modulation index obtained from Figure 3-9(a) two of the corrections being associated with the presence of the earth, and the third arising because of the directive antenna employed in the measurements. It will be recalled that the incident (ambient) field strength was measured at the receiving antenna and not at the blade location, but we can deduce the latter from the former on the assumption of a locally plane earth with reflection coefficient -1 appropriate to horizontal polarization. Since the separation R of the two places is small compared with the distance to the transmitter, it follows that

$$E^i(B) \simeq \frac{h_B}{h_R} E^i(R)$$

where h_R and h_B are, respectively, the heights above ground of the receiving antenna and the center of the blade. In addition, the ground affects the scattered signal received from the blade, and compared with the strength E^s in free space

$$E^s(R) = \xi E^s$$

with

$$\xi = \left| 2\sin\left(\frac{2\pi h_B h_R}{\lambda R}\right) \right| ,$$

where we have again made use of the same assumptions regarding the earth. Finally, there is the effect of the pattern factor $f(\alpha)$ of the receiving antenna (see [1], Figure VI-8). Since the antenna was directed towards the blade, the measured ambient field strength is lower than its true value by a factor $f(\alpha)$ with $\alpha = 20°$, and the net result of all three corrections is to multiply the modulation index m appearing in (3.3), (3.5) and (3.7) by

$$\frac{h_R}{h_B} \frac{f(\alpha)}{\xi}$$

Since $h_R = 5.2$ m , $h_B = 15.2$ m ,

$R = 140$ m , $\lambda = 0.56$ m

and $f(\alpha) \simeq -22$ dB $= 0.0794$

we have

$$\frac{h_R}{h_B} \frac{f(\alpha)}{\xi} = 0.265$$

and for the measured modulation index m = 0.62, the equivalent scattering area of the MOD-0 blade is, from (3.5)

$$A_e = 12.9 \text{ m}^2$$

Its scattering efficiency is therefore $\eta = 72$ percent.

For the MOD-0A blade the measured signal deviation implies a modulation index m = 0.28, and since the measurement conditions were identical to those described above, it now follows immediately that for the fiberglas blade

$$A_e = 5.8 \text{ m}^2 \quad \text{and} \quad \eta = 33 \text{ percent} ,$$

corresponding to a scattering cross section which is 6.9 dB below that for the metal blade. This last figure is believed reliable, but for the individual blades the deduced values of the equivalent scattering area are quite sensitive to the assumptions made concerning the ground, and to the height of the receiving antenna. It was therefore felt desirable to seek confirmation of the values from measurements on scale model blades under the (simulated) free space conditions that an anechoic chamber provides.

3.2 Scale Model Measurements

The measurements were all performed in an anechoic chamber 50 feet long, 30 feet wide and 15 feet high at a frequency of 12.18 GHz for which the wavelength is λ = 2.461 cm. A block diagram of the equipment is given in Figure 3-10. The test object was placed on a styrofoam pedestal and illuminated with a horizontally polarized electromagnetic wave, and the backscattering cross section was recorded as the pedestal was rotated through 360 degrees. Calibration was with respect to either a 14 or 10-inch diameter sphere whose backscattering cross sections at 12.18 GHz are 9.84×10^{-2} m^2 and 5.09×10^{-2} m^2 respectively.

As an initial test, data were obtained for metallic (aluminum) and wooden rectangular plates 18 x 1 x 1/8 inches in dimension at a range of 40 feet using the 14 inch sphere for calibration. The backscattering cross section of the metallic plate over a 60° range embracing the broadside peak is shown in Figure 3-11. The peak (specular) return is 14.7 dB above that of the sphere, implying σ_m = 2.88 m^2. The equivalent scattering area of the plate is therefore

$$A_e = \lambda \sqrt{\frac{\sigma_m}{4\pi}} , \qquad (3.8)$$

giving $A_e = 1.18 \times 10^{-2}$ cm, which is in excellent agreement with its physical area of 1.16×10^{-2} m^2. The corresponding pattern for the wooden plate is shown in Figure 3-12, and we observe that its broadside return is 11.3 dB below that for the aluminum plate.

The above measurements were made with the plate and, hence, the calibrating sphere quite close to the back wall of the anechoic chamber to obtain the maximum range available to us. Unfortunately this made it difficult to keep the room in balance as the plates were rotated and, in addition, produced a sphere return which varied by more than $\pm$ 1 dB as the sphere was rocked back and forth. The problem proved particularly troublesome when scale model blades were employed, and after much trial and error it was found that the only way to reduce

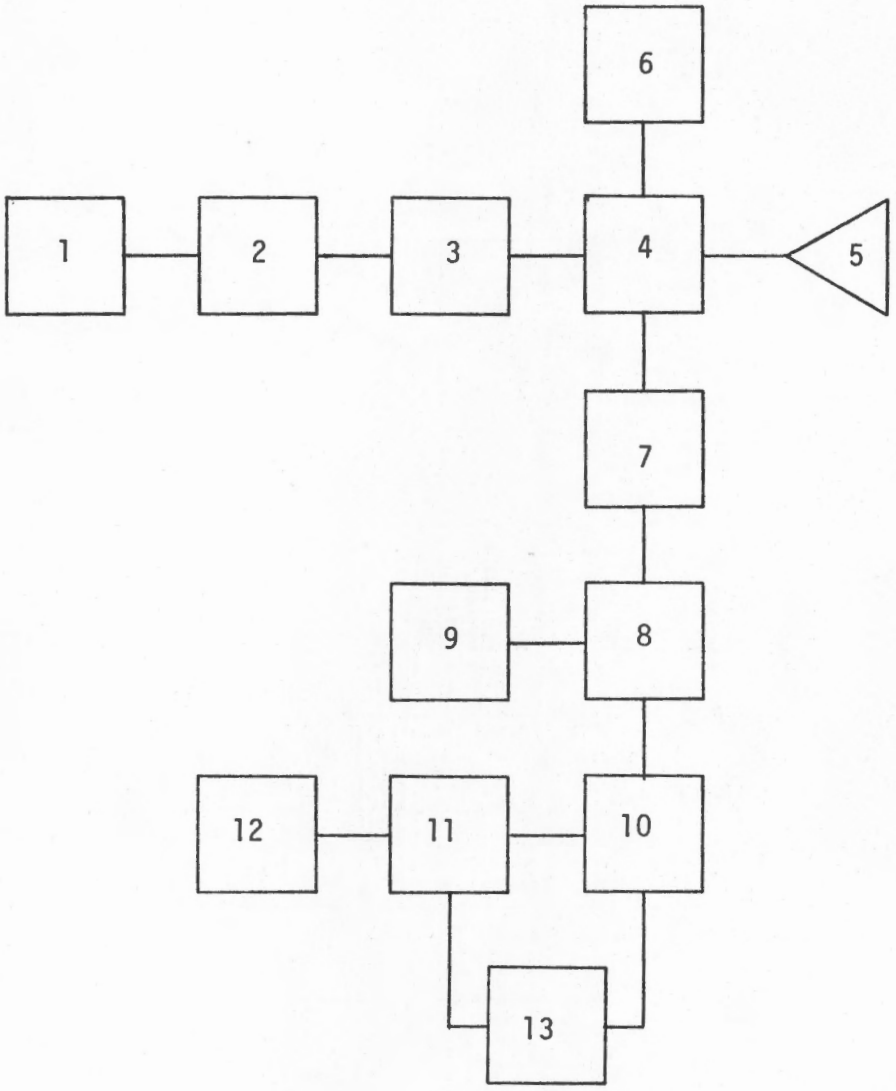

Figure 3-10: Block diagram of the scale model test equipment, where: 1 - short, 2 - attenuator, 3 - phase shifter, 4 - magic tee, 5 - horn, 6 - receiver, 7 - attenuator, 8 - directional coupler, 9 - frequency meter, 10 - directional coupler, 11 - stabilizer, 12 - klystron power supply, 13 - klystron.

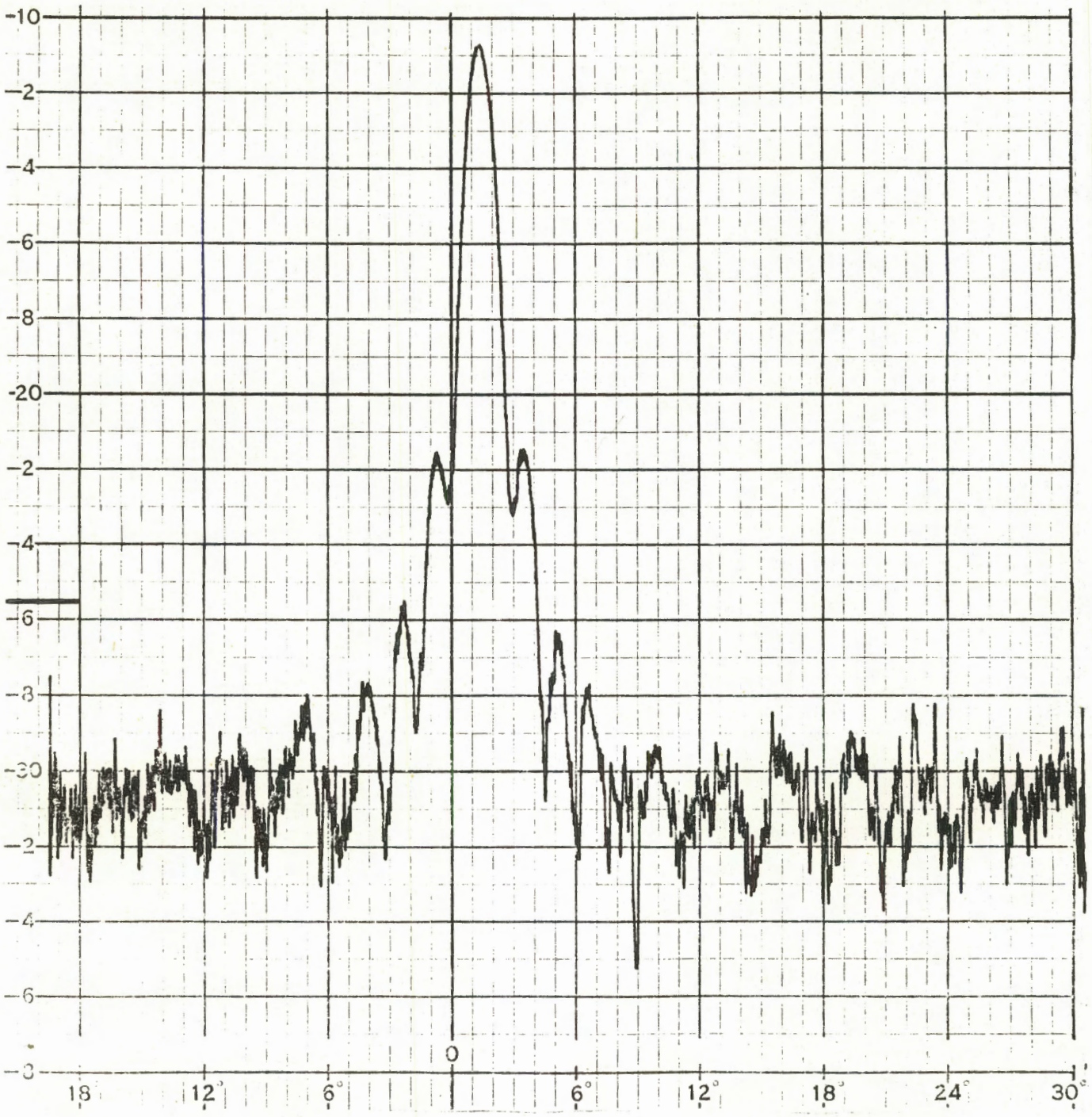

Figure 3-11: Backscattering pattern of the rectangular metallic plate.

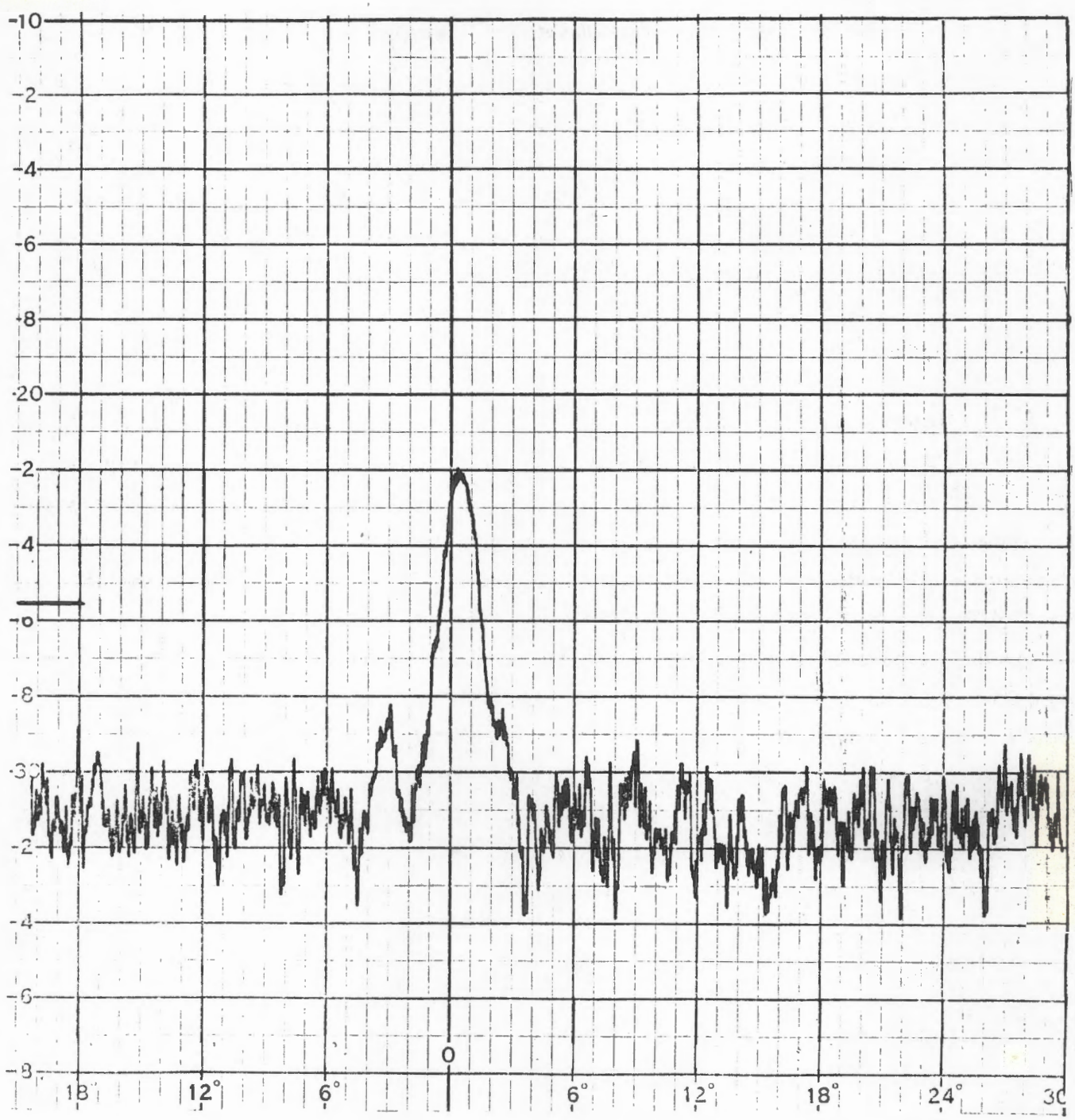

Figure 3-12: Backscattering pattern of the rectangular wooden plate.

the variations to an acceptable level was to increase the distance from the back wall to about 18 feet, thereby decreasing the range at which the measurements were made, and all of the blade data reported here were obtained at a range of 30 feet. This is about D^2/λ where D is the blade length, and the fact that it is less than the far zone distance by a factor 2 could lead to a decrease in the broadside scattering by as much as 0.5 dB.

3.2.1 Model Data

Three model blades were made, all 47.5 cm long and (nominally) 1:37.5 scale versions of the MOD-0 and MOD-0A blades. The MOD-0 model was cut from a block of wood and, to facilitate construction, was made with linear variations of blade thickness and twist from root to tip. The model was then coated with conducting (silver) paint. The second is also a model of the MOD-0 blade but was machined from a piece of G-10 laminated fiberglas (Pontiac Plastics, Inc.). Although intended to be identical in size to the previous one, its chord is somewhat greater close to the root. We shall refer to this as the MOD-0(FG) blade. The third blade is made of G-10 laminated fiberglas as well, and is a model of the MOD-0A blade. It was constructed to follow as closely as possible the blade-width variation specified by the B/D curve in Figure 3-4, but for simplicity linear approximations to the blade thickness and twist were adopted. Figure 3-13 is a photograph of the three blades. Their projected areas were measured by placing the models on sheets of graph paper and tracing round them with a pencil. The areas are as follows:

$$\begin{aligned} &\text{MOD-0} &&: A_p = 1.26 \times 10^{-2}\ m^2 \\ &\text{MOD-0(FG)} &&: A_p = 1.35 \times 10^{-2}\ m^2 \\ &\text{MOD-0A} &&: A_p = 1.36 \times 10^{-2}\ m^2 \end{aligned}$$

and the values are believed accurate to about one percent. From [2] the complex relative permittivity ε_r of laminated fiberglas at frequencies near 10 GHz is 4.37 + i0.16, giving rise to a power reflection coefficient $|\Gamma|^2$ = -9.0 dB. It is expected that a thin 'slab' of fiberglas such as a blade

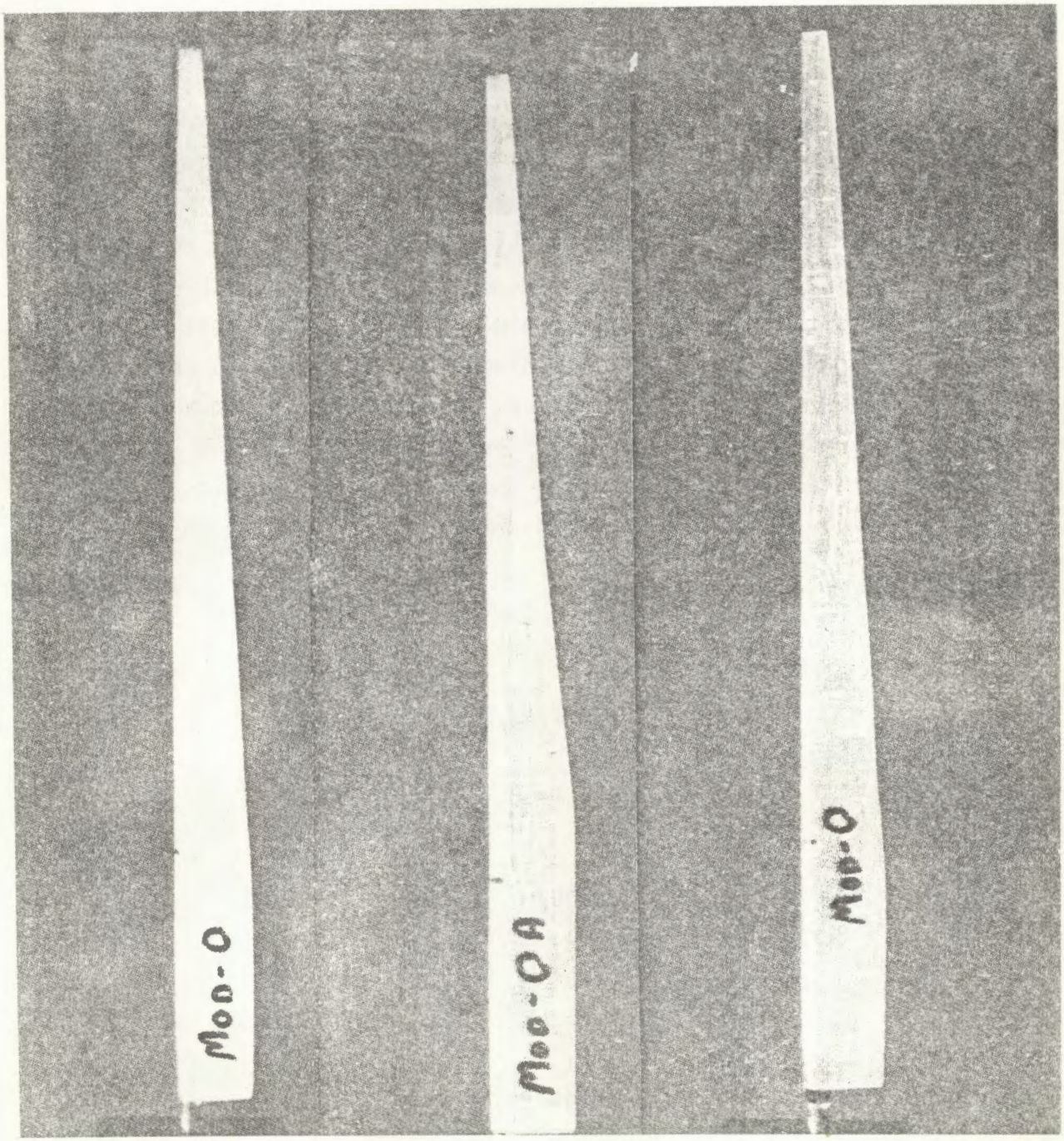

Figure 3-13: Photograph showing the scale models of MOD-0, MOD-0A and MOD-0A(FG) blades. The two on the right are fiberglas and the one on the left is metal coated.

would have a reflection coefficient somewhat different from this, and we also remark that ε_r shows only a few percent variation on decreasing the frequency to 100 MHz.

The peak 'broadside' cross sections of the blades are quite sensitive to their orientation. To ensure that the maximum backscattering cross sections were recorded, each blade was placed on top of the styrofoam support pedestal with its central chord vertical, and then adjusted in azimuth as well as rotation about its axis until the maximum return was observed. A pattern was now measured using horizontal polarization as the pedestal was rotated through 360°. Calibration was with respect to the 10-inch diameter sphere. The patterns for the three blades are shown in Figures 3-14 through 3-16, and it will be observed that because of the MOD-0 blades' twist, the peak returns on viewing the blades 'from the back' are substantially less than the maximum cross section σ_m. From a knowledge of σ_m, the equivalent scattering area A_e can be calculated using (3.8), and the scattering efficiency deduced from (3.6). The data are summarized in Table 3-1.

Blade	σ_m (dB) rel. sphere	σ_m (m^2)	$A_e \times 10^3$ (m^2)	η
MOD - 0	14.6	1.47	8.44	0.670
MOD-0(FG)	7.7	0.300	3.81	0.282
MOD-0A	6.5	0.277	3.32	0.244

Table 3.1: Peak returns.

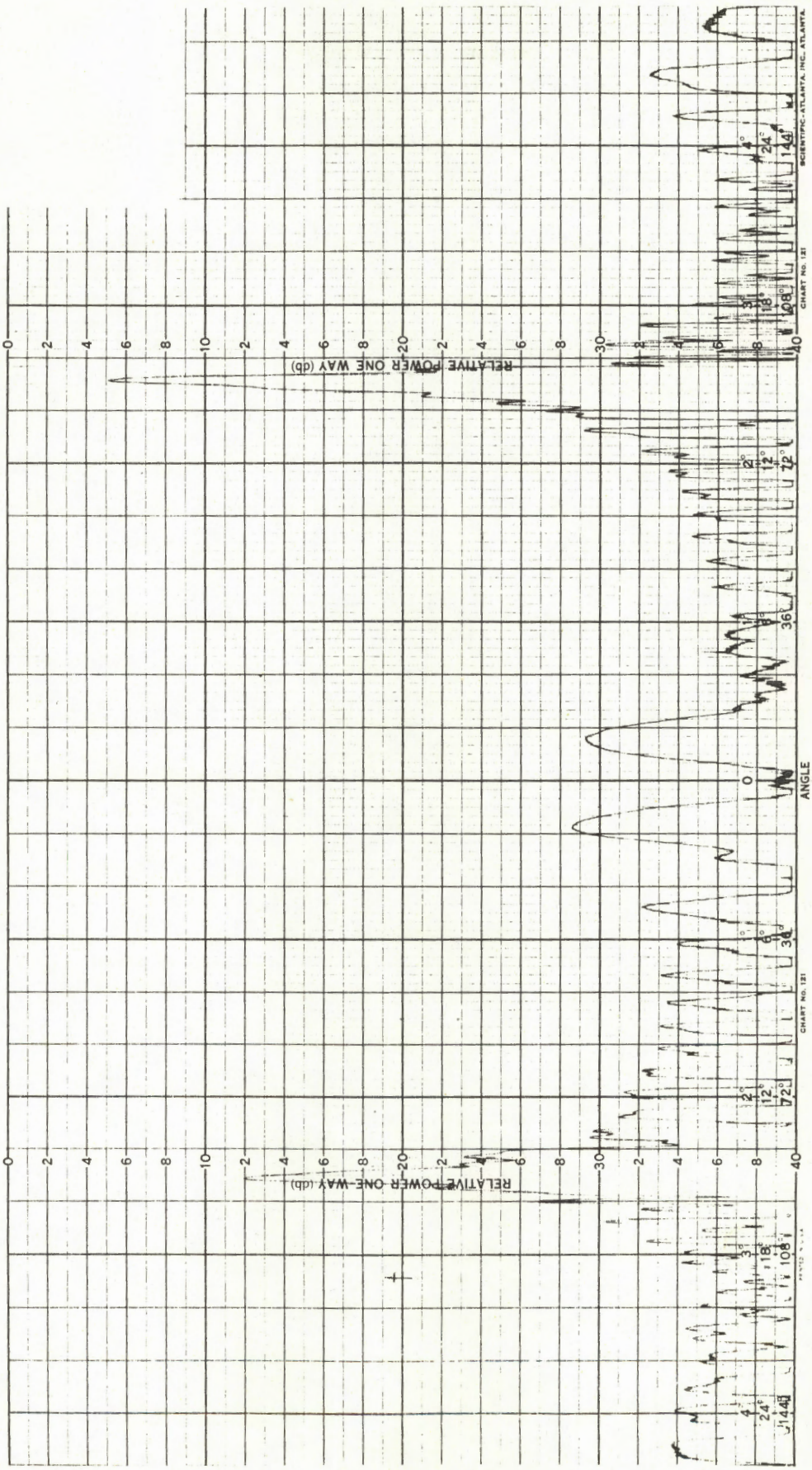

Figure 3-14: Maximum backscattering pattern of MOD-0 metal blade measured at 12.14 GHz.

014438-2-F

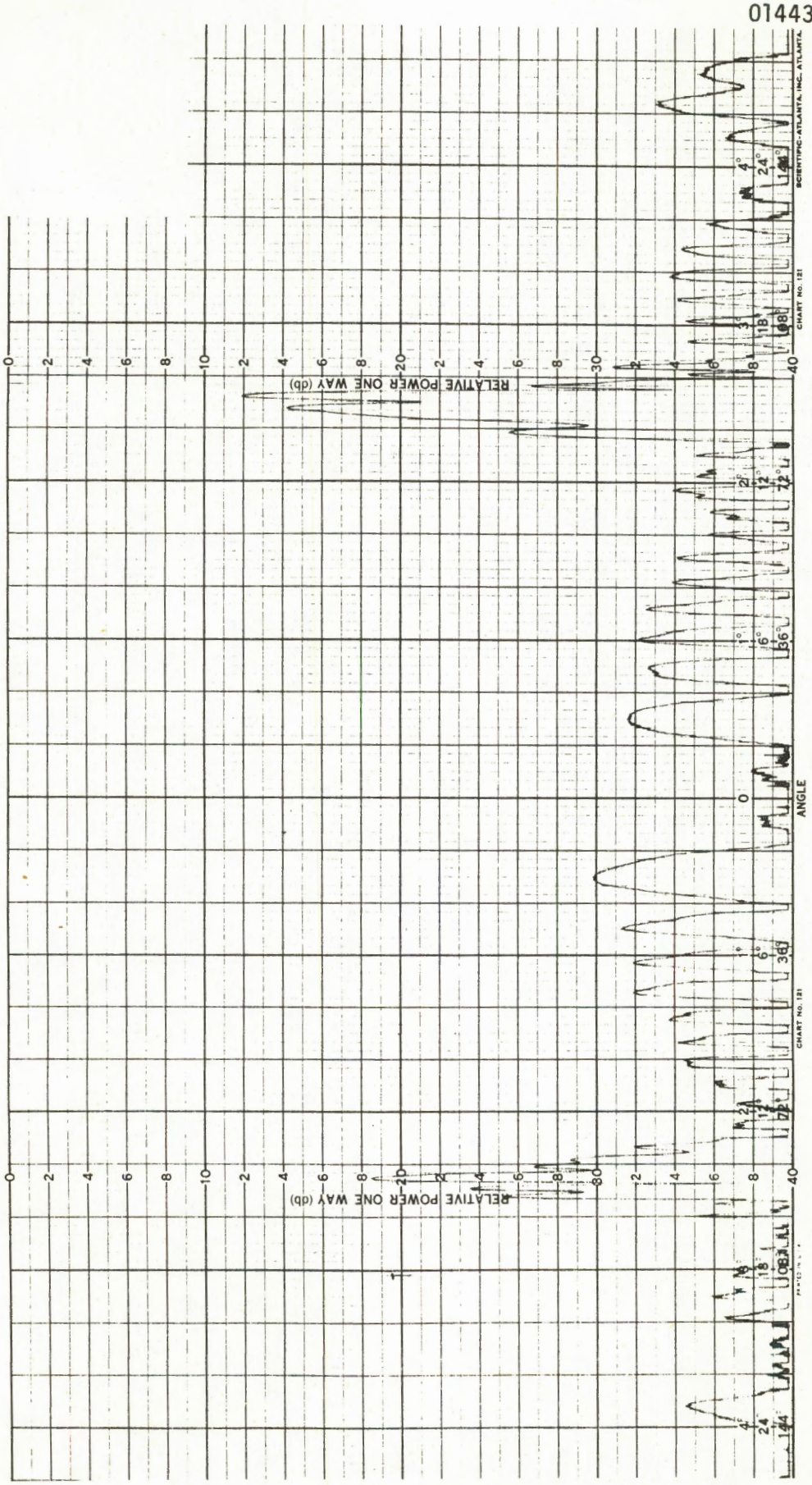

Figure 3-15: Maximum backscattering pattern of MOD-0(FG) fiberglas bladd measured at 12.14 GHz.

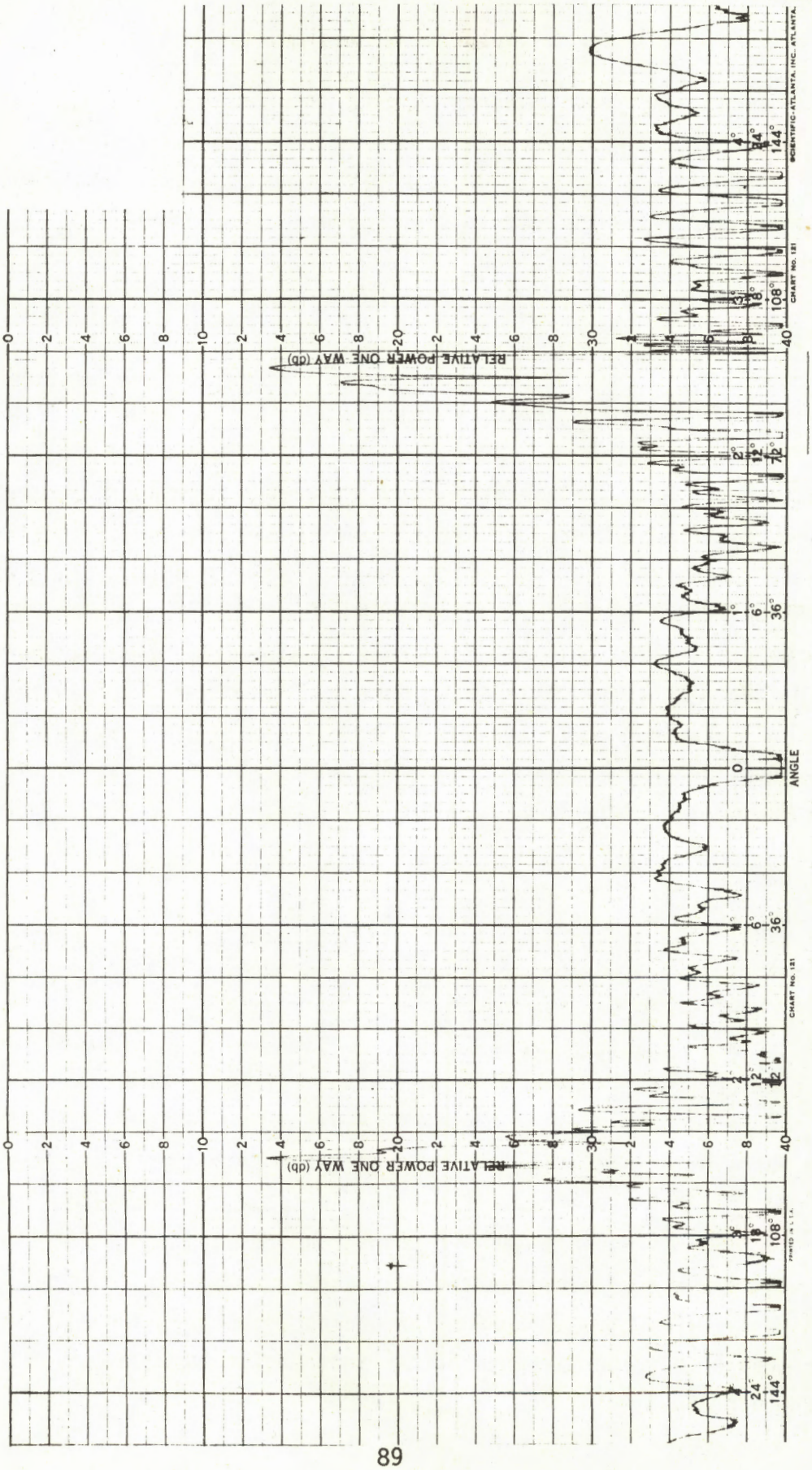

Figure 3-16: Maximum backscattering pattern of MOD-0A fiberglas blade measured at 12.14 GHz.

For the MOD-0 blade, η is within 5 percent of its value deduced from the field test at Plum Brook, a rather remarkable agreement. Comparison of the scattering efficiencies for the MOD-0 and MOD-0(FG) blades shows that the power reflection coefficient attributable to the fiberglas is $(0.282/0.670)^2 = -7.52$ dB. Using this same reflection coefficient we compute that a metal blade of the MOD-0A configuration would have a peak cross section $\sigma_m = 1.28\ m^2$ and a scattering efficiency $\eta = 0.587$.

3.2.2 Effect of Lightning Arrestor Strips

Because the MOD-0A blade is made of fiberglas (composite construction), it is necessary for the full scale blade to have some lightning protective device, and the scheme proposed [3] by the manufacturer (Hamilton Standard) is to attache 8-mil 6-inch wide aluminum tapes in the configuration shown in Figure 3-17. However, according to Mr. R.A. Wolf of NASA Lewis [4], it may be possible to get by with fewer tapes than those in Figure 3-17, and we therefore built up the full arrestor configuration in four stages, using 0.015-inch wide adhesive aluminum tape attached to the MOD-0A model. The tapes were, of course, applied to both sides of the blade, and the four stages are depicted in Figure 3-18.

At each stage the model was placed on the pedestal and adjusted in tilt and orientation to produce the maximum backscattering, and a pattern was then recorded showing the backscattering cross section for a full 360° rotation. The data for the peak scattering are summarized in Table 3.2, along with the corresponding values for the bare blade and a metallized version.

We observe that at stages Nos. 1 and 2 the maximum cross section is not much larger than for the blade without any arrestor tapes, whereas the addition of the two intermediate tapes and their associated bands greatly increases the scattering. Indeed, for the full configuration of tapes the scattering is only 0.2 dB less than for the analogous metal blade. It is therefore desirable that the tapes used for lightning protection not exceed those corresponding to stage 2.

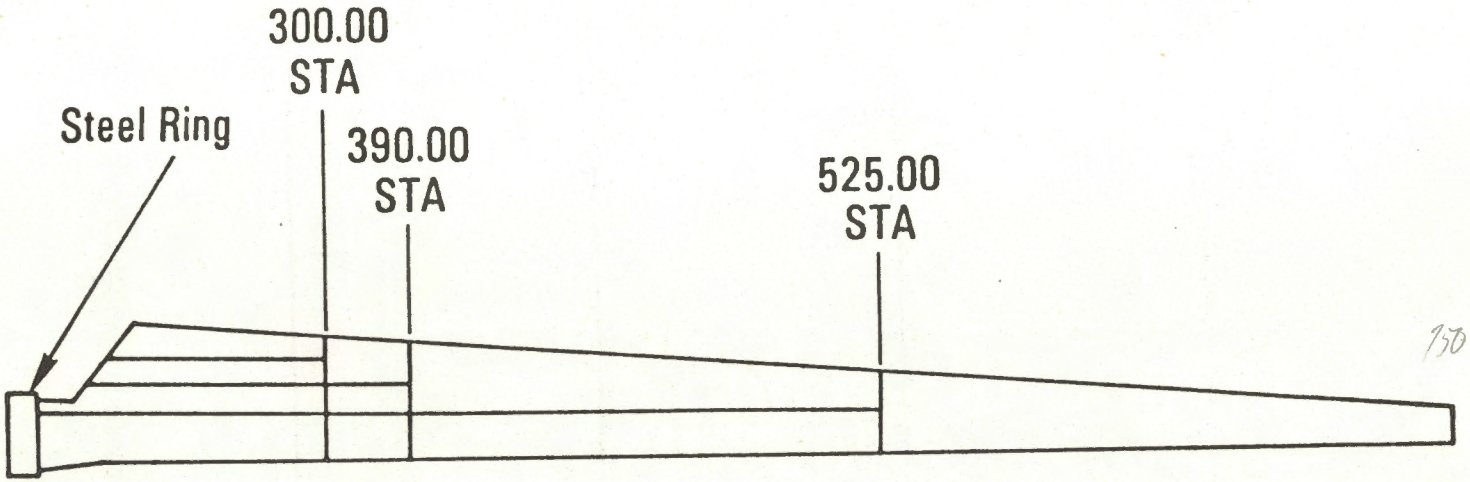

Figure 3-17: Lightning arrestor tape configuration [3].

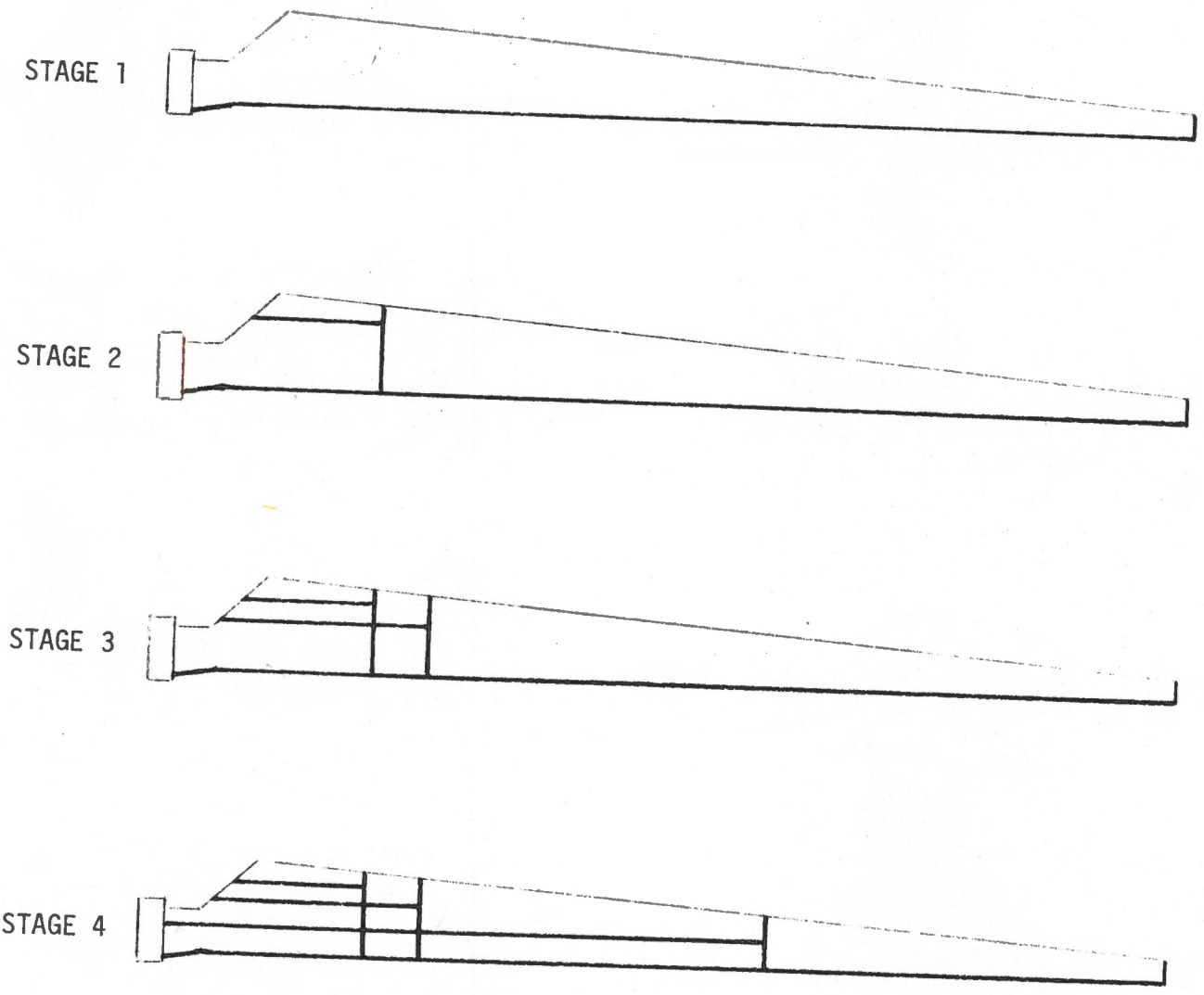

Figure 3-18: Tapes applied to model MOD-0A blade.

Stage	σ_m (dB) rel. sphere	σ_m (m^2)	$A_e \times 10^3$ (m^2)	η
Bare	6.5	0.227	3.32	0.244
#1	6.8	0.244	3.44	0.252
#2	7.2	0.267	3.60	0.265
#3	11.5	0.719	5.91	0.435
#4	13.8	1.22	7.70	0.566
Metal	----	1.28	7.88	0.587

Table 3.2: Data for various arrestor configurations.

3.3 Equivalent Scattering Areas

It is a trivial matter to determine the equivalent scattering areas of the full scale blades from a knowledge of their projected areas and the scattering efficiencies deduced from the model measurements. The results for the MOD-0 and MOD-0A blades, and for the MOD-0A blade with minimal (stage #2) lightning protection, are given in Table 3.3.

According to information supplied [5] by Mr. R.L. Puthoff of NASA Lewis, the MOD-1 blade (made of structural steel) is 1191 inches long (1210 inches from the center of rotation), with chord varying linearly from 144 inches at the root to 33.8 inches at the tip, and with a total twist of 11° distributed linearly over the span. The computed projected area is 62.5 m^2, and on the assumption of a scattering efficiency which is the average of those for the MOD-0 and (metallized) MOD-0A blades, its equivalent scattering area is as shown in Table 3.3. For all practical purposes, and certainly as regards the calculation of interference effects, it is sufficient to use the following values of A_e:

Blade	A_p (m^2)	η (%)	A_e (m^2)
MOD-0	18.0	67	12.1
MOD-0A	18.0	24	4.4
MOD-0A(#2)	18.0	27	4.8
MOD-1	62.5	63	39.4

Table 3.3: Equivalent scattering areas.

MOD-0 : 12 m^2
MOD-0A(#2) : 5 m^2
MOD-1 : 40 m^2 .

Since the range over which interference can exist is proportional to A_e, it is now obvious that the MOD-1 blade poses a substantially larger threat than either the MOD-0 or MOD-0A.

We have examined the possibility of reducing the scattering and, hence, A_e for the MOD-1 blade while maintaining its physical size. Apart from the size, the blade is similar to that of a helicopter, and in recent years considerable effort has been devoted to reducing the scattering from helicopter blades, albeit mostly for low angles of attack. If the metallic construction of the blade is retained, it would be necessary to apply some form of lossy coating that will reduce the power reflection coefficient through absorption, but because of the wide range of frequencies of interest here, and the relatively long wavelength ($\sim$ 30 cm) even at the highest frequency, a thin coating would have to be highly loaded to be effective. Since the entire surface of the blade must be covered to reduce the specular return, the weight penalty to achieve a cross section reduction of (say) 6 dB would be quite intolerable. We therefore see no possibility of significantly reducing the scattering efficiency of a metallic blade.

Were the MOD-1 blade constructed in a similar manner to the MOD-0A, its scattering efficiency would be about 7 dB lower when a (minimal) configuration of lightning arrestor strips was in place, and about 8 dB lower without any strips. Consistent with the retention of the blade's physical shape, the latter reduction is probably the largest that can be had, but we remark that since the power reflection coefficient of fiberglas is -9.0 dB, the insertion of some lossy material (e.g., a honeycomb structure with graded loading) into the hollow interior of the blade to suppress the contribution resulting from penetration through to the back surface could conceivably produce an additional dB. With a 9 dB reduction the scattering efficiency of the MOD-1 blade would be down to 22 percent, implying an equivalent scattering area of 14 m^2. This is little more than for the MOD-0 blade.

3.4 References

[1] Senior, T.B.A., D.L. Sengupta and J.E. Ferris (1977), "TV and FM Interference by Windmills", The University of Michigan Radiation Laboratory Report No. 014438-1-F.

[2] Harrington, R.F. (1961), "Time Harmonic Electromagnetic Fields", McGraw-Hill Book Co., Inc., New York; p. 452.

[3] letter dated 7 October 1977 from Mr. R.A. Wolf.

[4] telephone conversation with Mr. R.A. Wolf, 20 October 1977.

[5] telephone conversation with Mr. R.L. Puthoff, 6 December 1977.

APPENDIX 4: AMPLITUDE MODULATION OF ELECTROMAGNETIC SIGNALS BY SLOWLY ROTATING OBJECTS

4.1 Introduction

In a previous study [1] it was found that the signals scattered by the rotating blades of a windmill may combine with the direct signals to produce an amplitude modulated input signal to a TV receiver. Under some conditions the modulation waveforms appear in the form of repetitive pulses which, if sufficiently strong, produce video distortion on reception. It is therefore of interest to understand the nature of the amplitude modulation produced by the rotating blades of a windmill.

In general the modulation waveforms of the received signals are complicated functions of the windmill blade geometry, the rotation speed of the blades, and the directions of the transmitter and the receiver with respect to the windmill, and we present here the results of a theoretical and experimental study of the amplitude modulation produced by a slowly rotating object of simple shape. The scattering model employed is a rectangular metal plate which was found [1] useful before, but measured waveforms are also presented for rotating scale models of the MOD-0 windmill blade.

4.2 Rectangular Plate Analyses

4.2.1 Theory

We present here an approximate theory for determining the scattered far field when a plane electromagnetic wave is incident upon a rectangular metal plate in rotational motion. The approach taken is to first obtain an expression for the field scattered by a plate located in a fixed but arbitrary position, and then introduce the rotation by regarding the plate position as a function of time. Thus the field scattered by a rotating body is calculated

by assuming that at any given time it has the value corresponding to the instantaneous position of the body "frozen in its track" [2]. In the present case all material velocities are much less than the velocity of light, and also the rotation frequency is much less than the frequency of the incident electromagnetic wave. Under these conditions the approximation is known to yield accurate and meaningful results [2, 3].

At time t = 0 a rectangular metal plate of dimensions L_1 and L_2 is assumed located in the plane $\phi = \phi_s$ with its axis A-A' aligned along the z-axis of a rectangular coordinate system whose origin is at 0 (see Figure 4-1). The center of the plate is at 0 which is also the origin of a spherical coordinate system. The axis A-A' of the plate is now rotated in the x-z plane (i.e., around the y-axis) with angular frequency Ω such that at time t its position is as shown in Figure 4-2, where

$$\theta_s = \Omega t \ . \tag{4.1}$$

The plate is illuminated by a plane electromagnetic wave incident from the direction (θ_o, ϕ_o), with magnetic vector (in the z direction)

$$\vec{H}^i = \hat{z}\, H_o \exp\left[ik\left(x \sin\theta_o \cos\phi_o + y \sin\theta_o \sin\phi_o + z \cos\theta_o\right)\right] , \tag{4.2}$$

where H_o is the amplitude of the magnetic vector, and $k = 2\pi/\lambda$ is the propagation constant in free space. An r.f. time dependence $\exp(i\omega t)$ is assumed and suppressed.

According to the physical optics approximation, the surface current density at an arbitrary point on the illuminated side of the plate is

$$\vec{J}_s = 2\hat{n} \times \vec{H}^i \tag{4.3}$$

where $\hat{n}$ is the unit normal to the plate, with $\vec{J}$ zero on the shadow side. To obtain $\vec{H}^i$ in a form suitable for calculating the far zone scattered field,

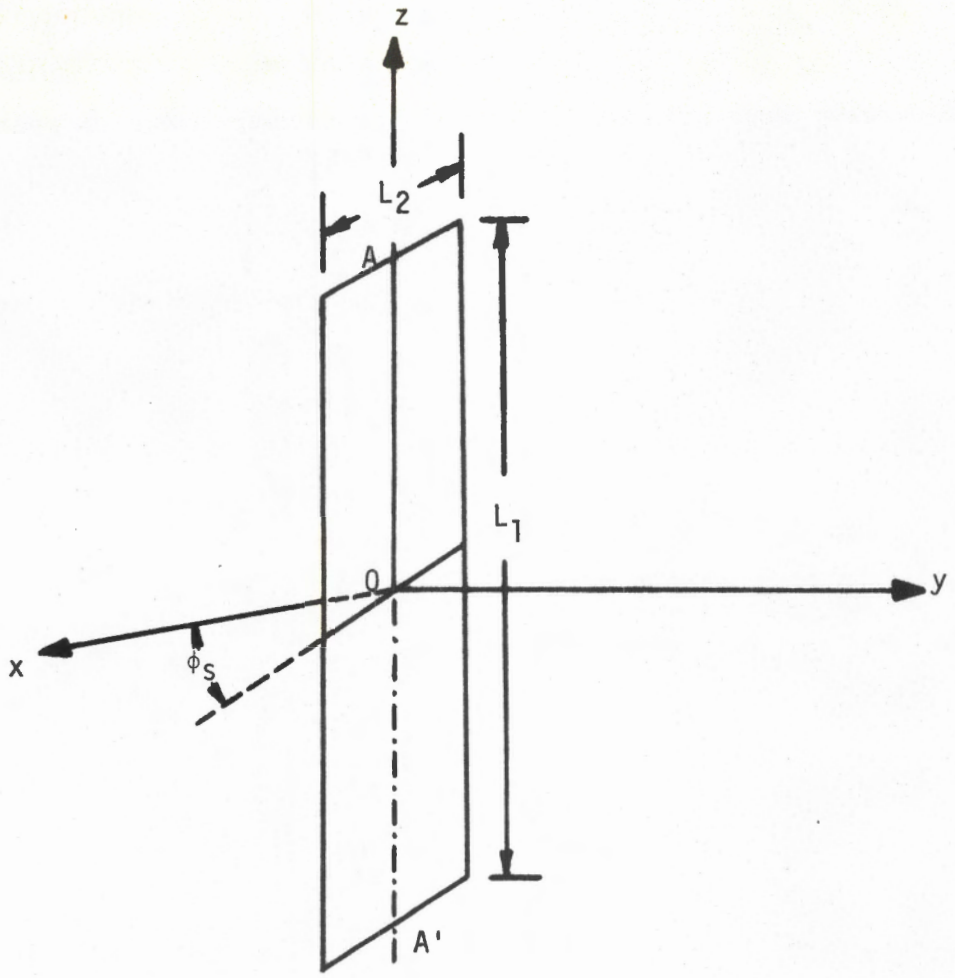

Figure 4-1: Skewed rectangular plate at time t = 0. The skew angle is ϕ_s.

we first perform a coordinate rotation about the y-axis in Figure 4-2. The new coordinate system (ξ, ν, η) is defined such that the η-axis is aligned along the axis A-A' of the plate at time t. The unit vectors in the two coordinate systems are related by the following:

$$\left.\begin{aligned} \hat{x} &= \hat{\xi} \cos\theta_o + \hat{\eta} \sin\theta_s \quad , \quad \hat{y} = \hat{\nu} \, , \\ \hat{z} &= -\hat{\xi} \sin\theta_s + \hat{\eta} \cos\theta_s \quad , \quad \hat{\xi} \times \hat{\nu} = \hat{\eta} \end{aligned}\right\} \tag{4.4}$$

and hence, from (4.2) and (4.4), the incident magnetic field is

$$\vec{H}^i = (-\hat{\xi} \sin\theta_s + \hat{\eta} \cos\theta_s) \exp\left[ik\,(\alpha\xi + \beta\nu + \gamma\eta)\right] \tag{4.5}$$

where

$$\left.\begin{aligned} \alpha &= \sin\theta_o \cos\phi_o \cos\theta_s - \cos\theta_o \sin\theta_s \quad , \\ \beta &= \sin\theta_o \sin\phi_o \quad , \\ \gamma &= \cos\theta_o \cos\theta_s + \sin\theta_o \cos\phi_o \sin\theta_s \quad . \end{aligned}\right\} \tag{4.6}$$

We now perform another coordinate rotation about the η-axis to obtain a coordinate system (x', y', z') such that the plate lies in x'z' plane with y'-axis normal to the plate. The (x', y', z') system is related to the (ξ, ν, η) system by

$$\left.\begin{aligned} \hat{\xi} &= \hat{x}' \cos\phi_s - \hat{y}' \sin\phi_s \quad , \\ \hat{\nu} &= \hat{x}' \sin\phi_s + \hat{y}' \cos\phi_s \quad , \\ \hat{\eta} &= \hat{z}' \\ \text{with} \quad \hat{x}' \times \hat{y}' &= \hat{z}' = \hat{\eta} \, , \end{aligned}\right\} \tag{4.7}$$

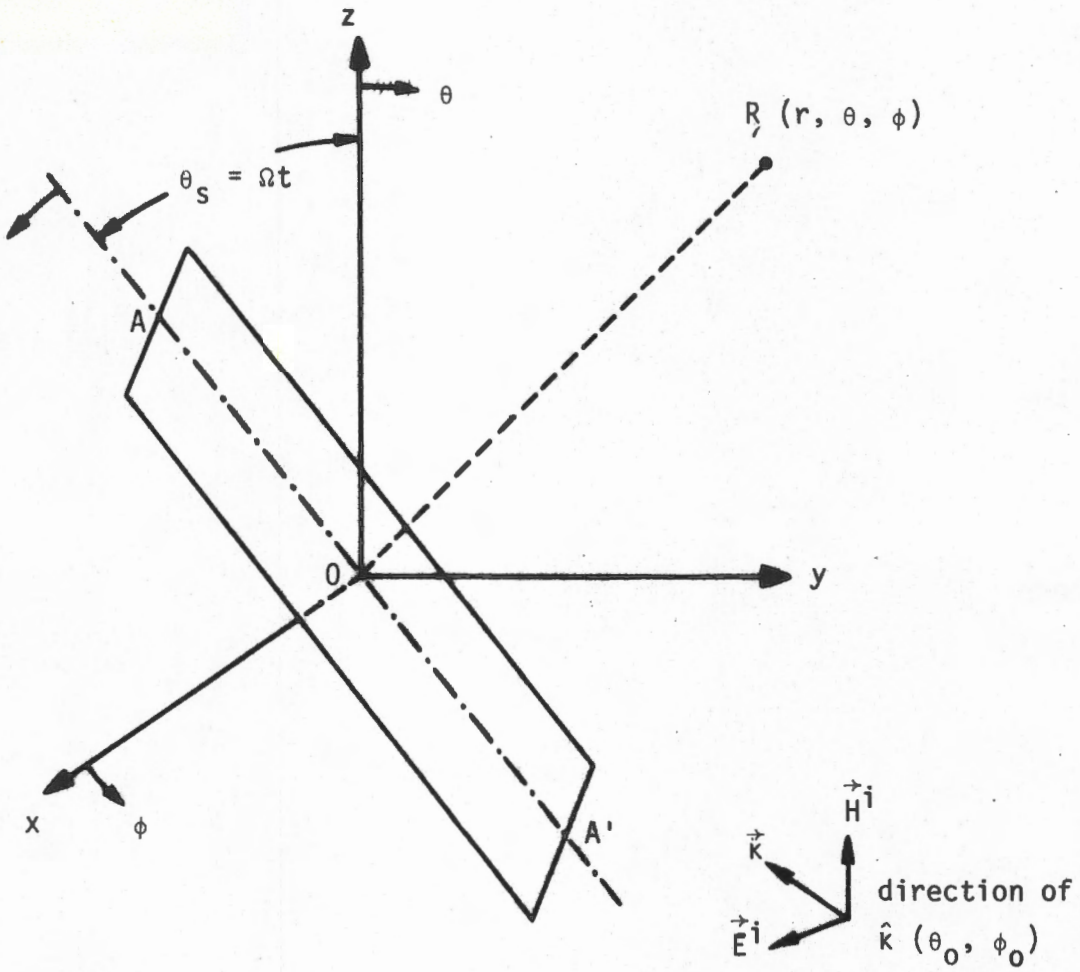

Figure 4-2: Rotating skewed rectangular plate, with the incident field direction and the receiver location shown. The line AA' is rotating in the xz plane.

and since the unit normal $\hat{n}$ to the plate is

$$\hat{n} = \hat{y}' = -\hat{\xi} \sin \phi_s + \hat{\nu} \cos \phi_s \quad , \tag{4.8}$$

the incident field becomes

$$\vec{H}^i = (-\hat{\xi} \sin \theta_s + \hat{\nu} \cos \theta_s) \exp [ik \{(\alpha \cos \phi_s + \beta \sin \phi_s) x' + (-\alpha \sin \phi_s + \beta \cos \phi_s) y' + \gamma z'\}] \quad . \tag{4.9}$$

From (4.3), (4.8) and (4.9) the induced current density at a point $\vec{r}'$ on the plate is then

$$\vec{J}_s (\vec{r}') = \vec{j}\, 2H_o \exp [ik \{(\alpha \cos \phi_s + \beta \sin \phi_s) x' + \gamma z'\}] \quad , \tag{4.10}$$

where

$$\vec{j} = \hat{\xi} \cos \theta_s \cos \phi_s + \hat{\nu} \cos \theta_s \sin \phi_s + \hat{\eta} \sin \theta_s \cos \phi_s \quad ,$$

i.e.,

$$\vec{j} = \hat{x} \cos \phi_s + \hat{y} \cos \theta_s \sin \phi_s \tag{4.11}$$

The electric Hertz vector at a far field point R (r, θ, φ) due to the current distribution $\vec{J}_s(\vec{r}')$ is

$$\vec{\pi} = \frac{Z}{4i\pi k} \frac{\exp (-ikr)}{r} \int_S \vec{J}_s (\vec{r}') \exp (ik \hat{r} \cdot \vec{r}') \, ds' \quad , \tag{4.12}$$

where

$$\left.\begin{aligned} \hat{r} &= \hat{x} \sin \theta \cos \phi + \hat{y} \sin \theta \sin \phi + \hat{z} \cos \theta \quad , \\ \vec{r}' &= \hat{x}'x' + \hat{z}'z' \quad , \\ ds' &= dx'\, dz' \quad , \\ &\text{S is the surface area of the plate,} \end{aligned}\right\} \tag{4.13}$$

and Z is the intrinsic impedance of free space. Hence, from (4.10) - (4.13),

$$\vec{\pi} = \frac{\vec{j}Z}{2i\pi k} \frac{\exp(-ikr)}{r} H_o \int_{-L_1/2}^{L_1/2} \int_{-L_2/2}^{L_2/2} \exp[ik(Ax' + Bz')]\, dx'\, dz'$$

$$= \vec{j} \frac{ZH_o L_1 L_2}{2i\pi k} \frac{\exp(-ikr)}{r} \operatorname{sinc} \frac{L_1}{\lambda} B \operatorname{sinc} \frac{L_2}{\lambda} A \quad , \tag{4.14}$$

with

$$A = (p \cos\theta_s - q \sin\theta_s) \cos\phi_s + u \sin\phi_s \quad , \tag{4.15}$$

$$p = \sin\theta_o \cos\phi_o + \sin\theta \cos\phi \quad , \tag{4.16}$$

$$q = \cos\theta_o + \cos\theta \quad , \tag{4.17}$$

$$u = \sin\theta_o \sin\phi_o + \sin\theta \sin\phi \quad , \tag{4.18}$$

$$B = p \sin\phi_s + q \cos\phi_s \quad , \tag{4.19}$$

$$\operatorname{sinc}[x] = \frac{\sin\pi x}{\pi x} \quad , \tag{4.20}$$

and since the scattered electric field is simply

$$\vec{E} = k^2 \vec{\pi} \quad , \tag{4.21}$$

the transverse components of the scattered electric field are:

$$E_\phi = i E_o \frac{L_1 L_2}{\lambda} \frac{\exp(-ikr)}{r} [\sin\phi \cos\phi_s - \cos\phi \sin\phi_s \cos\theta_s] \cdot \operatorname{sinc}\left[\frac{L_1}{\lambda} B\right] \operatorname{sinc}\left[\frac{L_2}{\lambda} A\right] \quad , \tag{4.22}$$

$$E_\theta = -i E_o \frac{L_1 L_2}{\lambda} \frac{\exp(-ikr)}{r} \cos\theta [\cos\phi \cos\phi_s + \sin\phi \sin\phi_s \cos\theta_s] \cdot \operatorname{sinc}\left[\frac{L_1}{\lambda} B\right] \operatorname{sinc}\left[\frac{L_2}{\lambda} A\right] \quad . \tag{4.23}$$

where $E_o = Z H_o$. Note that in the plane $\theta = \frac{\pi}{2}$, the component $E_\theta \equiv 0$. This implies that the cross polarized component of the scattered field vanishes in the horizontal plane, and henceforth our discussion will pertain only to the ϕ component of the scattered electric field.

As evident from (4.22), E_ϕ is equivalent to a superposition of the fields produced by a pair of crossed dipoles located at the origin O and oriented along the x- and y-axes. The strengths of the two dipoles are proportional to the areas of the plate projected on the xz and yz planes respectively, and are functions of the plate orientation (θ_s, ϕ_s), the incident field direction (θ_o, ϕ_o) and the receiving direction (θ, ϕ). If we now assume that the plate is rotating according to (4.1), the modulation envelope of the scattered field produced by the rotation is

$$f_m(t) = f_{mx}(t) - f_{my}(t) , \tag{4.24}$$

where

$$f_{mx}(t) = \sin\phi \cos\phi_s \operatorname{sinc}\left[\frac{L_1}{\lambda}(p \sin\Omega t + q \cos\Omega t)\right] \cdot \operatorname{sinc}\left[\frac{L_2}{\lambda}\{(p \cos\Omega t - q \sin\Omega t)\cos\phi_s + u \sin\phi_s\}\right] , \tag{4.25}$$

is the contribution of the x-directed dipole and

$$f_{my}(t) = \cos\phi \sin\phi_s \cos\Omega t \operatorname{sinc}\left[\frac{L_1}{\lambda}(p \sin\Omega t + q \cos\Omega t)\right] \cdot \operatorname{sinc}\left[\frac{L_2}{\lambda}\{(p \cos\Omega t - q \sin\Omega t)\cos\phi_s + u \sin\phi_s\}\right] . \tag{4.26}$$

is the contribution of the y-directed dipole. Equation (4.24) will be referred to as the modulation waveform produced by a rotating skewed plate. When the plate rotates in its own plane, i.e., the xz plane so that $\phi_s = 0$, the modulation waveform reduces to

$$f_m(t)\big|_{\phi_s=0} = f_{mx}(t)\big|_{\phi_s=0} = \sin\phi \operatorname{sinc}\left[\frac{L_1}{\lambda}(p \sin\Omega t + q \cos\Omega t)\right] \cdot \operatorname{sinc}\left[\frac{L_2}{\lambda}(p \cos\Omega t - q \sin\Omega t)\right] , \tag{4.27}$$

in agreement with the results reported earlier [1].

4.2.2 Discussion of Results

In this section we discuss briefly the nature of the modulation waveforms under various situations and make some general observations on the basis of the above theory.

Rotating Skewed Plate ($\phi_s \neq 0$)

(i) If the receiver lies in the forward direction defined by $\theta = \pi - \theta_o$, $\phi = \pi + \phi_o$, then $p = q = u = 0$ and

$$f_m(t) = \sin\phi \cos\phi_s - \cos\phi \sin\phi_s \cos\Omega t , \tag{4.28}$$

showing that the modulation envelope is a sinusoidal function of time with a frequency equal to the rotation frequency of the plate.

(ii) If the receiver lies in the specular direction with respect to the plane of rotation, i.e., $\theta = \pi - \theta_o$, $\phi = \pi - \phi_o$, then $p = q = 0$ and $u = 2 \sin\theta_o \sin\phi_o = 2 \sin\theta \sin\phi$. In this case the modulation function is

$$f_m(t) = (\sin\phi \cos\phi_s - \cos\phi \sin\phi_s \cos\Omega t)\,\mathrm{sinc}\left[\frac{2L_2}{\lambda} \sin\theta_o \sin\phi_o \sin\phi_s\right], \tag{4.29}$$

and the modulation envelope is again a sinusoidal function of time with frequency equal to the rotation frequency of the plate.

(iii) For arbitrary incident and receiving directions the modulation waveform is a complicated function of time having a repetition period equal to that of the plate rotation. The exact waveform in such cases may be obtained numerically from (4.24).

Rotating Non-Skewed Plate ($\phi_s \equiv 0$)

For a rectangular plate rotating in its own plane the incident field induces on the plate only x-directed electric dipoles to contribute to the scattered field. The modulation waveform then simplifies to the expression given in (4.27). This case was discussed in [1], but for completeness we quote the following observations which are important to the interpretation of our experimental results:

(i) The modulation waveform is a periodic function having a frequency equal to twice the rotation frequency of the plate.

(ii) For a plate in the xz plane, the specular and forward directions are $\theta = \pi - \theta_o$, $\phi = \pi - \phi_o$ and $\theta = \pi - \theta_o$, $\phi = \pi + \phi_o$, respectively, and in both cases $p = q = 0$, making $f_m(t)$ independent of time. Although these are the directions of maximum scattering, no time-varying modulation will be produced by the rotation of the plate.

(iii) In the special case $\theta_o = \theta = \pi/2$ for which $p = \cos\phi_o + \cos\phi$ and $q = 0$, the modulation waveform can be written (without the factor $\sin\phi$) as:

$$f_{m_1}(t) = \operatorname{sinc}\left[\frac{L_1}{\lambda}(\cos\phi_o + \cos\phi)\sin\Omega t\right]\operatorname{sinc}\left[\frac{L_2}{\lambda}(\cos\phi_o + \cos\phi)\cos\Omega t\right]. \tag{4.30}$$

For a plate of high aspect ratio, $L_1 >> L_2$, and the time dependence of $f_{m_1}(t)$ is primarily determined by the first factor. For a sufficiently small rotation frequency of the plate, the modulation function now has the form of a sinc pulse in time repeating at twice the rotation frequency of the plate, and if its width $2t_1$ in time is measured by the separation between the minima on both sides of the maximum:

$$2t_1 = \frac{1}{\pi f_s}\sin^{-1}\left[\frac{1.5\,\lambda}{L_1(\cos\phi_o + \cos\phi)}\right], \tag{4.31}$$

where f_s is the rotation frequency of the plate. Equation (4.31) should be used when the receiver is away from the specular direction. However, if the receiver is near to the specular direction, i.e., $\phi_o = \pi - (\phi + 2\Delta\phi)$ where $2\Delta\phi$ is very small, the second factor in (4.30) can be assumed unity, and the first factor written as

$$f_{m_1}(t) \simeq 1 - \frac{1}{3}\left[\frac{L_1\ \Delta\phi\ \sin\ \phi}{\lambda}\right]^2 + \frac{1}{3}\left[\frac{L_1\ \Delta\phi\ \sin\ \phi}{\lambda}\right]^2 \cos\ 2\ \Omega t, \qquad (4.32)$$

showing that near the specular direction the modulation waveform is a continuous sinusoidal function of time with frequency $2f_s$.

4.3 Rectangular Plate Experiments

4.3.1 Experimental Procedures

Experiments were carried out in an anechoic chamber to measure the amplitude modulation of the signals scattered by a rectangular metal plate rotating about an axis through its center when illuminated by a plane electromagnetic wave. The frequency of the incident electromagnetic field was 12.18 GHz, coresponding to the wavelength λ = 2.461 cm, and block diagram of the experimental equipment is shown in Figure 4-3. An incident field polarized with its electric vector in the horizontal plane was radiated from a horn antenna, and the scattered field received by a similar horn. The plate and both horns were in the far field of each other according to the $2D^2/\lambda$ criterion, and throughout the measurements the phase centers of all three lay in the same horizontal plane, i.e., $\theta = \theta_o = \pi/2$. The received signal was fed to a spectrum analyzer the vertical output of which was connected to the vertical input to an oscilloscope where the time-varying modulation waveform was observed. The settings of the spectrum analyzer and the oscilloscope were adjusted for best display of the modulation envelope. In particular, the analyzer sweep was stopped so that the vertical output contained only the amplitude modulation on the 12.18 GHz signal introduced by the scatterer. The location of the transmitting horn was held constant, and changes in the directions of incidence and scattering were made by moving the receiving horn and/or rotating the pedestal on which the scatterer was placed using the positioner control (see Figure 4-4).

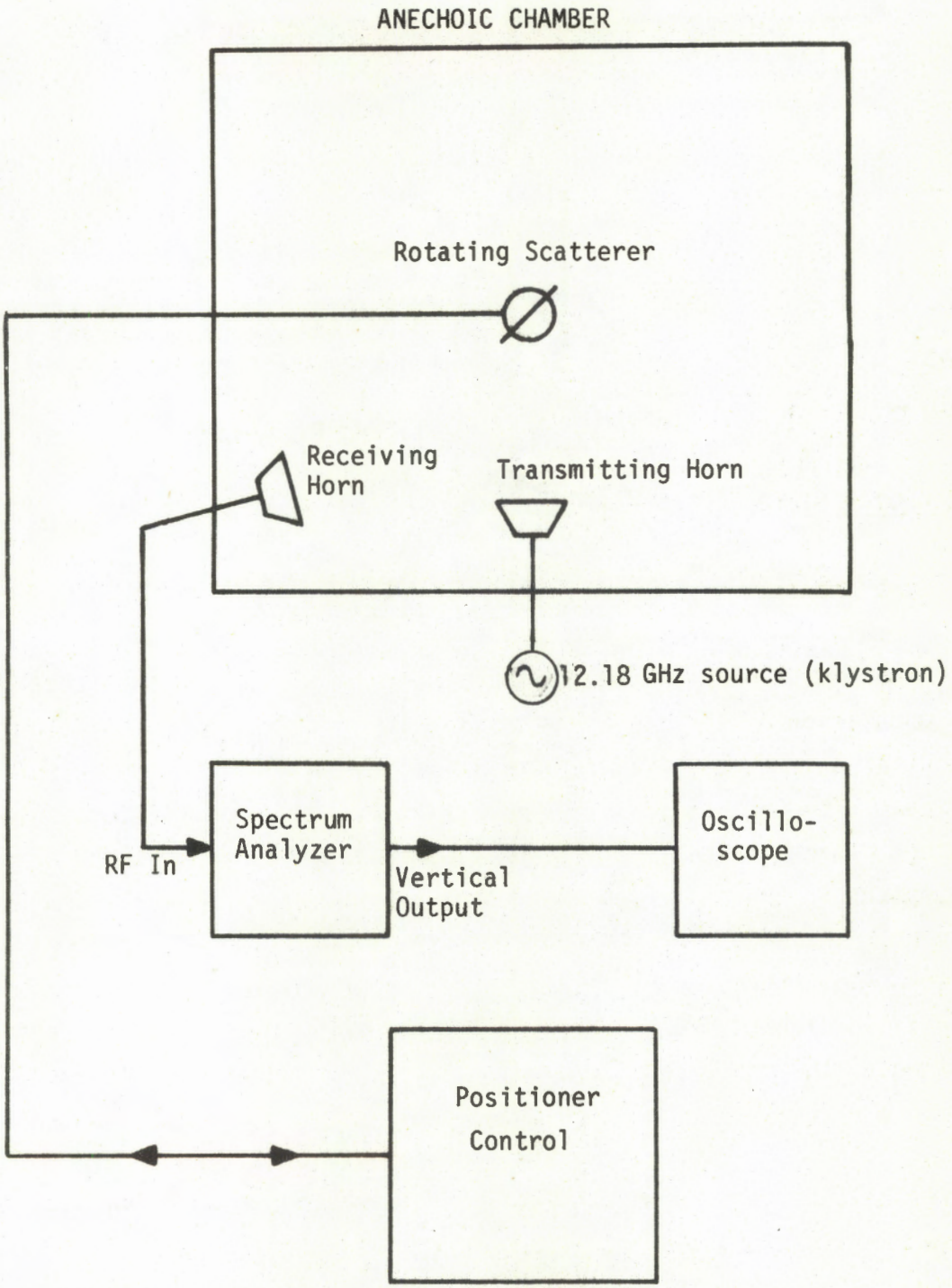

Figure 4-3: Block diagram of the experimental equipment.

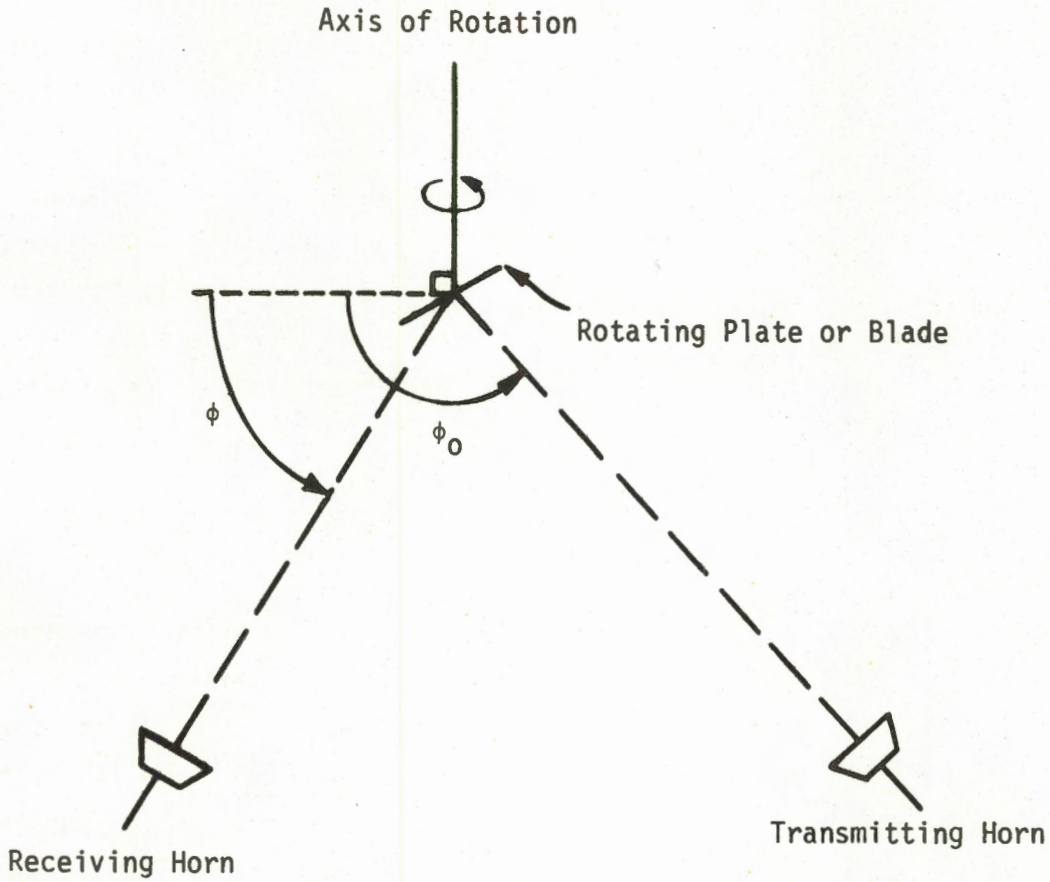

Figure 4-4: The experimental set-up. ϕ and ϕ_o were changed by rotating the scatterer around the vertical axis.

At the frequency used the dimensions of the brass plate were $L_1 = 5\lambda$ and $L_2 = 2\lambda$. In one experiment the plate was skewed, corresponding to $\phi_s = 3°$, and its major axis was rotated in a vertical plane at 10 Hz. Due to mechanical problems with the motor and drive mechanisms, f_s sometimes differed from 10 Hz, and in these cases the value of f_s will be noted explicitly. In the non-skewed case the plate was rotated at 10 Hz in its own, i.e., the vertical, plane. In all of the experiments the center of the plate remained fixed in position. Because of difficulties experienced in extracting the modulation waveform from the received signal, it proved impossible to obtain absolute values for the magnitude of the modulation, so the only data presented are relative. However, the waveform shapes are preserved and can be compared with the theoretical predictions.

4.3.2 Results for Non-Skewed Plates

Some modulation waveforms observed in non-specular directions are reproduced in Figures 4-5 through 4-7 along with the corresponding theoretical curves. The results clearly show that the modulation waveforms have the form of sinc pulses, and repeat at twice the rotation frequency of the plate. The agreement between theory and experiment is rather good. The observed and calculated modulation pulse widths $2t_1$ are listed in Table 4.1, and also agree well.

ϕ_o	ϕ	$2t_1$ (msec)	
		Observed	Calculated
145°	85°	12.5	13.4
100°	10°	12.0	12.1
120°	30°	~29 (unstable display)	30.6

Table 4.1: Observed and calculated pulse widths for non-skewed plates.

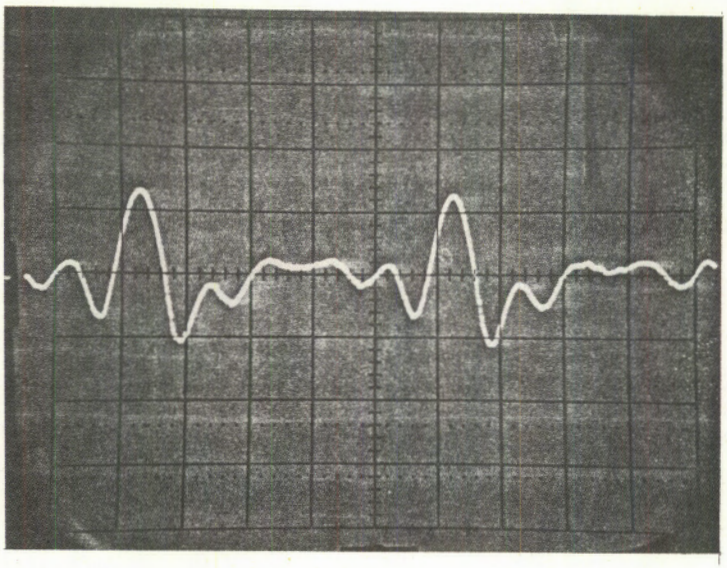

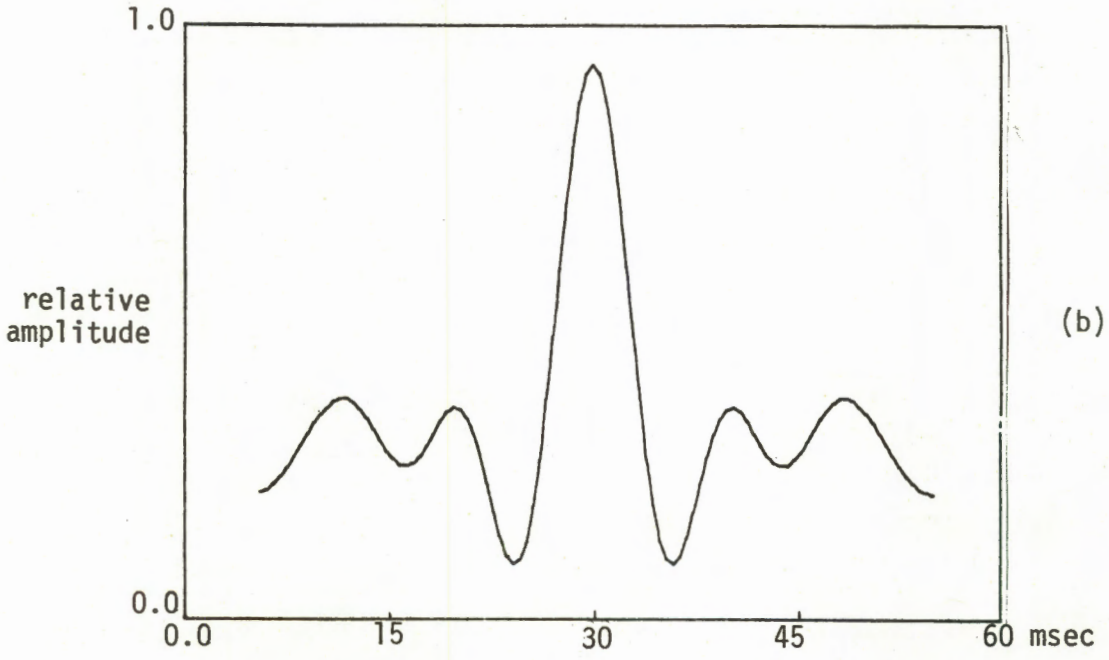

Figure 4-5: Experimental (a) and theoretical (b) non-specular modulation waveforms for a rectangular plate with ϕ_o = 145° and ϕ = 85°.

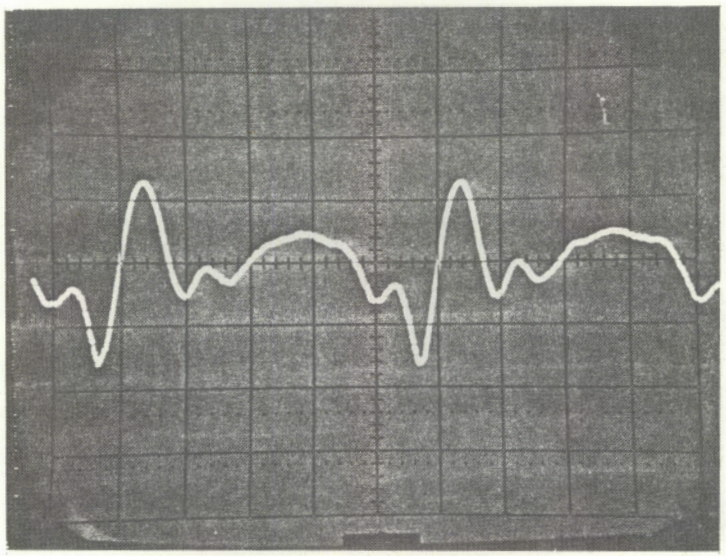

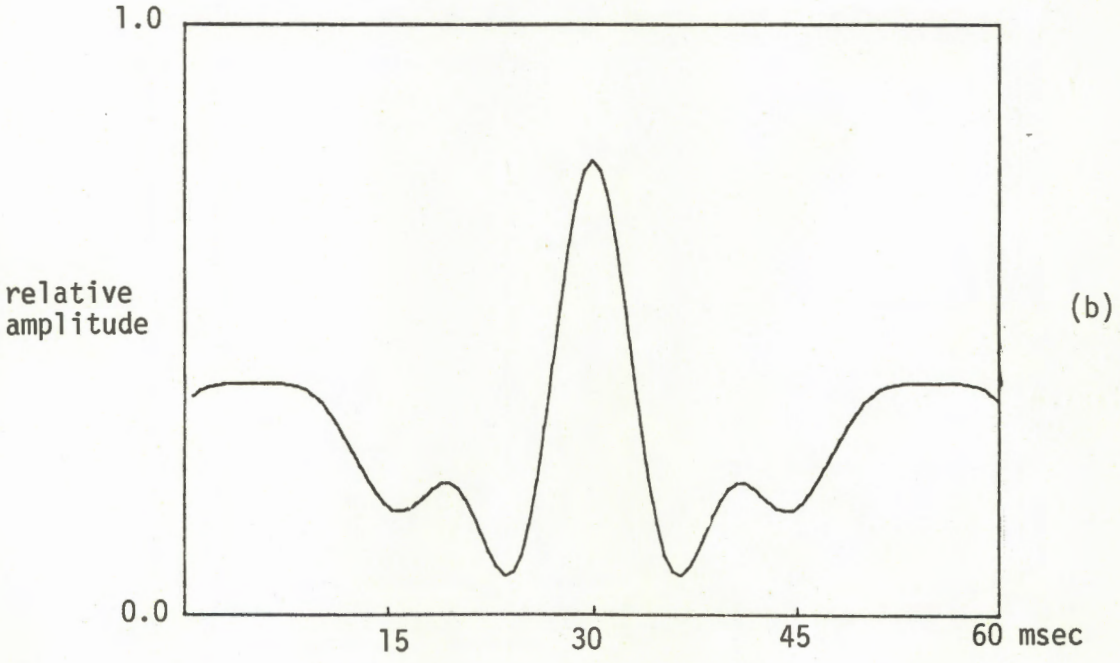

Figure 4-6: Experimental (a) and theoretical (b) non-specular modulation waveforms for a rectangular plate with ϕ_o = 100° and ϕ = 10°.

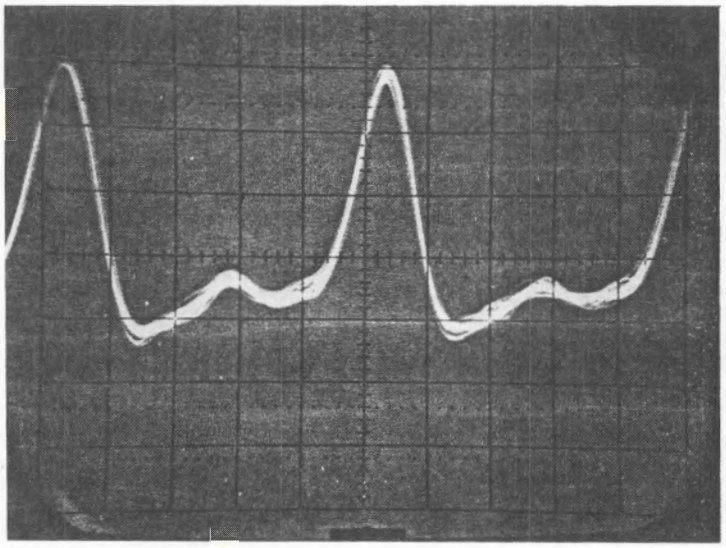

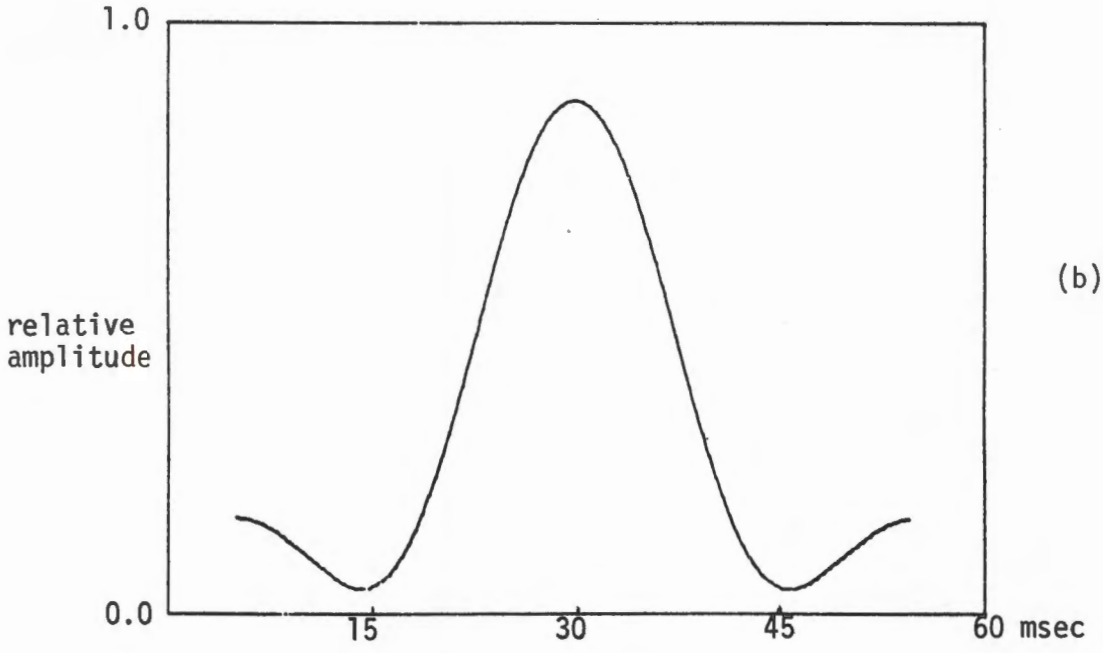

Figure 4-7: Experimental (a) and theoretical (b) non-specular modulation waveforms for a rectangular plate with ϕ_o = 120°and ϕ = 30°.

The observed waveforms in two different directions of specular scattering are shown in Figures 4-8(a) and (b) and as predicted by the theory, there is no modulation. For scattering in a direction slightly ($\Delta\phi$ = 5°) away from specular, the observed modulation waveforms for three different directions of incidence are presented in Figures 4-9(a) through 4-9(c). As predicted, the waveforms are sinusoidal with frequency $2f_s$ and large magnitude.

4.3.3 Results for Skewed Plates

In an attempt to simulate more closely the situation for actual windmill blades which are necessarily non-planar and do not lie in their plane of rotation, experiments were carried out with the rectangular plate skewed through an angle ϕ_s = 3° (see Figure 4-1), and some of the results obtained are presented in Figures 4-10 through 4-13. Comparison with the theoretical prediction shows agreement at least as regards the general shapes of the modulation waveforms and (see Table 4.2) the widths of the main pulses.

ϕ_o	ϕ	$2t_1$ (msec)	
		Observed	Calculated
95°	95°	50	50.6
125°	30°	54	50.6
90°	30°	12-13 (unstable display)	11.8
120°	120°	10	9.4

Table 4.2: Observed and calculated pulse widths for skewed plates.

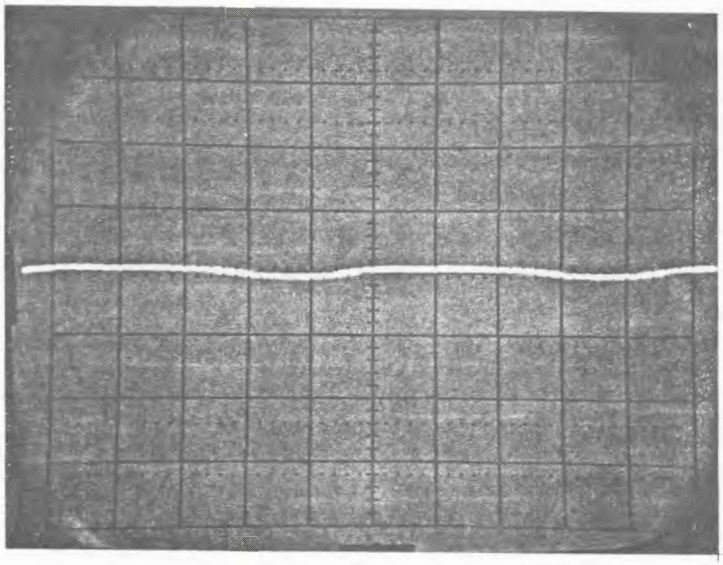

0.05 volts/ division

(a)

10 msec/division

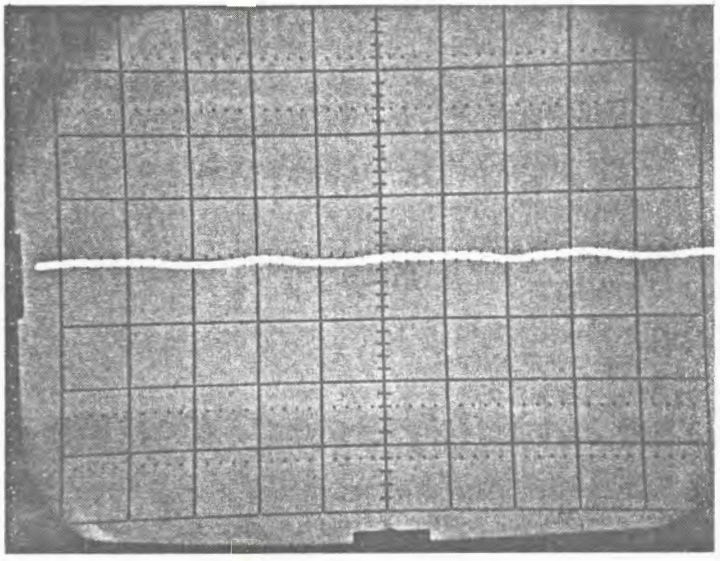

0.05 volts/ division

(b)

10 msec/division

Figure 4-8: Experimental specular modulation waveforms for a rectangular plate with (a) $\phi_0 = 120°$ and $\phi = 60°$, and (b) $\phi_0 = 135°$ and $\phi = 45°$.

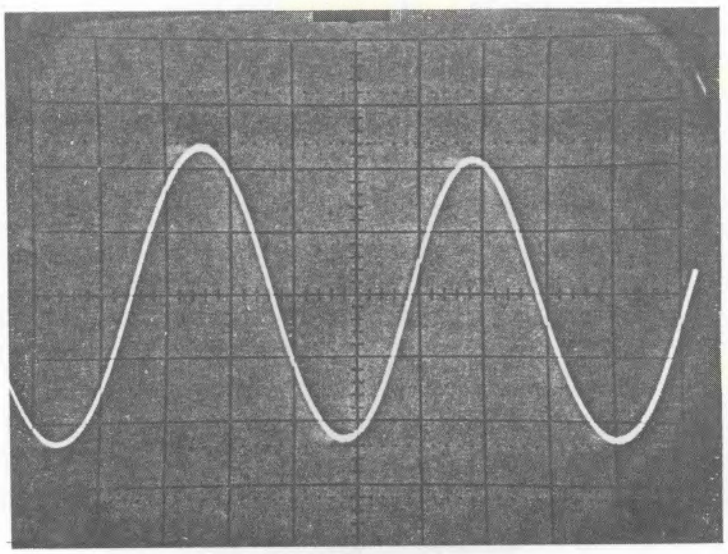

0.1 volts/division

(a)

10 msec/division

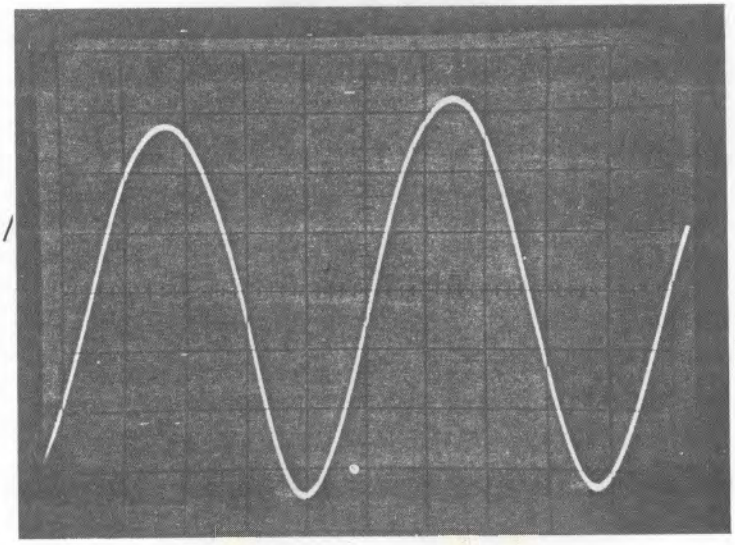

0.1 volts/division

(b)

10 msec/division

Figure 4-9.

0.5 volts/
division

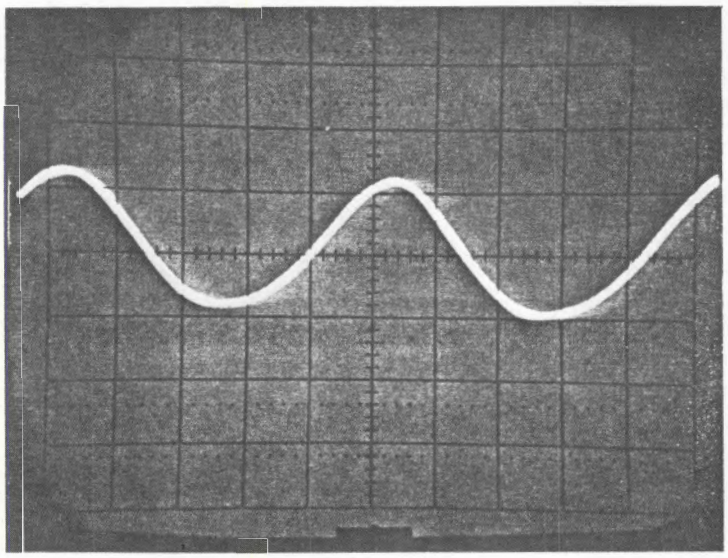

(c)

10 msec/division

Figure 4-9: Experimental near-specular ($\Delta\phi$ = 5°) modulation waveforms for a rectangular plate with (a) ϕ_o = 110° and ϕ = 80°; (b) ϕ_o = 115° and ϕ = 55° for f_s = 11 Hz; and (c) ϕ_o = 95° and ϕ = 95°.

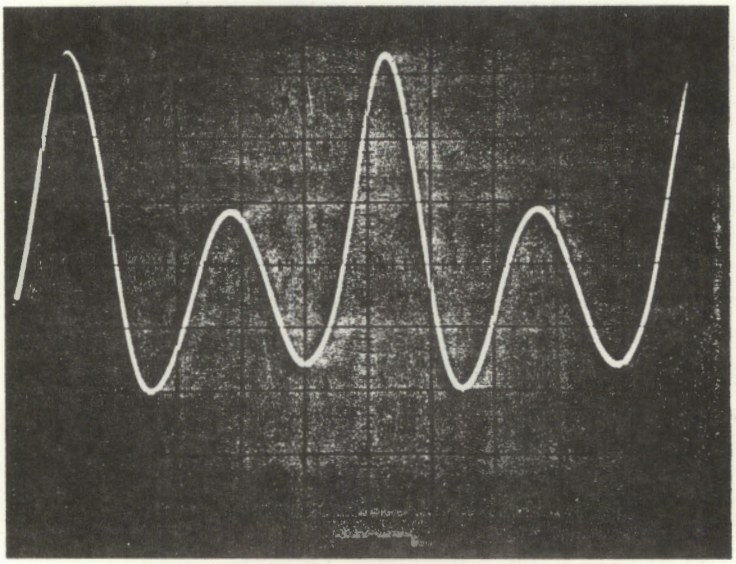

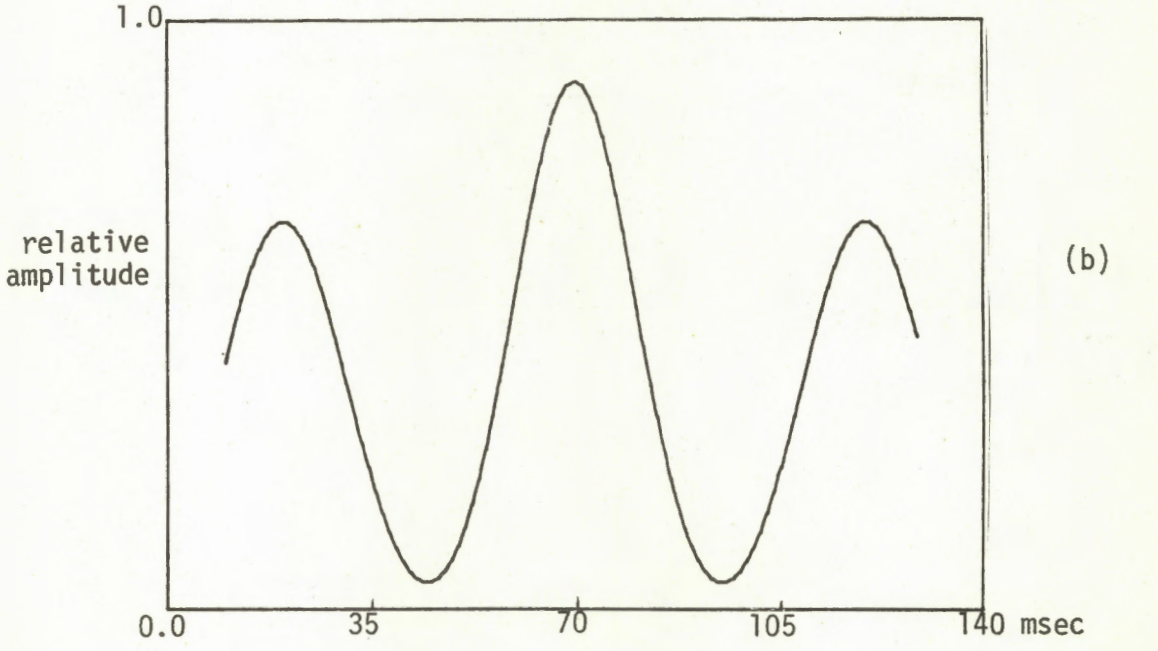

Figure 4-10: Experimental (a) and theoretical (b) non-specular modulation waveforms for a rectangular plate with $\phi_o = 95°$, $\phi = 95°$ and $\phi_s = 3°$.

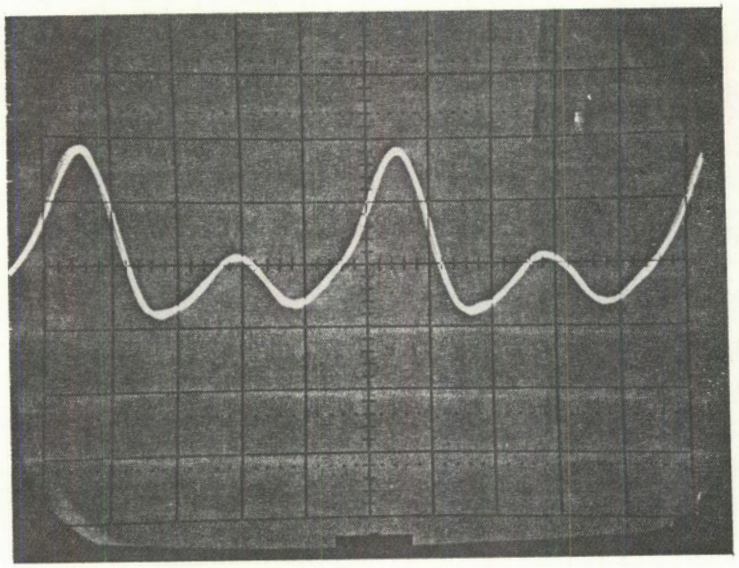

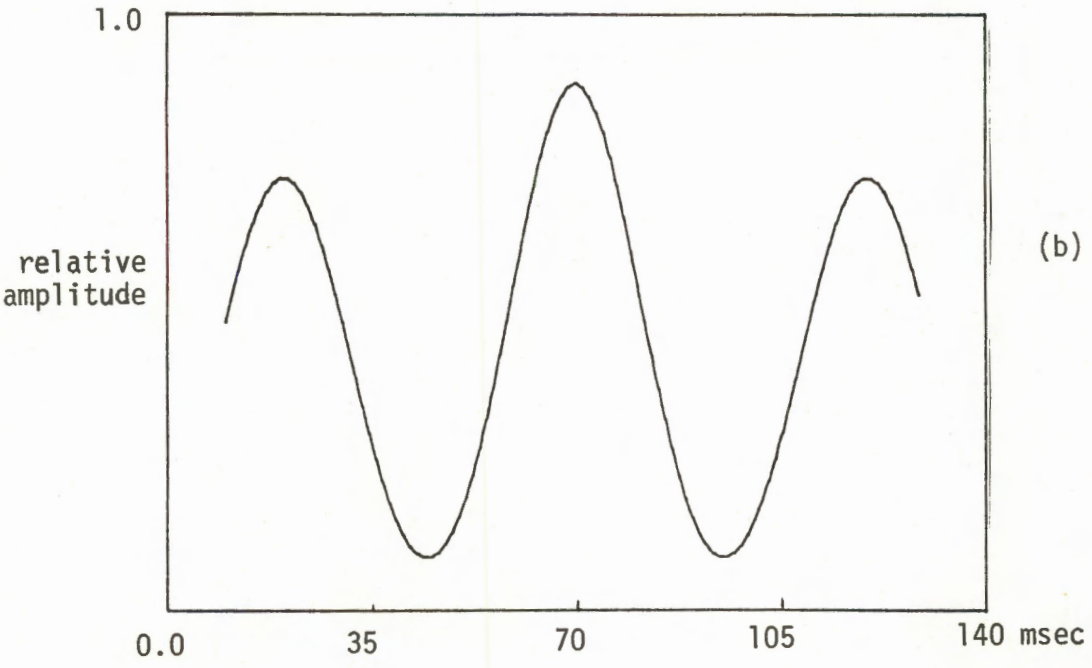

Figure 4-11: Experimental (a) and theoretical (b) non-specular modulation waveforms for a rectangular plate with $\phi_o = 125°$, $\phi = 65°$ and $\phi_s = 3°$.

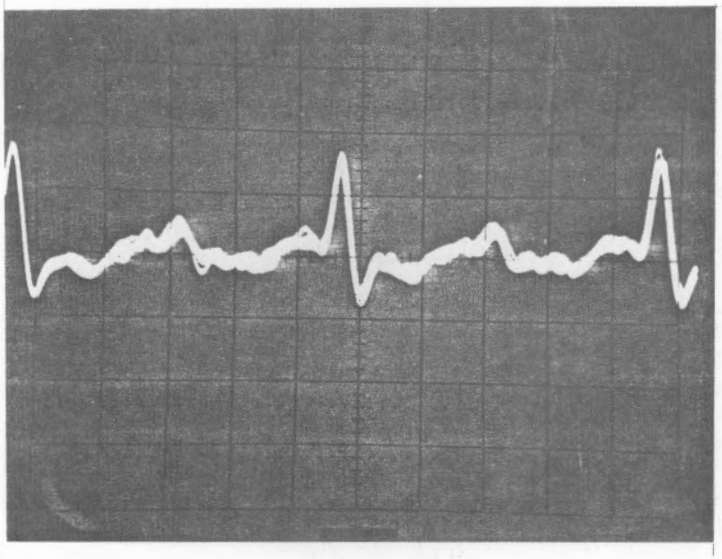

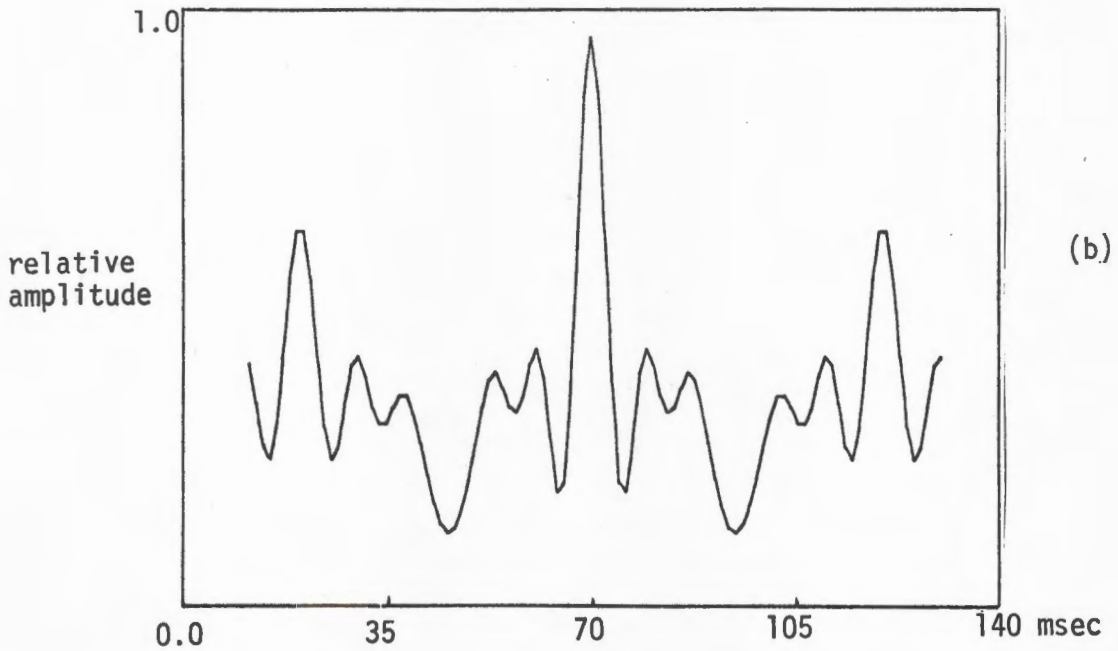

Figure 4-12: Experimental (a) and theoretical (b) non-specular modulation waveforms for a rectangular plate with $\phi_o = 90°$, $\phi = 30°$ and $\phi_s = 3°$.

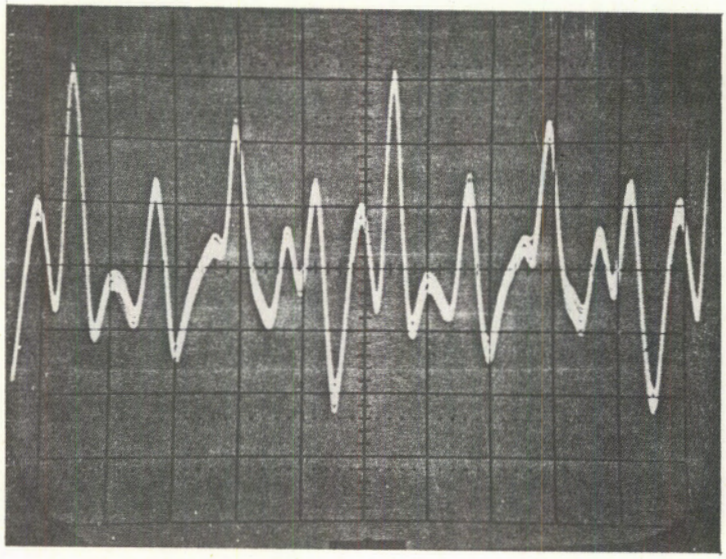

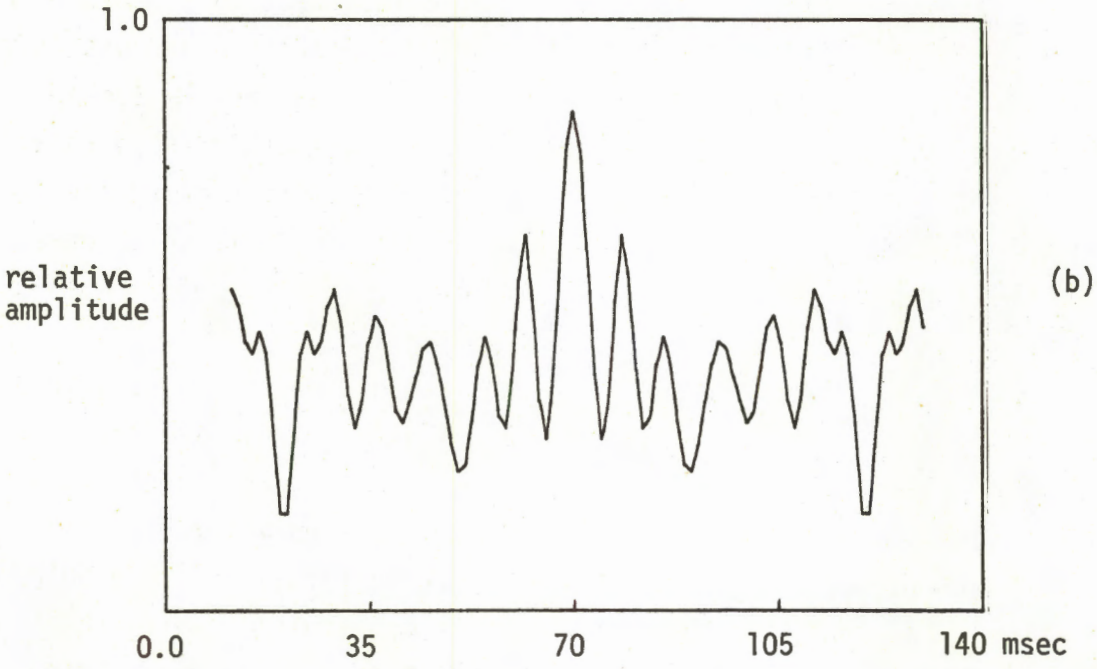

Figure 4-13: Experimental (a) and theoretical (b) non-specular modulation waveforms for a rectangular plate with $\phi_o = 120°$, $\phi = 120°$ and $\phi_s = 3°$.

The shape of the modulation waveforms is much more complicated than in the case of a non-skewed plate, but a key feature is the fact that because of the asymmetry the period is now $1/f_s$ instead of $1/2f_s$ (see Section 4.2) when the plate was non-skewed. Although the shape of the waveform is strongly dependent on the directions of incidence and scattering, the pulsed nature is clearly evident.

4.4 Experiments With Model Windmill Blades

Two identical scale models of the MOD-0 windmill blade were cut from a piece of wood. The blades were nominally 1:37.5 in scale, with length 19.2λ and width varying linearly from 1.55λ at the root to 0.57λ at the tip at the frequency 12.18 GHz. One blade was sprayed with several coatings of silver (metallic) paint and was, in fact, the model used in our laboratory measurements of the backscattering behavior (see Section 3.2.1), whereas the other was left bare. Using threaded rods inserted in their ends, the blades were attached symmetrically to a hub on a horizontal rod so as to allow the blades to rotate in a vertical plane. The observed modulation waveforms thus contained the returns from both blades, but because of their separation in time, each waveform could be separately identified.

The observed waveforms for a blade rotation frequency f_s = 2.5 Hz with incidence at ϕ_o = 120° and reception in the broadside (ϕ = 90°) direction are shown in Figures 4-14(a) through 4-14(c). The first is for the case of the blades at zero pitch angle, i.e., their base chords in the plane normal to the axis of rotation, and the second for a pitch angle of approximately 45°. In both figures the large pulses on the left are due to the metal blade, while the smaller ones on the right are caused by the wooden blade, and Figure 4-14(c) is an expanded view of the wooden blade waveform of Figure 4-14(a).

The modulation waveforms produced by the metal blade are similar to those for the skewed rectangular plate (Figures 4-10 through 4-13), and the asymmetry

0.2 volts/
division

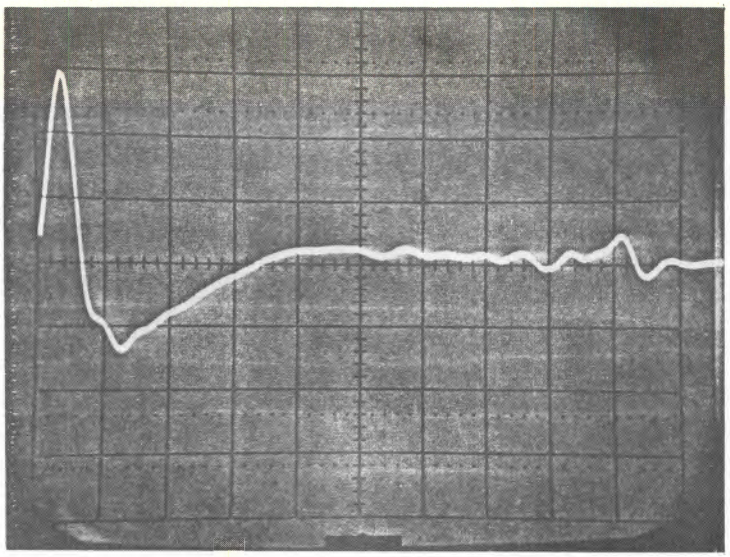

(a)

20 msec/division

0.2 volts/
division

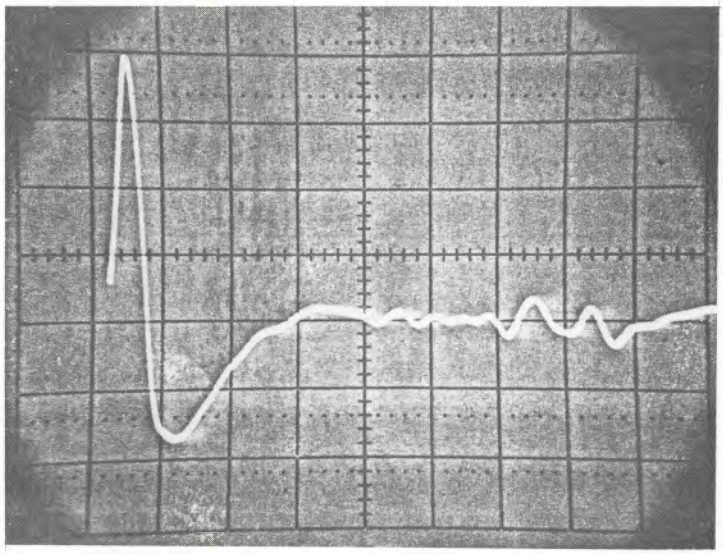

(b)

20 msec/division

Figure 4-14: Experimental modulation waveforms for metal (on left) and wooden (on right) blades for ϕ_0 = 120°, ϕ = 90°, and f_s = 2.5 Hz: (a) blade pitch $\cong$ 0, (b) blade pitch $\simeq$ 45°.

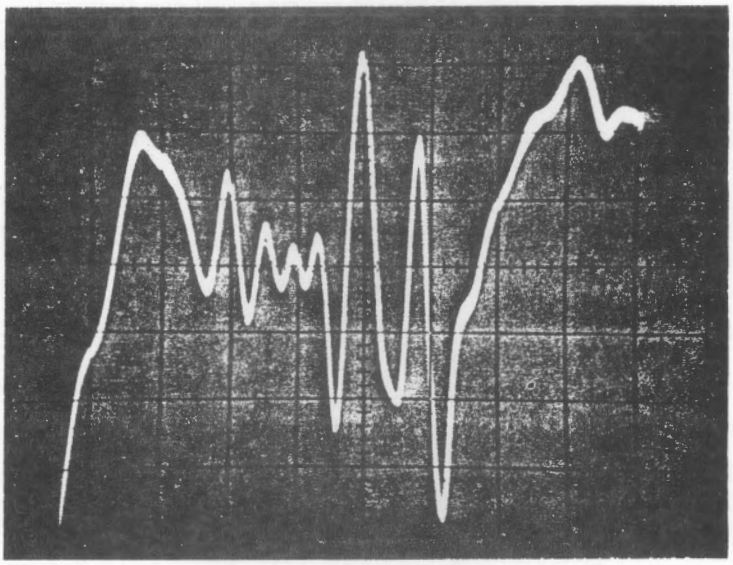

Figure 4-14(c): Expanded view of the modulation waveform for the wooden blade with 0° pitch.

and narrower width of the pulses in Figure 4-14 can be attributed to the asymmetry and larger size of the blade. We remark that a non-zero pitch to the blade seems to produce a slight decrease in the width of the main pulse. With the wooden blade, the waveform is smaller in amplitude by about 13 dB, but its overall shape resembles that for the full scale MOD-0A (fiberglas) blade observed at Plum Brook.

4.5 Conclusions

The waveforms of the amplitude modulation of an incident electromagnetic wave produced by a slowly rotating object has been investigated both theoretically and experimentally, and the key features diagnosed. The nature of the modulation waveform depends on the orientation and electrical dimensions of the object, its rotation speed and, most strongly, the directions of incidence and scattering. For a rectangular metal plate rotating in its plane, the modulation is independent of time in the directions of specular and forward scattering, i.e., in the directions where the scattering is a maximum. In directions near specular or forward, the modulation waveform is a sinusoid whose frequency is twice the rotation frequency; and away from these directions, the waveform consists of sinc-like pulses repeating at twice the rotation frequency. The widths of the pulses are inversely proportional to the maximum linear dimension of the plate. When the metal plate is skewed, the modulation waveform in the specular and forward directions is sinusoidal with frequency equal to the rotation frequency; in other directions the waveform is primarily pulse-like, with the pulses repeating at the rotation frequency and the width of the main pulses being inversely proportional to the plate dimension. In view of the results obtained with a scale model windmill blade, it would appear that as regards the modulation waveform a skewed rectangular plate is a satisfactory model of an actual blade provided the dimensions are comparable and the skew angle approximates the average departure (including pitch as well as twist angle) of the blade surface from its plane of rotation.

4.6 References

[1] T.B.A. Senior, D.L. Sengupta and J.E. Ferris, "TV and FM Interference by Windmills", The University of Michigan Radiation Laboratory Report No. 014438-1-F, February 1977.

[2] J. Van Bladel, "Electromagnetic Fields in the Presence of Rotating Objects", Proc. IEEE, Vol. 64, No. 3, pp. 301-318, March 1976.

[3] R.E. Kleinman, "Electromagnetic Scattering by a Linearly Oscillating Target", AFCRL-TR-75-0554, Physical Sciences Research Papers No. 648, Microwave Research Laboratory, Air Force Cambridge Research Laboratories, Hanscom Air Force Base, Mass, 01731, 20 October 1975.

APPENDIX 5: MEASUREMENTS OF TV INTERFERENCE

The results of two measurement programs to investigate and record the TV interference produced by a windmill are reported here. The first program was a series of field tests using the NASA/ERDA 100 Kw wind turbine generator located at the NASA Lewis Plum Brook Facility near Sandusky, Ohio. The second was a series of simulations performed in a laboratory environment where the interference to TV reception was studied under conditions simulating those experienced in the field, i.e., the direct signal was combined with an artificially-generated multipath signal so that the total input to the TV receiver was amplitude modulated by a repetitive pulse whose shape approximated that observed at Plum Brook. In both cases the primary sources were the actual transmitters of the TV channels available locally. The tests were similar to those reported in [1] but differed from the preliminary ones in the wider variety of circumstances investigated, the more precise nature of the laboratory simulations, and the more detailed video recordings that resulted.

5.1 Field Tests

The field testing was carried out on six visits to Plum Brook during the period April to November 1977. The main objectives of these tests were (i) to investigate and quantify the way in which the interference depends on the various parameters involved, e.g., the orientation of the WTG, the pitch angle of the blades, TV channel number (and therefore frequency), distance from the WTG, receiver used, etc.; (ii) to determine the nature of the modulation that the interference produces for later simulation in the laboratory; and (iii) to obtain reproducible recordings of the interference seen on one or more TV channels. All of the objectives were achieved and some of the recordings made were included on the video tape supplied to the sponsor.

5.1.1 Test Procedure

The relevant features of the WTG and a systematic procedure for conducting the tests were described in [1] and will not be repeated here.

A typical set-up for performing the tests is shown in Figure 5-1 where we included only those components which are pertinent to the data collection. The RF signals used were the TV Channels 3, 5, 8, 25 and 43 whose transmitters are located at Cleveland, approximately 83 Km from the WTG, and Channel 13 with the transmitter at Toledo, about 67 Km away. With any given station a portion of the signal is reflected off the turbine blades and this, together with the direct signal, is picked up by the receiving antenna and fed simultaneously to a TV receiver and a spectrum analyzer. The receiving antenna used was a commercially available directional antenna for TV reception. A horizontal plane pattern of the antenna measured at 600 MHz is shown in Figure 5-2. The TV picture was observed to see if there was any video distortion, and the detected signal was fed to a video recorder whenever the data was felt to be worth preserving. The spectrum analyzer was tuned to the audio carrier frequency and its vertical output was recorded on paper tape for later evaluation. This provided a recording of the received signal level as a function of time and included any modulation pulse produced by scattering from the turbine blades.

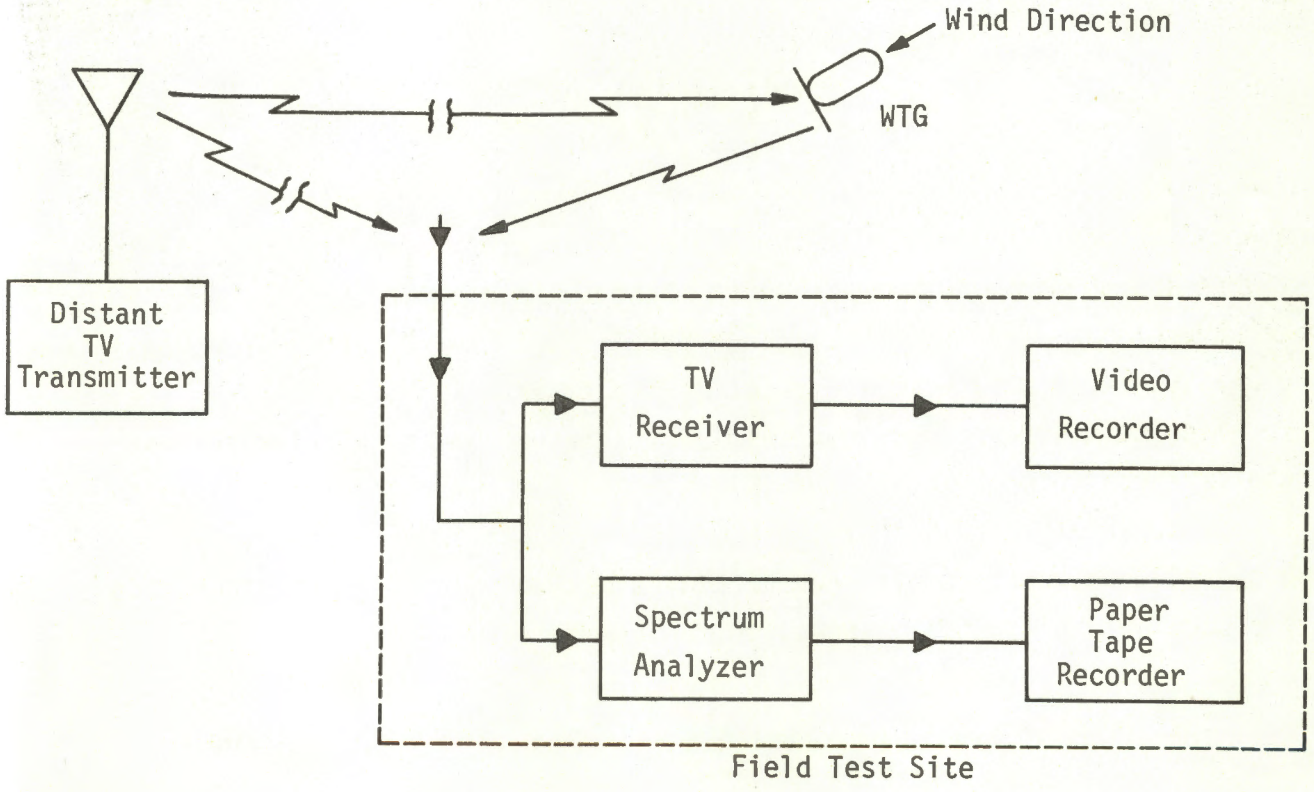

Figure 5-1: Schematic diagram of a typical field test set-up.

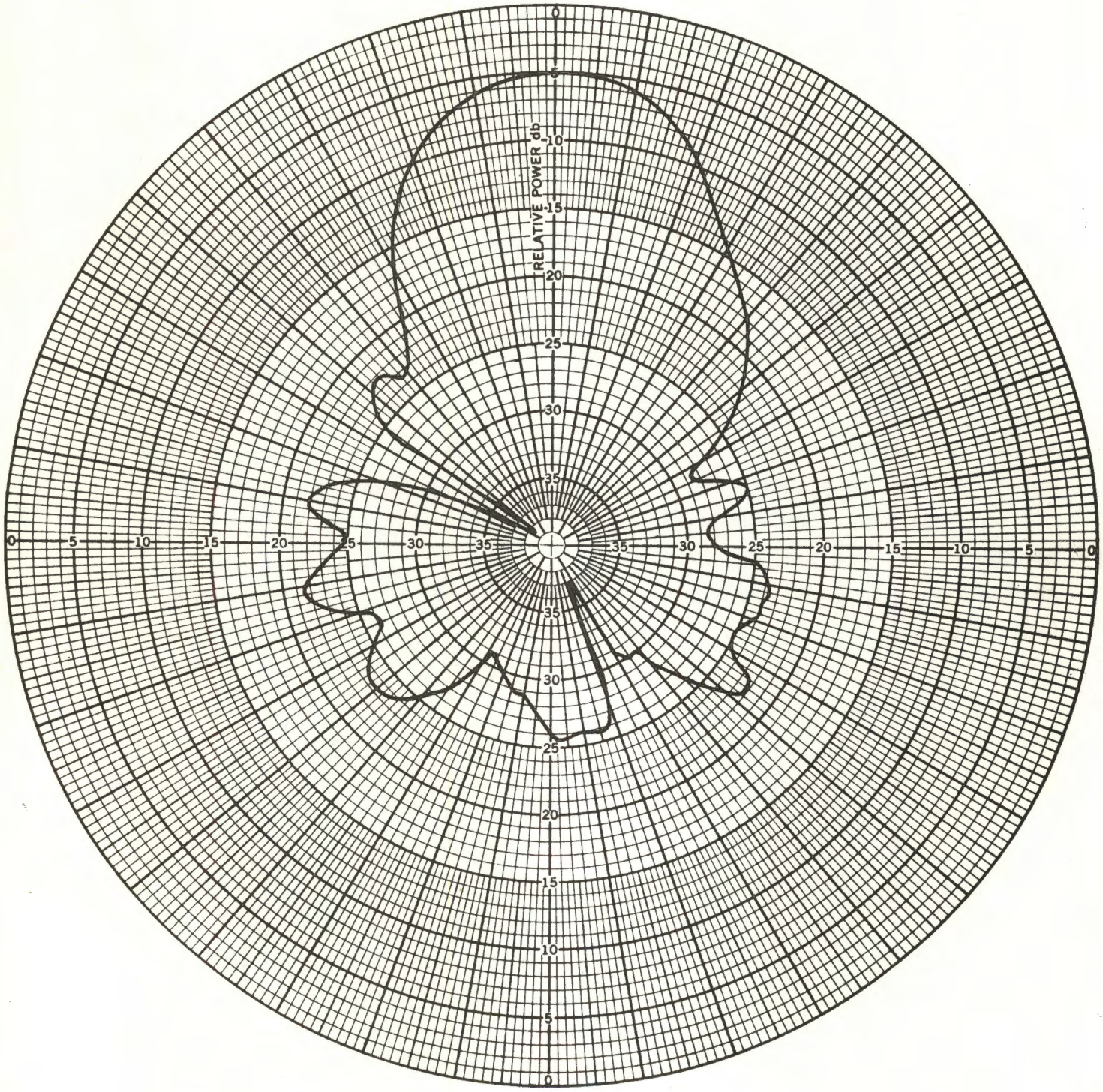

Figure 5-2: Free space horizontal plane pattern of the TV receiving antenna measured at 600 MHz.

The signal scattered by a rotating blade combines with the direct signal to produce an effectively amplitude modulated signal at the receiver. Thus, as a function of time, the output of the spectrum analyzer will vary above and below the ambient level of the direct signal, and it is conventional to quote the total variation of the field amplitude in dB. Simple formulas are given in [1] from which the percentage of amplitude modulation of the received signal can be obtained from the dB variation observed in the output of the spectrum analyzer. For future reference, the relationship between the percent modulation (m x 100) and the total dB variation in the received signal level is plotted in Figure 5-3.

5.1.2 Video Recording

One of the objectives of the field tests was to obtain a video recording of the interference produced by an actual WTG at one or more sites in the vicinity of the machine. It was required that the tape be reproducible using, for example, the facilities of The University of Michigan TV Center, to create copies which were free of additional distortion, and since it had been found impossible to copy the tape made during our 1976 visits to Plum Brook, tapes were made on most of our 1977 visits and tested for reproducibility. It is fortunate that we did so, and it was not until the middle of the year that a reproducible recording was obtained.

The first visit to Plum Brook was made on 26 April 1977 to check up the sites and test equipment to be used on future trips. Since the 60 Hz AC power needed to run the equipment was not available at most of these sites, power was obtained from the same portable diesel generator that we had used before. Such testing as was done indicated that the frequency of the AC power was stable, and all the instrumentation appeared to function satisfactorily using the power supplied by the generator. On our next visit to Plum Brook two weeks later, a black and white video recording of the interference was made by feeding the video signal directly to the tape recorder from the TV circuitry as before. Unfortunately it was found impossible to reproduce the tape and after much debate it was concluded that transients in the power supply

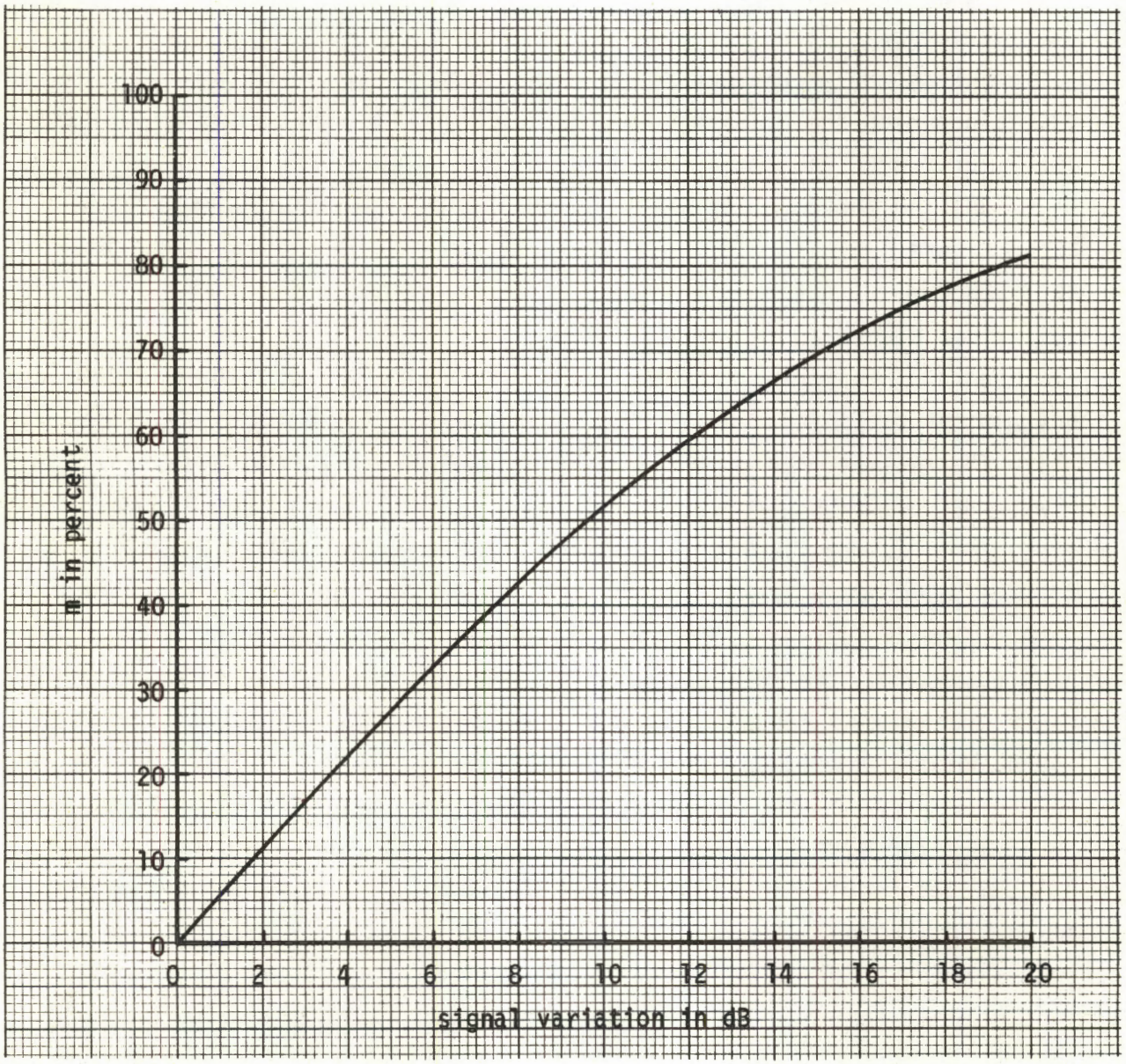

Figure 5-3: Percent modulation as a function of the total dB variation of the observed signal.

for the generator that were not detectable in the field were causing the tape recorder to malfunction. To overcome the difficulty it was recommended that we use a 60 Hz crystal-controlled line source to supply power to the tape recorder, and on our third trip a recording was made with the audio and video signals as well as the required sync signals fed directly into the video recorder. This time the tape was reproducible, but not with the fidelity desired. It now appeared that the wind turbine interference itself caused the circuitry of the video recorder to improperly synchronize the video picture, thereby adding video degradation to that rightfully attributable to the WTG. The only solution appeared to be to use a TV camera to photograph the TV screen and then to record its signal, a procedure which is both costly and cumbersome.

To check out this new approach some color recordings were made in the laboratory and, on our next visit to Plum Brook in late June, a less expensive black and white TV camera was used to record some typical WTG interference. These tapes were successfully copied, and we were now confident of our ability to make a reproducible color video tape recording of the interference effects in the field.

Two visits to Plum Brook were made in early November to observe and record the interference on color video tape. On the first of these visits the wind conditions were erratic and judged unsatisfactory for our purposes, but on the second the conditions were more favorable, and the video distortion produced by a WTG was duly recorded. Two TV receivers were used: a 1976 Zenith model 17GC 45 which has been rated superior for its rejection of interference, and a 1977 Curtis Mathis model B317. The receivers and all test equipment were located inside the WTG control center building 150 m from the WTG, thereby eliminating the need for a portable power supply. The receiving antenna was located on the roof of the building and oriented to receive the transmissions from Cleveland and Toledo. Tests were conducted using TV Channels 3, 5, 8, 25 and 43 from Cleveland and 13 from Toledo. The geometry of the test set-up with some of the angles and distances involved is shown in Figure 5-4, and a block diagram of the equipment used for the measurements is given in Figure 5-5.

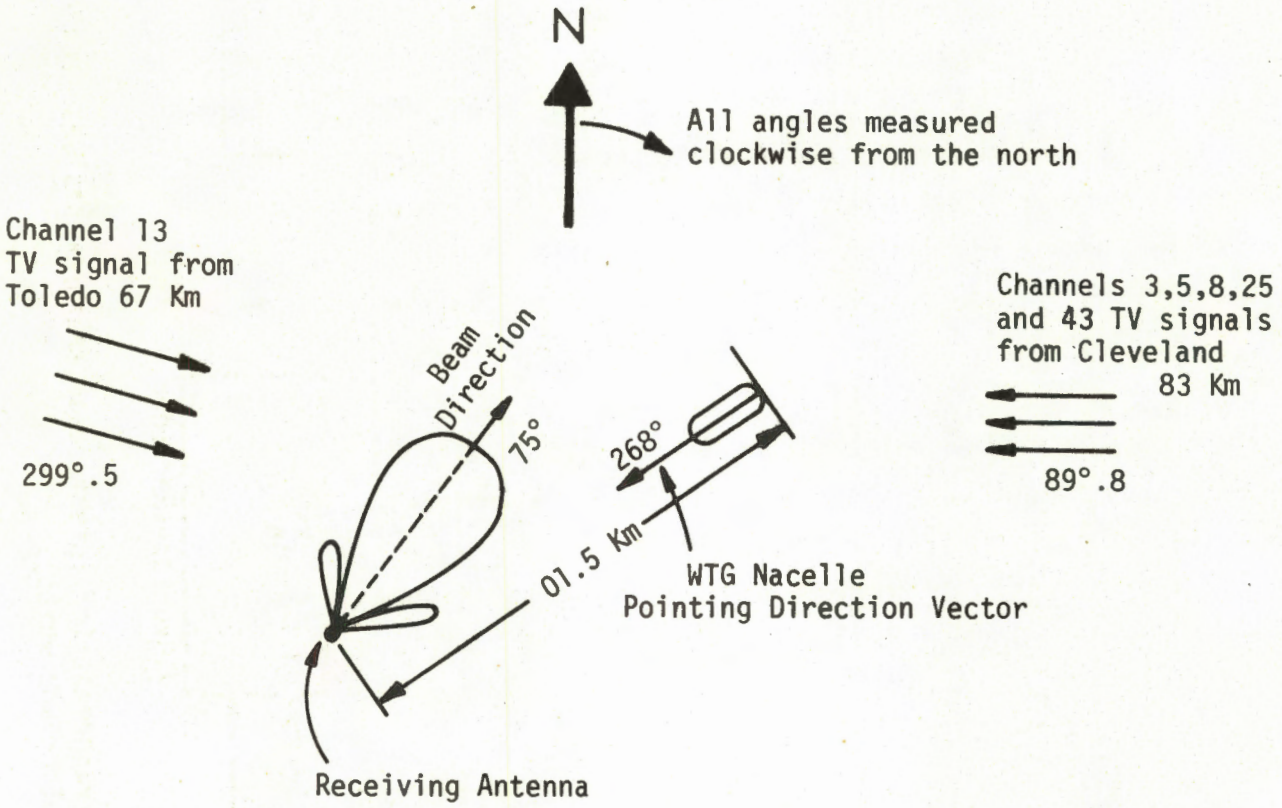

Figure 5-4: Conventions for measuring various angles during field tests.

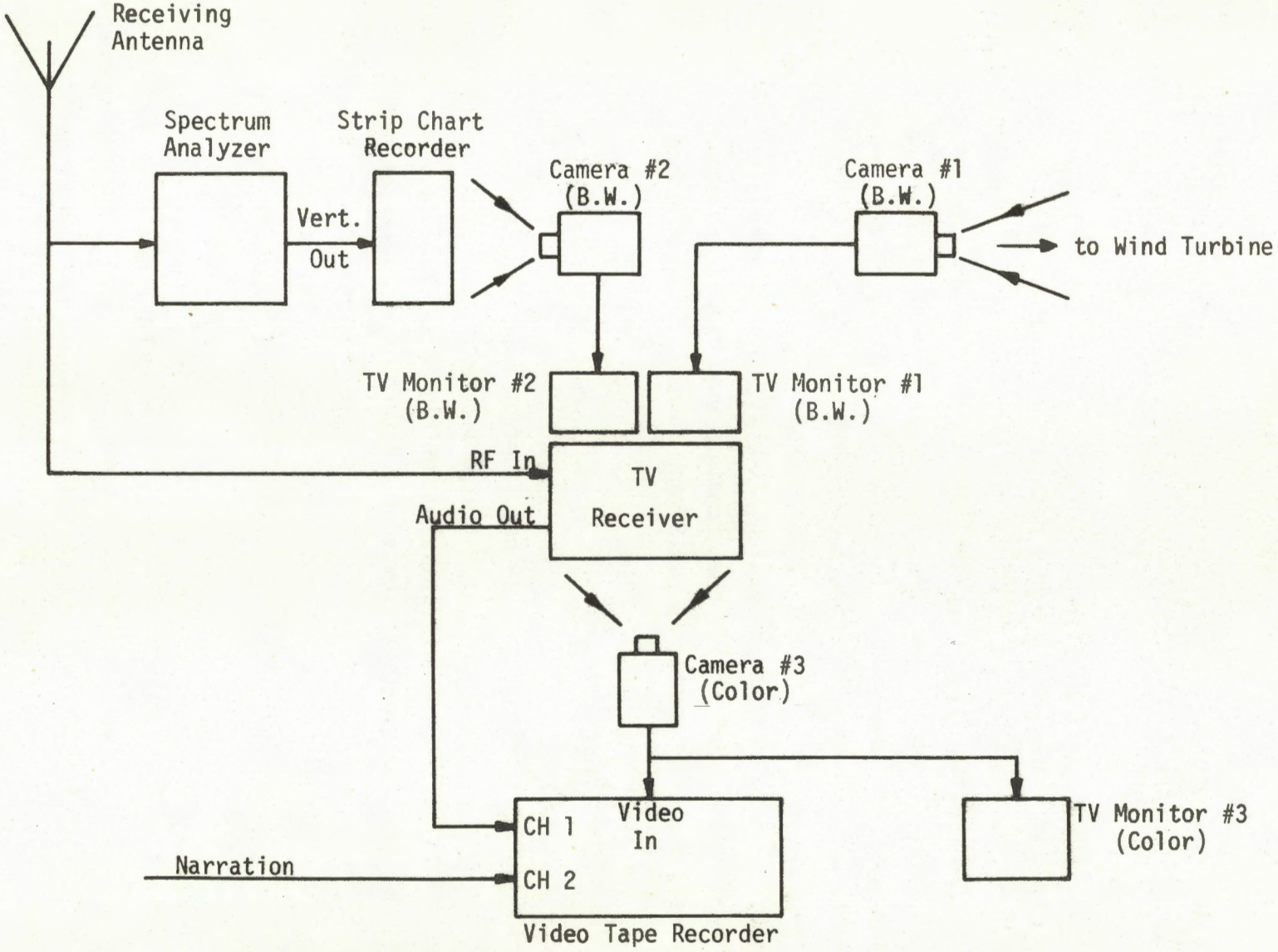

Figure 5-5: Experimental arrangement for interference measurements and recordings (B.W. denotes black and white).

For each TV channel a color video recording of the observed interference was made to include the following:

(i) 20 seconds of the program material being observed on the test receiver, accompanied by a narration of pertinent data;

(ii) 10 seconds showing the WTG (monitor #1) and the total received signal including the modulation pulses (monitor #2);

(iii) 15 seconds showing simultaneously the program on the test receiver and both monitors, thereby enabling the viewer to visually correlate the WTG blade position with the modulation pulses and the interference.

The original tape of these recordings is available for inspection. A condensed (and edited) version has been combined with the recordings of the laboratory simulations (see Section 5.2.3) and furnished to the sponsor.

5.1.3 Interference Studies

The video recording was only one facet of our field studies, and though it proved more time consuming than we had expected, a variety of other investigations were performed during our visits to the Plum Brook Facility. These have led to a rather complete understanding of the nature of WTG interference to TV reception, and most of the results obtained have been referred to either implicitly or explicitly in the preceding appendices. The key findings are summarized at the end of this section, but before doing so, a few comments would appear to be in order.

For any given TV transmission, the region about a WTG where the interference can exceed a level judged "acceptable" is called [1] the interference zone. It is defined as the region where the modulation index can be greater than a threshold value established on the basis of the field tests and laboratory simulations (see Section 5.2), and a method for computing the interference zone in any given case is described in [2]. The zone consists of two distinct parts: a specular (or backward) part whose shape is a cardioid with center at the WTG and maximum directed towards the transmitter, and a narrow (forward)

lobe about the line joining the transmitter to the WTG and directed away from the transmitter. Theoretically at least, the interference distance (i.e., to the boundary of the zone) is a maximum in the forward direction.

The nature of the observed interference differs in the two parts of the zone. In the backward part, the (delayed) multipath signal is produced by specular reflection off the surface of a blade. This leads to a ghost image on the TV screen which, at low or moderate levels of interference, 'jitters' horizontally in synchronism with the blade rotation, thereby causing video distortion. However, in the forward portion of the zone there is little or no delay between the direct and multipath signals at the receiver, and the interference now appears as an intensity modulation of the picture, again in synchronism with the blade rotation. Though a somewhat larger value of the modulation index could be acceptable in the forward direction, a single threshold has been selected (see Section 5.2) for the entire zone, namely 0.15 (15 percent), corresponding to a 2.6 dB variation of the total field.

In our previous study [1] the measurements were confined to the backward region, and it was therefore desirable to examine the interference in the forward portion of the zone. The measurements were carried out during the period 20-22 June and were somewhat limited because of the difficulty of finding test sites appropriate to the available TV transmitters and the orientation and pitch angles of the WTG blades at the time of the experiment, but did show the nature of the interference in the forward region. The site chosen was such that the WTG was almost in line between the TV transmitter of Channel 43 and the test receiver (Zenith model 17GC 45). The distance d (see Figure 5-6) between the receiver and the WTG was varied from 0.4 to 0.1 Km in increments of 0.08 Km. The ambient signal level received was -65 dB m (i.e., 3.2×10^{-7} watts) which, in the absence of any windmill interference, is sufficient to produce a distortion-free picture on the test receiver. At the extreme distance d = 0.4 Km, the recorded signal from the output of the spectrum analyzer is displayed in Figure 5-7 and clearly shows the modulation pulses caused by the rotating WTG blades. The modulation index was 2.5 dB (13 percent) which is slightly less than the threshold, and no unacceptable video distortion of the received picture

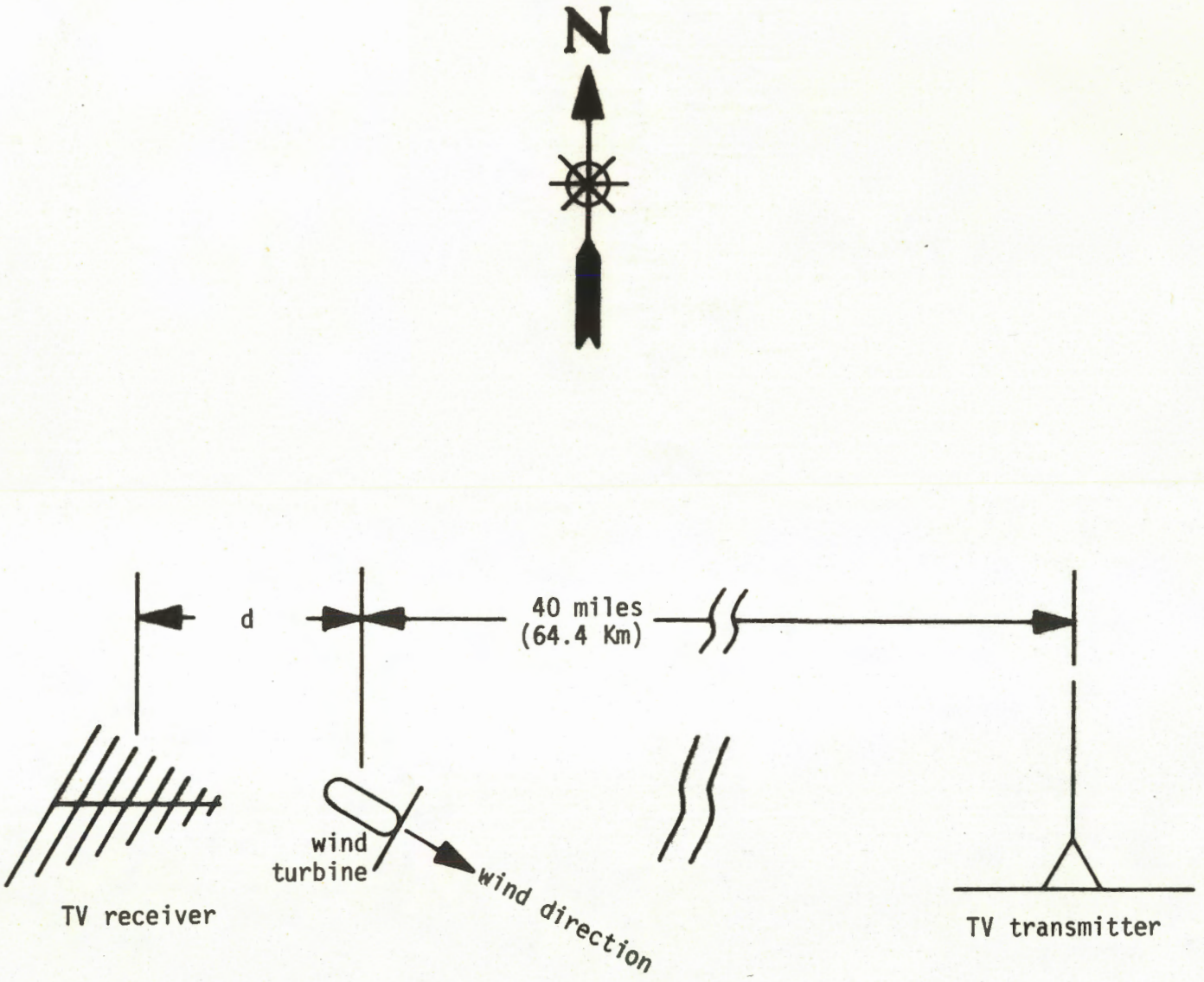

Figure 5-6: Geometry for interference measurements in the forward region of the WTG.

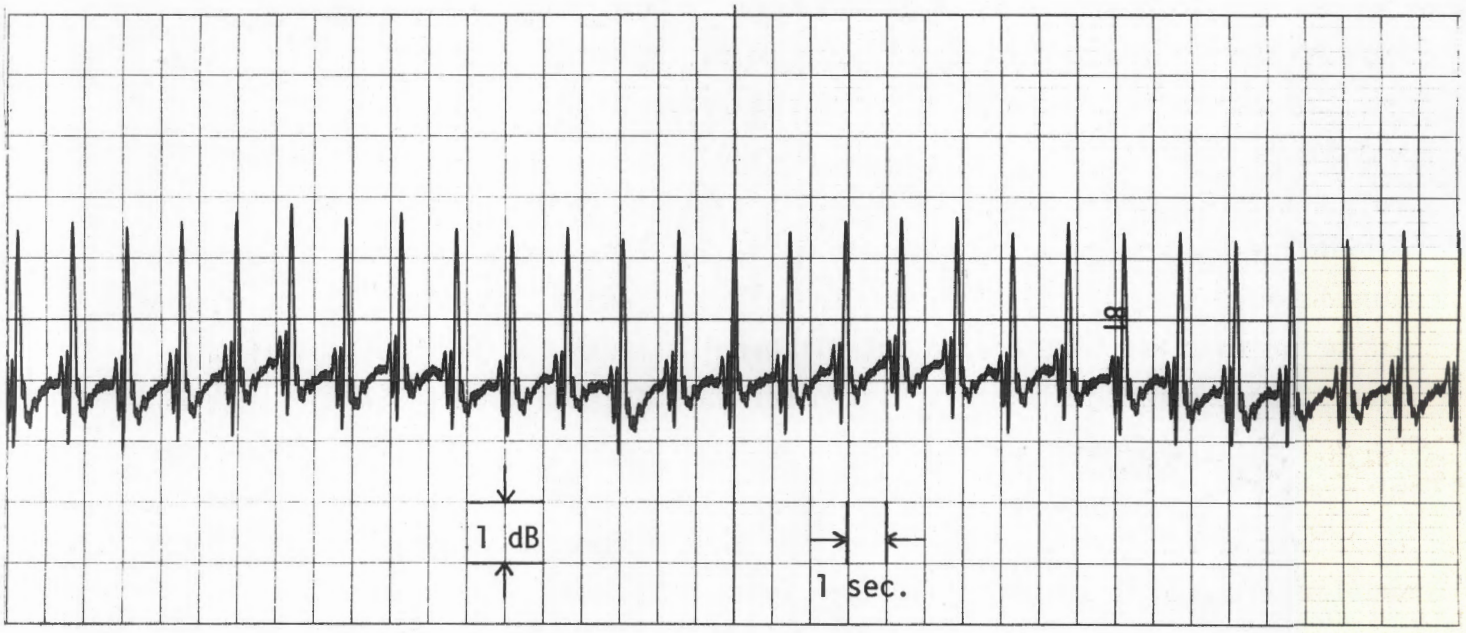

Figure 5-7: Received signal showing the modulation pulses due to the forward scattering by the WTG blades. WTG-to-receiver distance = 0.4 Km. WTG blade rotation frequency = 20 rpm.

was observed. Unfortunately, as the range d was decreased, the modulation index remained below the threshold due to the changing azimuth and pitch angle of the blades forced by the wind conditions, and such interference as was observed never did become objectionable. The study was not pursued further because of the difficulty in finding a suitable test site.

Rather detailed measurements of the interference in the backward (specular) portion of the interference zone were made in late November from the WTG control center building during the recording of the video tape referred to in the previous section. The results of the measurements are summarized in Tables 5-1 and 5-2 for the two test receivers. Unfavorable wind conditions prevented any measurements on Channel 43 with the Curtis Mathis receiver, but with both receivers the interference on Channels 8, 13 and 25 was fairly strong and produced significant video distortion. On Channels 3, 5 and 43, however, the modulation was below the threshold due to the different azimuth and pitch angles of the blades, and no video distortion was observed. As seen from Tables 5-1 and 5-2, the two receivers responded similarly to the interference effects, and the results confirm our previous findings that the orientation and pitch angles of the blades with respect to the receiving antenna beam significantly affect the modulation pulse shape and modulation index and, hence, the video distortion observed.

The conclusions from the field tests can be summarized as follows:

1. In the backward portion of the interference zone the observed video distortion is a horizontal jittering of the received picture in synchronism with the WTG blade rotation, whereas in the forward portion the interference produces intensity fluctuations of the picture, also in synchronism with the blade.

2. In the backward region significant interference is observed only when a blade is positioned to direct a specular reflected signal to the receiver. The azimuth and pitch angles of the blades are key factors affecting the

TV Channel	Ambient Signal Level (dBm)	Antenna Beam Position (degrees)	Turbine Azimuth (degrees)	Turbine (rpm)	Turbine Blade Pitch (degrees)	Percent Modulation	Interference Present?
3	-65	75	268	40.8	-8 to -10	11.5	No
5	-66	75	268	40.8	-1 to -2	8.6	No
8	-70	75	268	40.8	-6 to -2	56.0	Yes
13	-73	75	269	40.5	-10 to -7	38.2	Yes
25	-77	75	268	40.8	-9 to -4	38.2	Yes
43	-78	75	269	40.7	-3 to 6	14.3	No

Table 5-1: Interference measurement data for 1976 Zenith TV model 17GC 45. Distance of the WTG from the receiver ≈ 0.15 Km. For other parameters see Figure 5-2.

TV Channel	Ambient Signal Level (dbm)	Antenna Beam Position (degrees)	Turbine Azimuth (degrees)	Turbine (rpm)	Turbine Blade Pitch (degrees)	Percent Modulation	Interference Present?
3	-62.5	75	260	21.0	-15 to -22	9.2	No
5	-65.5	75	264	20.1	-24 to -18	10.3	No
8	-66.0	75	264	20.1	-18 to -14	33.2	Yes
13	-71.0	75	264	20.5	-21 to -17	45.4	Yes
25	-76.0	75	264	20.1	-25 to -20	33.2	Yes
43	-----	--	---	----	----------	----	---

Table 5-2: Interference measurement data for 1977 Curtis Mathis TV model B317. Distance of the WTG from the receiver ≈ 0.15 Km. For other parameters see Figure 5-4.

level of interference. In particular, for given transmitter and receiver locations, interference is observed only if the wind is such as to position the WTG appropriately.

3. Each blade contributes individually and the scattered signal is a sync-like pulse which usually appears when the blade is close to horizontal.

4. All other conditions being equal, the interference and the resulting video distortion increase with increasing TV channel number, i.e., frequency.

5. Although few of the test sites were such that the distance of the receiver from the WTG could be progressively changed, it was verified that the interference decreases with increasing distance from the WTG.

6. In the backward region the observed video distortion shows no significant dependence on the ambient level of the received signal provided the signal is well above the noise level of the receiver.

7. For a given level of interference, the backward region video distortion appears independent of the receiver used.

5.2 Laboratory Tests

With the information available from the field tests and from the other investigations carried out under this program, it was possible to simulate the interference that a windmill produces, and thereby examine the video distortion under the controlled environment that a laboratory affords. The tests were performed by studying the video reception of a test receiver for an applied signal consisting of the direct (desired) one combined with a portion which was amplitude modulated so as to simulate the multipath situation. The direct signals were those of the locally available TV channels, and the reception provided by two commercial TV receivers was examined for varying modulation and ambient signal levels at the input to the test receiver.

The main objectives of the simulation studies were to (i) observe and characterize the nature of the video interference; (ii) investigate the dependence (if any) on the test receiver used and the ambient signal level; (iii) determine the dependence on the modulation applied; and (iv) establish the modulation levels for which the time-dependent interference is (a) first perceived, and (b) the most severe that would still be judged acceptable to the average viewer. The threshold level obtained from (iv)b is a key ingredient in the determination of the interference zone about a windmill [2].

5.2.1 Experimental Set-Up

Figure 5-8 shows a block diagram of the equipment used in the measurements. The desired TV signal was received by a commercial log-periodic antenna whose beam direction could be adjusted via a rotor control and which was mounted on the roof of the building about 120 feet above ground level. With the UHF channels it was found desirable to boost the received signal using a pre-amplifier, but this was by-passed at VHF where the signals were stronger. The signal was then passed through a set of variable attenuators so its value could be adjusted to any level, and thence to a coaxial T-junction where it was split into two branches, the direct and multipath lines, as shown in Figure 5-8. The direct line carried the signal representing the direct signal from the transmitter to the receiver, and its value could be controlled by another attenuator. The multipath line carried the signal simulating that produced by reflection off the moving blades of a windmill, and to effect the simulation, the signal was delayed in time and then amplitude-modulated with a repetitive pulse of the required shape. The signals were re-combined at a second T-junction and the resulting composite signal was fed to the test receiver and a spectrum analyzer. The latter was always tuned to the audio carrier frequency of the TV channel, and its vertical output was applied to a strip chart recorder to give hard copy of the input signal to the test receiver on a function of time. The output of the recorder was used to determine the effective amplitude modulation (in dB) of the signal input to the test receiver, and this could be set to a desired level using the attenuators and the DC bias at the AGC terminal of the VHF (or UHF) tuner.

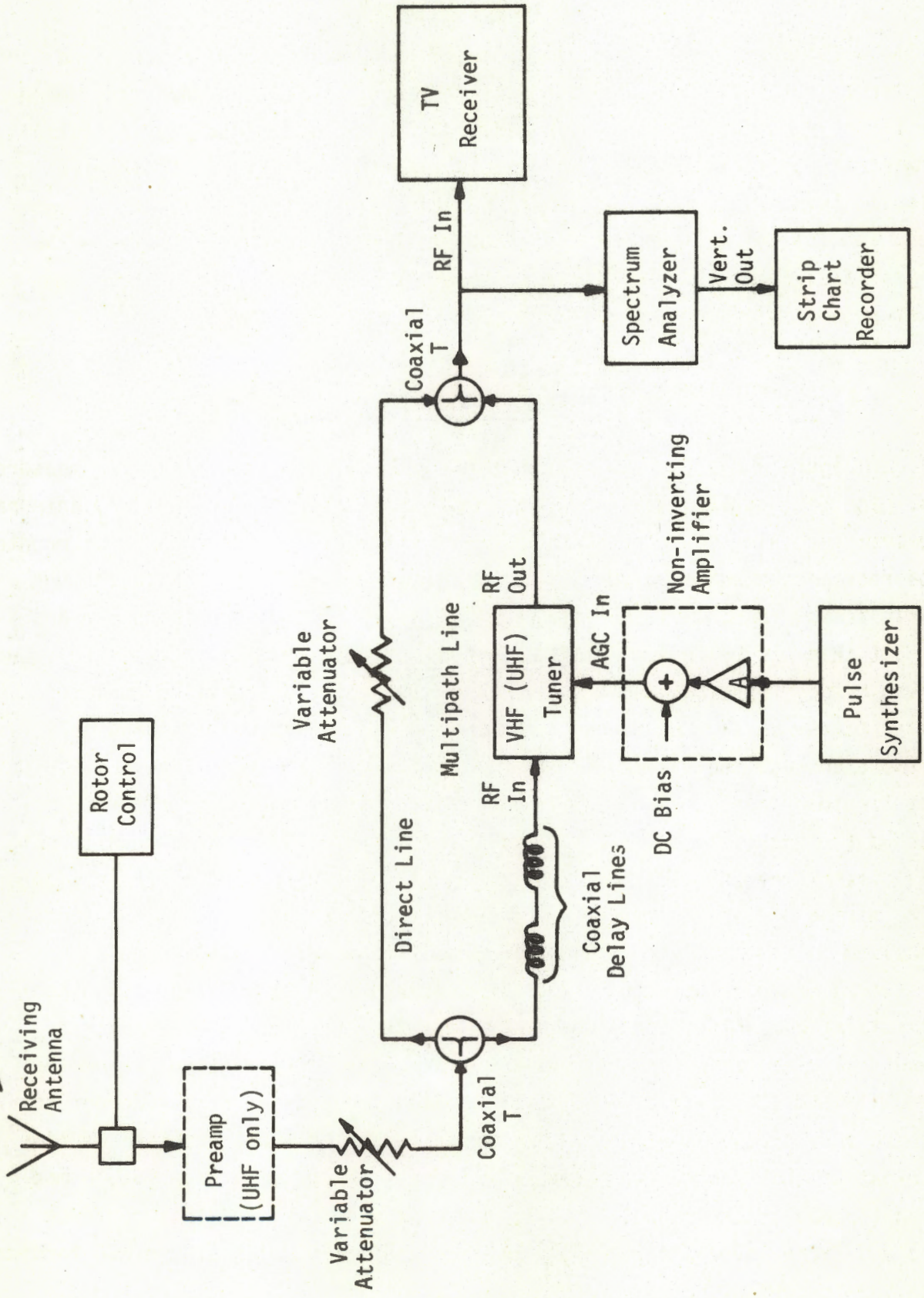

Figure 5-8: Experimental set-up for simulation and measurement of interference produced by a WTG.

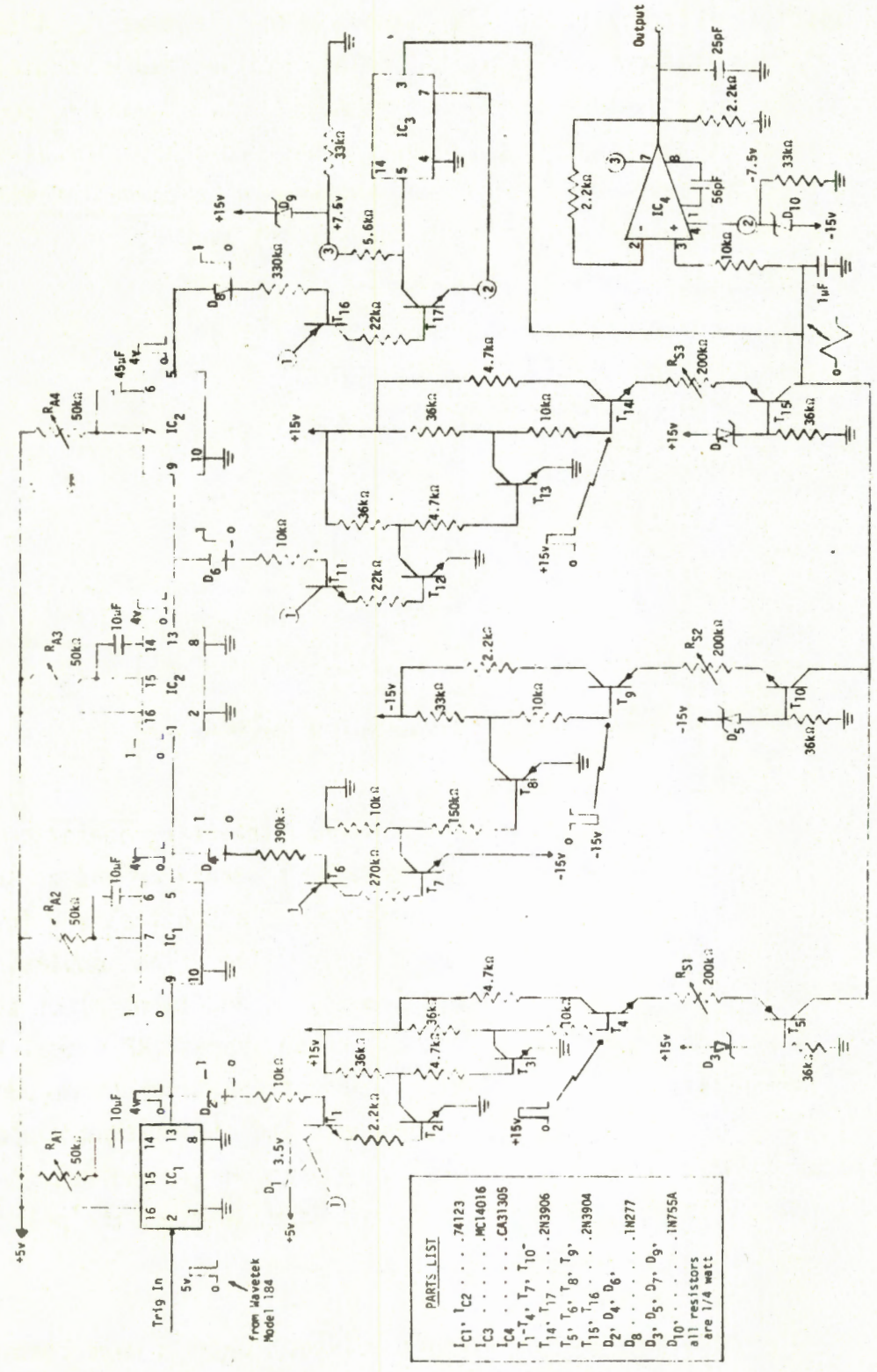

Figure 5-9: Circuit diagram of the modulation pulse synthesizer. Inset shows the list of parts.

The modulator itself consisted of three stages. The first was a circuit whose schematic diagram is shown in Figure 5-9. This synthesized a modulation pulse of the form in Figure 5-10 whose parameters A_1, A_2, t_1, t_2 and t_3 could be independently adjusted to produce a pulse of the desired shape. Provision was also made so that the pulse repetition frequency could be chosen at will, but all the experiments were carried out with the prf set at 2 Hz.

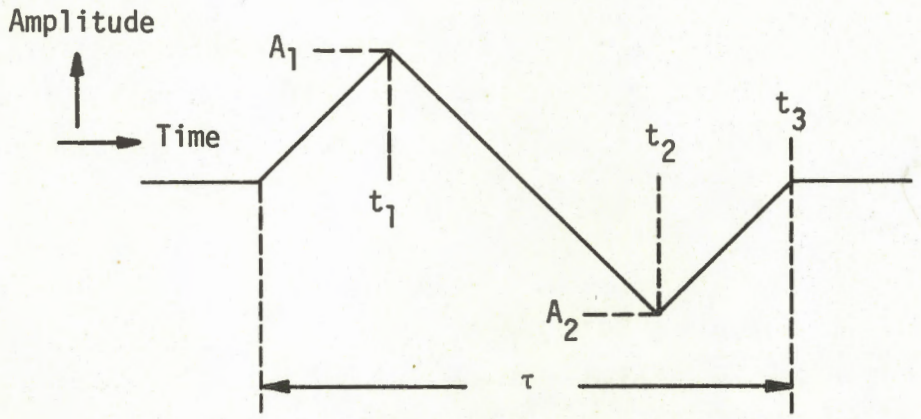

Figure 5-10: Sketch of the synthesized pulse.

The second stage of the modulator was a simple non-inverting operational amplifier to amplify (or attenuate) the pulse from the synthesizer and to introduce the required DC bias. The third and final stage was a modified VHF (or UHF) tuner whose input was the RF signal from the delay line. The modulation pulse from the non-inverting amplifier was applied to the AGC terminal of the tuner so that the DC portion of the pulse controlled the average RF signal level while the pulse itself differentially varied the gain of the tuner to produce the desired modulation. This average level represents the signal that would be scattered off the windmill blades if the blades were stationary, and was, in general, less than the RF signal level in the direct line, whereas the pulse simulates the effect of blade rotation.

As noted earlier, the direct and delayed (modulated) signals were combined at the second T-junction. Figure 5-11(a) is typical of the modulation applied to the input to the receiver as measured by the strip chart recorder, and should

be compared with the example shown in Figure 5-11(b) of the modulation of the received TV signal on Channel 43 measured at Plum Brook. Since the blades were rotating at 20 rpm, the pulse repetition period in Figure 5-11(b)is 1.5 s, but in all our laboratory tests a repetition period of 0.5 s was adopted. This corresponds to a blade rotation frequency of 60 rpm which is somewhat larger than for a typical WTG. The choice of 2 Hz for the prf was made purely for convenience and implies that the periodicity of the interference phenomena observed in the simulation is slightly smaller than would be found in practice. However, this does not effect the nature of the interference phenomena, and in all other respects the laboratory study provided a realistic simulation of the interference that could result from a windmill in the vicinity of the receiver.

5.2.2 Test Procedure

The tests were made using a 1976 Zenith model 17GC 45 and a 1967 Airline model GEN 12349A color TV receiver. The first is a 17 inch model rated superior in its interference rejection capability and the second is a 14 inch model typical of an older receiver. The RF signals were the TV Channels 2, 4, 7, 9 and 50 whose transmitters are located near Detroit (Michigan) approximately 60 Km from the laboratory where the measurements were performed, and Channels 11, 13 and 24 originating in Toledo (Ohio) approximately 90 Km away. The tests were carried out using all of these channels and three similar types of modulation pulse having widths τ = 50, 100 and 200 ms with a 500 ms repetition period (prf = 2 Hz). The 100 ms width is typical (see Figure 5-11(b)) of the major portion of the modulation pulse produced by the windmill at Plum Brook on Channel 43; and the 50 and 200 ms pulses were intended to simulate the modulation produced by larger and smaller windmills respectively, and/or by the MOD-0 windmill at higher and lower TV channel frequencies.

Conditions within the backward portion of a windmill interference zone were simulated by introducing a time delay between the direct and multipath signals at the receiver, and by suitably attenuating the multipath signal relative to the direct one. As indicated in Figure 5-8, two sections of coaxial line were used which together produced 625 ns delay at all of the TV channel

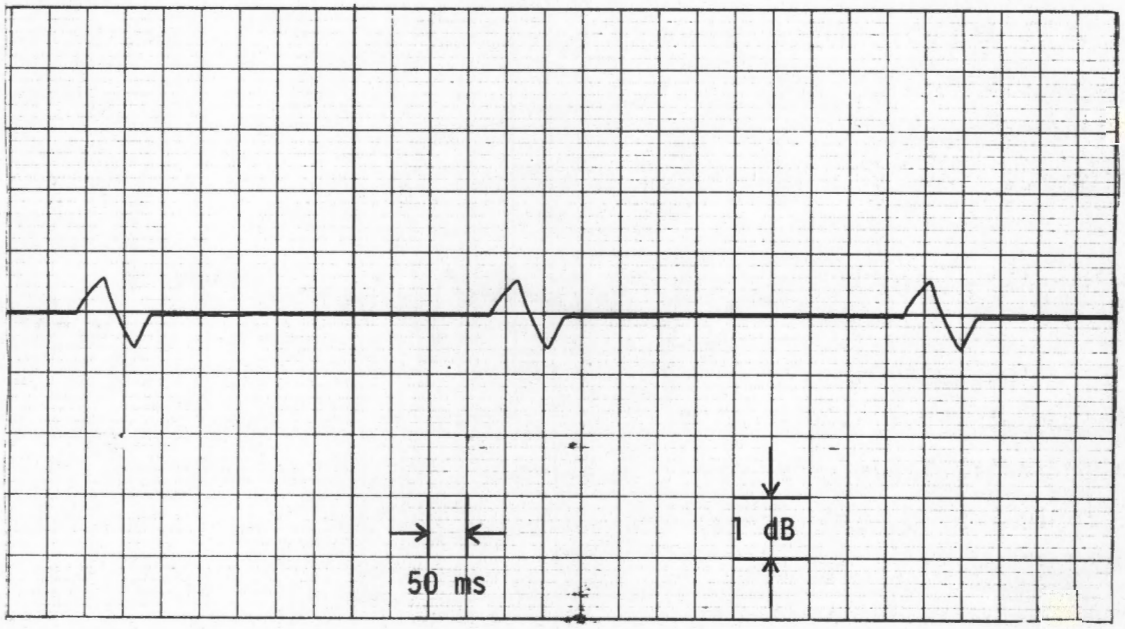

Figure 5-11(a): Modulation pulses applied to the input of the test receiver during the simulation test on Channel 50.

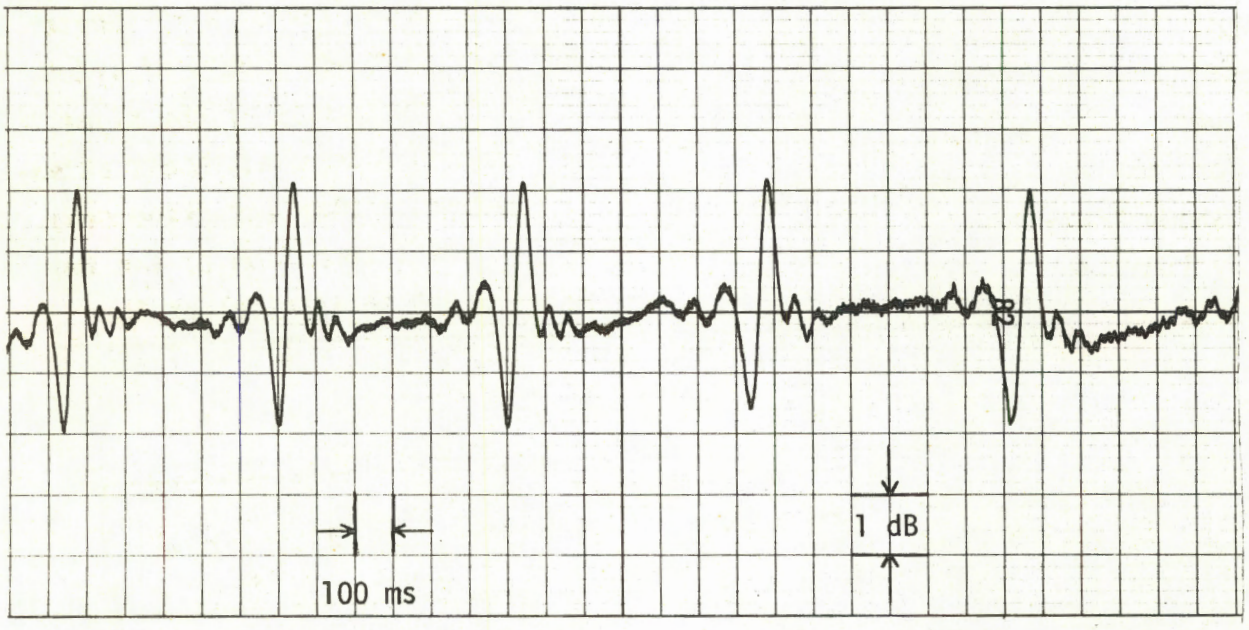

Figure 5-11(b): Modulation pulses at the input of the test receiver observed during the Channel 43 field tests at Plum Brook.

frequencies. This corresponds approximately to the time delay between the direct and multipath signals in the field test measurements in the WTG control center building at Plum Brook (see Section 5.1.3). Different lengths of coaxial line would be required to simulate conditions in other portions of the backward interference zone, leading to different shifts of the ghost picture away from the direct picture, but not otherwise changing the nature of the interference. However, no other lengths were used in the test. With shorter lengths it proved difficult to distinguish the four distinct levels of video distortion discussed later, and with longer lengths the losses at the higher frequencies became excessive. For the two sections of line used, their attenuation characteristics as a function of the TV channel number (or frequency) are shown in Table 5-3. It will be observed that the attenuation of the two delay lines is negligible at the lowest frequency, but substantial at the highest.

TV Channel No.	TV Channel Audio Carrier Frequency (MHz)	Attenuation (dB)
2	59.75	1
4	71.75	7
7	179.75	9
9	191.75	9
11	203.75	10
13	215.75	10
24	535.75	14
50	687.25	18

Table 5-3: Measured attenuation versus TV channel number (or frequency) for the two delay lines.

For the forward portion of the windmill interference zone, the conditions were simulated by eliminating the direct line in Figure 5-8, so that only the modulated signal was applied to the inputs to the test receiver and the spectrum analyzer.

For given TV channel and modulation pulse width, each simulation test had two parts. The first served to establish the critical modulation level as a function of the ambient RF signal strength at the input to the test receiver. This critical level is defined as the smallest modulation index m_c in dB (or percent) required to produce video distoriton detectable by an observer viewing the received picture from a distance of 5 feet. Although the criterion is obviously subjective, the same observers were used throughout the experiment, and the results were reproducible when the tests were repeated at a later time. In the second part of the test, the modulation index m was increased in small steps from zero and the degree of video distortion observed. Four categories of video reception were distinguished: (i) no video distortion, corresponding to $m < m_c$; (ii) distortion judged acceptable for at least small periods of viewing time. This corresponds to $m_c < m < m_o$, the upper limit m_o being the threshold modulation level specifying the interference zone around a windmill; (iii) distortion judged unacceptable and intolerable for prolonged viewing, and (iv) disruptive distortion, occasionally resulting in picture break-up due to loss of vertical sync by the test receiver.

The simulation measurements for the backward portion of the interference zone used the entire experimental set-up shown in Figure 5-8. The first part of the test involved the following steps with each TV receiver.

(i) Set the modulation pulse width to the desired value.
(ii) Set the channel selector switch of the test receiver to the desired TV channel and tune the spectrum analyzer to the audio carrier frequency of the desired TV channel.
(iii) Rotate the receiving antenna for maximum received signal strength.
(iv) Increase the modulation level until the critical modulation level is reached as judged by an observer viewing the received picture at a distance of 5 feet from the test receiver.

(v) Record the ambient signal strength and the output from the spectrum analyzer.

(vi) Obtain the critical modulation level m_c in dB from the strip chart recording.

(vii) Decrease the signal level by 5 dBm.

(viii) Repeat steps (iv) - (vi) until the signal level is too low for satisfactory reception.

(ix) Select a new TV channel and repeat steps (ii) - (viii) until all desired TV channels have been tested.

(x) Adjust the modulation pulse width to a new value and repeat steps (ii) - (ix).

The above procedure allowed us to study independently the effects of the ambient signal strength, the TV channel frequency and the modulation pulse width on the critical modulation level.

In the second part of the test, steps (i) - (iii) were repeated prior to the following:

(xi) Adjust the ambient signal level to a desired value.

(xii) Increase the applied modulation in four stages, and note the category in which the video distortion falls.

(xiii) At each stage in (xii), record the spectrum analyzer output on the strip chart recorder and obtain the applied modulation level in dB.

For the tests simulating the forward portion of the interference zone, the direct line in Figure 5-8 was eliminated, and the measurements performed using the procedure described above.

5.2.3 Presentation of Results

A rather extensive series of laboratory simulations was performed. For a number of commercial TV channels, the received signals were amplitude modulated in the manner described in Section 5.2.1, and the video distortion observed under controlled conditions as a function of the modulation index. The modulation level is given in dB and can be converted into percent modulation using Figure 5-3. Since the RF signals were those of the local TV channels, the state of the received signals depended on the propagation characteristics at the times the tests were carried out. Occasionally a particular channel was unavailable or the signal was such that meaningful data could not be obtained, and this accounts for the missing entries in the subsequent tabulations of the data.

As simulations of the backward portion of the interference zone, Tables 5-4(a), (b) and (c) show the critical modulation index m_c necessary to produce minimum observable video distortion in the Zenith test receiver picture for signals of various levels on each of the TV channels. The results given are for three cases where the modulation pulses have the same shape and prf but different time-widths. Data which are of questionable accuracy are marked with symbols whose meaning is explained below Table 5-4(c). Due to systematic and, occasionally, erratic variations in the signal level on Channel 13, all of the data for this channel are suspect, but for completeness the results have been included in the tables. The analogous data for the Airline test receiver are shown in Tables 5-5(a), (b) and (c). Because a pulse width as large as 200 ms is not felt to be realistic for existing windmills at the higher frequencies, we have not presented any data for τ = 200 ms on Channels 24 and 50.

The degrees of video distortion observed in the backward region for the two receivers are shown in Tables 5-6 and 5-7(a) and (b). The four levels of modulation index are those for the onset of the types of video distortion defined in Section 5.2.2, and data are given for pulse widths τ = 50 and 100 ms, the latter being typical of the MOD-0 windmill. With the Zenith receiver, the results were similar at all of the signal levels considered, and for this reason

Audio Carrier Level $\left(\frac{dB}{mW}\right)$	Channel No.							
	2	4	7	9	11	13	24	50
	Frequency (MHz)							
	59.75	71.75	179.75	191.75	203.75	215.75	535.75	691.75
	m_c (dB)							
-50	---	1.9	0.9	---	---	---	0.9	---
-55	3.4	1.9	0.9	---	0.8	3.6**	1.2	---
-60	4.3	1.9	1.0	---	0.8	3.5**	0.9	0.8
-65	5.8*	2.2	1.0	∿0.6	0.8	3.6**	1.0	0.9
-70	5.3*	2.5	1.2	0.7	0.9	4.0**	1.2	0.9
-75	∿7.0*	2.6	1.3	0.9	0.8	3.3**	1.1	0.8
-80	---	3.6*#	1.6	1.3#	1.2	3.8**#	1.2	0.8
-85	---	4.0*#	1.7	---	1.3#	3.5**#	---	---

(a) τ = 50 ms,

Audio Carrier Level $\left(\frac{dB}{mW}\right)$	Channel No.							
	2	4	7	9	11	13	24	50
	Frequency (MHz)							
	59.75	71.75	179.75	191.75	203.75	215.75	535.75	691.75
	m_c (dB)							
-50	4.0	---	0.9	---	---	---	---	---
-55	3.4	1.0	0.8	---	0.8	3.8**	---	0.6
-60	4.6	1.2	1.0	0.8	0.9	4.0**	0.6	0.7
-65	4.9	0.9	1.0	0.8	0.8	3.0**	0.7	0.7
-70	4.8	1.1	1.2	1.1	0.9	2.9**	0.9	2.0#
-75	---	1.0	1.5#	1.6	1.0	3.0**	1.2#	2.0#
-80	---	2.6#	1.6#	2.1#	1.3#	3.0**#	---	---
-85	---	2.7#	1.7#	2.0#	1.6#	3.2**#	---	---

(b) τ = 100 ms

Audio Carrier Level $\left(\frac{dB}{mW}\right)$	Channel No.					
	2	4	7	9	11	13
	Frequency (MHz)					
	59.75	71.75	179.75	191.75	203.75	215.75
	m_c (dB)					
-50	---	1.5	0.6	---	---	---
-55	3.5	2.0	0.8	---	1.6	1.4**
-60	3.4	1.4	0.7	~0.8	2.0	1.9**
-65	3.8	2.0	0.8	0.9	2.0	1.9**
-70	4.0	3.0	0.8	0.7	2.0	2.1**
-75	5.0	3.2	1.2	0.8	2.4	2.7**
-80	5.1	5.2#	1.6	1.1#	2.5#	2.7**#
-85	5.0	---	2.0	1.2#	3.1#	---

(c) τ = 200 ms

Legend:

* ghost very dominant - data unreliable

\# signal extremely weak: received picture very snowy - data accuracy unreliable

** ambient signal variations large - data mostly unreliable

Table 5-4: Backward region critical modulation index m_c (in dB) required to produce minimum observable video distortion as a function of ambient audio carrier signal level on various TV channels. Test receiver: 1976 Zenith Model 17GC 45. (a) τ = 50 ms, (b) τ = 100 ms, (c) τ = 200 ms.

Audio Carrier Level $\left(\frac{dB}{mW}\right)$	Channel No.						
	2	4	7	11	13	24	50
	Frequency (MHz)						
	59.75	71.75	179.75	203.75	215.75	535.75	691.75
	m_c (dB)						
-50	---	---	---	---	---	---	---
-55	---	0.3**	1.4	0.5	0.9	---	0.8
-60	0.4	0.3**	1.4	0.5	1.2	0.8	0.8
-65	0.4	0.3**	1.3	0.3	1.1	0.8	0.8
-70	0.5	0.3**	1.0	0.3	0.8	0.5	0.8
-75	0.5	0.3**	0.7	0.3	0.5	0.6	0.6
-80	---	---	0.9	<0.3#	0.4	0.6	0.6
-85	---	---	1.4#	0.7	0.4	0.7#	---

(a) τ = 50 ms

Audio Carrier Level $\left(\frac{dB}{mW}\right)$	Channel No.						
	2	4	7	11	13	24	50
	Frequency (MHz)						
	59.75	71.75	179.75	203.75	215.75	535.75	691.75
	m_c (dB)						
-50	0.8	---	2.2	---	---	---	---
-55	0.5	1.5	2.1	0.9	2.9	---	1.9
-60	0.4	1.4	1.5	0.8	3.3	1.6	1.8
-65	0.5**	1.3	1.8	0.8	3.1	1.5	1.6
-70	0.4**	1.6	1.2	0.8	2.5	1.9	1.8
-75	0.4**	1.8	1.2	0.8	2.2	1.8	1.8#
-80	0.4**	1.8	1.2	0.6#	2.0#	1.8	2.0#
-85	0.4**#	---	---	0.8#	2.0#	---	---

(b) τ = 100 ms

Audio Carrier Level (dB/mW)	Channel No.				
	2	4	7	11	13
	Frequency (MHz)				
	59.75	71.75	179.75	203.75	215.75
	m_c (dB)				
-50	---	---	1.5	---	---
-55	1.0	---	1.5	---	2.9
-60	1.0	0.4	2.4	1.4	2.1
-65	1.7	0.4	2.2	1.4	2.6
-70	1.9	0.6	2.8	1.6	2.5
-75	2.7	0.9	2.8	1.5	3.3
-80	2.0	1.9#	3.6	1.0	3.8
-85	3.3#	---	3.6	1.0	4.0

(c) τ = 200 ms

Legend:

* ghost very dominant - data unreliable

\# signal extremely weak: received picture very snowy - data accuracy unreliable

** ambient signal variations large - data mostly unreliable

Table 5-5: Backward region critical modulation index m_c (in dB) required to produce minimum observable video distortion as a function of ambient audio carrier signal level on various TV channels. Test receiver: Airline Model GEN12349A. (a) τ = 50 ms, (b) τ = 100 ms, (c) τ = 200 ms.

Channel No.	Degree of Observed Video Distortion				
	1	2	3	4	
	m_c (dB)	m_o (dB)	m (dB)	m (dB)	
7	1.1	2.8	3.1	18	τ = 100 ms
50	0.7	2.6	3.0	8	
50	0.8	2.0	2.9	4	τ = 50 ms

Table 5-6: Degree of observed backward region video distortion (and the modulation index required) with an ambient audio carrier signal level of -60 dBm for two TV channels and two pulse widths, τ = 50 and 100 ms. Test receiver: 1976 Zenith Model 17GC 45.

Audio Carrier Level (dB/mW)	Degree of Observed Video Distortion				
	1	2	3	4	
	m_c (dB)	m_o (dB)	m (dB)	m (dB)	
-55	1.4	1.8	4.0	7.3	Channel 7
-60	1.4	1.9	3.8	8.0	
-65	1.3	2.0	2.8	8.5	
-70	1.0	2.1	3.2	7.5	
-55	0.8	2.0	4.0	4.2+	Channel 50
-60	0.9	1.4	3.6	4.2+	
-65	1.0	1.8	3.7	4.3+	
-70	0.8	1.6	3.9	4.0+	

(a) τ = 50 ms

Audio Carrier Level (dB/mW)	Degree of Observed Video Distortion				
	1	2	3	4	
	m_c (dB)	m_o (dB)	m (dB)	m (dB)	
-55	2.1	2.5	5.4	7.6	Channel 7
-60	1.5	2.6	7.5	8.0	
-65	1.8	2.7	6.1	7.8	
-70	1.2	3.0	5.5	7.9	
-55	1.9	2.8	4.3	4.8+	Channel 50
-60	1.8	2.6	4.2	5.0+	
-65	1.6	2.5	4.4	5.1+	
-70	1.7	2.7	4.4	5.1+	

(b) τ = 100 ms

+ modulation pulse distortion

Table 5-7: Degree of observed backward region video distortion (and the modulation index required) as a function of ambient audio carrier signal level for two TV channels and two pulse widths, (a) τ = 50 ms and (b) τ = 100 ms. Test receiver: Airline Model GEN12349A.

Audio Carrier Level (dB/mW)	τ = 50 ms		τ = 100 ms	
	Channel 7	Channel 50	Channel 7	Channel 50
	m_c (dB)			
-50	20	--	29	--
-55	17	--	25	--
-60	15	--	20	--
-65	14	16	15	17
-70	6.5	12	5.5	13
-75	3.5	8	3.5	10
-80	2.5#	4	3.5	5
-85	1.5#	2	2	4

Table 5-8: Forward region critical modulation index m_c (dB) required to produce minimum observable video distortion as a function of ambient audio carrier signal level on two TV channels for two pulse widths. Test receiver: 1976 Zenith Model 17GC 45.

Audio Carrier Level (dB/mW)	m_c (dB)
-55	2.2
-60	2.9
-65	3.0
-70	3.2
-75	3.2
-80	2.8#
-85	2.6#

Table 5-9: Forward region critical modulation index m_c (dB) required to produce minimum observable video distortion as a function of ambient audio carrier signal level on TV Channel 50 for τ = 100 ms. Test receiver: Airline Model GEN12349A.

Table 5-6 shows data only for the ambient signal level -60 dBm. The choice of TV channel was based on the dependability and consistency of the data.

For the forward portion of the interference zone the modulation index m_c required for minimum observable video distortion is given in Tables 5-8 and 5-9 for the Zenith and Airline test receivers respectively.

In addition to the above, a color video recording (along with narrations of pertinent data) of the observed video distortions due to simulated backward region interference was prepared to include the following for the TV channel numbers shown in parentheses:

(i) 30 seconds of the direct program material being observed on the test receiver (7);

(ii) 30 seconds showing the effect of the stationary windmill (7);

(iii) a set of 30 seconds intervals, each showing the observed minimum video distortion at the critical modulation level (m_c) as a function of ambient audio carrier signal level (7);

(iv) sets of 30 seconds intervals showing the degree of observed video distortions versus modulation level (m) at a constant level of -60 dBm for the ambient audio carrier signal (4, 7, 24 and 50);

(v) summary of effects for TV Channel 50 shown in 30 seconds intervals containing the observed video distortions for $m = m_c$, m_o and for increasing values of $m > m_o$ until the received picture is disrupted due to loss of vertical sync.

5.2.4 Discussion

In the light of the results presented in Section 5.2.3 the following observations are made.

Backward Region Simulations

(i) The value of m_c on any given channel is reasonably independent of the ambient signal level for both test receivers. The slight tendency for m_c to increase with decreasing signal (see Tables 5-4 and 5-5) can be attributed to the fact that at lower signal levels the poorer quality of the pictures forced more than the minimum required modulation to maintain a uniform criterion for the nature of the observed video distortion.

(ii) With the Airline receiver, m_c decreases with decreasing τ on all channels except Channel 2. There is no such trend with the Zenith receiver: indeed, on some channels the behavior is just the opposite.

(iii) The Zenith receiver is less sensitive to interference on the lowest two TV channels whereas the Airline receiver is quite sensitive there. Overall, the Zenith is less susceptible to interference than the Airline receiver.

(iv) Both receivers show similar vulnerability on the highest TV channels, with the Zenith being slightly more vulnerable than the Airline.

(v) The range of modulation index for which the interference is acceptable is larger for the Zenith than for the Airline (see Tables 5-6 and 5-7).

Forward Region Simulations

(vi) For both receivers the critical modulation index is now dependent on the ambient signal level and decreases with decreasing level.

(vii) With a strong ambient signal ($\gtrsim$ -65 dBm), however, the Zenith receiver is extremely insensitive to interference, which could explain why no video distortion was observed in the field tests described in Section 5.1.3. Overall, the Airline receiver is much more sensitive to interference than the Zenith.

Modulation Threshold Level m_o

To compute the interference zones associated with a windmill it is necessary to know the modulation threshold m_o defined as the largest value of the amplitude modulation index m of the received signals for which the resulting video distortion is still judged acceptable for short periods of viewing. The modulation index is proportional to the amplitude of the interfering signal and because this increases with increasing frequency and decreases with increasing distance from the windmill, the maximum extent of the interference zones is determined by the modulation threshold at the highest TV frequency (or channel number) of interest. As seen from Tables 5-6 and 5-7, the lowest values of m_o obtained with the two receivers on Channel 50 are 1.4 dB (∿8 percent) and 2.5 dB (∿14 percent) for pulse widths 50 and 100 ms respectively. These values apply to the backward portion of the interference zone. In the forward portion, m_o depends quite strongly on the ambient signal strength (see Table 5-8), increasing with increasing signal strength, and because of this, it is not possible to assign a unique value of m_o for this region. However, the data in Table 5-8 indicate that for the pulse lengths and receivers considered, the minimum m_o is larger than the values for the backward region, and since a width τ = 100 ms is typical of the pulse produced by existing windmills, it is recommended that the single modulation threshold m_o = 2.6 dB (∿15 percent) be used for the entire interference zone. This is, in fact, the value that has been used in the Site Assessment Handbook [2], and we remark that it will over estimate the size of the forward portion of the zone.

5.3 Conclusions

Video distortion effects on TV reception caused by the NASA/ERDA 100 Kw WTG, located at Plum Brook (Ohio), have been observed and quantified by conducting a number of field tests using two commercial TV receivers receiving TV signals from Cleveland and Toledo, both in Ohio. The primary reason for the observed distortion is the pulse amplitude modulation of the received signals produced by the rotating blades of the WTG. These modulation pulses have been

recorded and characterized, and no video distortion has been observed when the modulation pulse level is less than a threshold value. The two test receivers responded similarly to the windmill interference which has been found to depend on the windmill blade orientation, pitch, the existing wind speed, the distance of the receiver from the windmill and the TV channel number (or frequency). No significant audio distortion due to a WTG has been observed.

Tests have been conducted in the laboratory simulating the conditions of the field tests by amplitude modulating the received TV signals with repetitive pulses having shapes similar to those obtained in the field. The interference effects have been observed to be similar to those found during the field tests. For a selected number of TV channels, the video distortions produced have been studied as functions of the ambient RF signal and modulation levels. On the basis of these results, a single modulation threshold level has been established for determining the interference zones associated with existing windmills.

Finally, video recordings of the distortions obtained from field and laboratory tests have been edited and combined into a single recording which has been delivered to the sponsor.

5.4 References

[1] Senior, T.B.A., D.L. Sengupta and J.E. Ferris, "TV and FM Interference by Windmills", The University of Michigan Radiation Laboratory Final Report No. 014438-1-F, February 1977, Contract No. E(11-1)2846, ERDA, Washington, D.C.

[2] Senior, T.B.A. and D.L. Sengupta, "Wind Turbine Generator Siting and TV Reception Handbook", The University of Michigan Radiation Laboratory Technical Report No. 014438-1-T, January 1978, Contract No. EY-76-S-02-2846.A001, DOE, Washington, D.C.